DISCOVERY OF SMALL MOLECULE INTERACTORS OF HUMAN ARFGAP1 AND THEIR POTENTIAL USE FOR THE TREATMENT OF PARKINSON'S DISEASE

by

Katherine A. Strynatka

Submitted in partial fulfilment of the requirements

for the degree of Doctor of Philosophy

at

Dalhousie University

Halifax, Nova Scotia

December 2023

Dalhousie University is located in Mi'kma'ki,

the ancestral and unceded territory of the Mi'kmaq.

We are all Treaty people.

TABLE OF CONTENTS

LIST OF TABLES

LIST OF FIGURES

ABSTRACT

Parkinson's disease (PD), a movement disorder affecting primarily elderly patients, is the second most common neurodegenerative disease. The majority of cases are idiopathic, however, a subset of patients have genetic variations that highly predispose them to the disease. The most common genetic variant is in the *LRRK2* gene, encoding a protein with both GTPase and protein kinase enzymatic domains. All known PD predisposing variants result in an increase in its kinase activity. LRRK2 kinase inhibitors were trialed as a potential treatment but were found to be toxic to the kidney and lung. Thus, alternate approaches in treating LRRK2-mediated PD may offer benefit. The GTPase activating protein ArfGAP1 was identified as a regulator of LRRK2 activity. We hypothesized that inhibiting ArfGAP1 activity may be a viable approach to treat LRRK2-mediated PD. We performed a cell-based high-throughput small molecule screen testing over 100,000 compounds for potential inhibition of human ArfGAP1 in a cell-based assay. Five compounds consistently showed reversal of ArfGAP1 toxicity to cells. I tested three candidates for their ability to directly bind purified ArfGAP1 using microscale thermophoresis. The results suggest that all three compounds bind ArfGAP1. Fruit fly models expressing human LRRK2, and the most common PD pathogenic version LRRK2-G2019S, in dopaminergic neurons of the fly brain were used to test the efficacy of the three compounds using an age-related motor deficit phenotype. This proof of concept experiment determined that one of the compounds increased movement in flies expressing human LRRK2, but not the LRRK2-G2019S variant.

LIST OF ABBREVIATIONS USED

5-HT	Serotonin
AD	Alzheimer disease
AMP	Ampicillin
ArfGAP1	Arf1 GTPase activating protein 1
ATG9	Autophagy-related 9
BSA	Bovine serum albumin
CAM	Chloramphenicol
cDNA	Complementary DNA
CNS	Central nervous system
COMT	Catechol-o-methyltransferase
DA	Dopamine
FDA	Food and Drug Administration
FPLC	Fast protein liquid chromatography
GBA	β-Glucocerebrosidase
GDI	GDP dissociation inhibitor 1

GFP	Green fluorescent protein
GTP	Guanosine triphosphate
GWAS	Genome-wide association studies
HIP	Haploinsufficiency profiling
HOP	Homozygous profiling
HTS	High-throughput screen
iPSC	Induced pluripotent stem cells
IPTG	Isopropyl β-D-1-thiogalactopyranoside
LB	Luria-Bertani broth
LiAc	Lithium acetate
LIMP2	Lysosomal integral membrane protein 2
LRRK2	Leucine-rich repeat kinase 2
MAP	Mitogen-activated protein
MPTP	1-methyl-4-phenyl-1,2,3,6-tetrahydropyridine
MST	Microscale thermophoresis
Ni-NTA	Nickel-nitriloacetic acid

NSF	N-ethylmaleimide sensitive factor
NTA	Nitriloacetic acid
OD	Optical density
ORF	Open reading frame
PBS	Phosphate-buffered saline
PD	Parkinson’s disease
PEG	Polyethylene glycol 3500
Pgk1	Phosphoglycerate kinase 1
PINK1	PTEN-induced kinase 1
PVDF	Polyvinylidene difluoride
SDS	Sodium dodecyl sulphate
SDS-PAGE	Sodium dodecyl sulphate-polyacrylamide gel electrophoresis
SN	Substantia nigra
SNARE	Soluble NSF attachment protein receptor
SNpc	Substantia nigra pars compacta
Snc1	Suppressor of npr1-1

TBS	Tris-buffered saline
TBST	Tris-buffered saline with Tween
TEMED	Tetramethylethylenediamine
TRIM	Tripartite motif-containing
VPS35	Vacuolar protein sorting 35

INTRODUCTION

Genetic Causes of Parkinson's Disease

Parkinson's Disease Overview

Parkinson's disease (PD) is a neurodegenerative disorder that is most prevalent in the elderly, affecting 1-2% of people over the age of 60 and up to 5% for those over 85 years of age (Islam & Moore, 2017). PD is characterized by symptoms including rigidity, bradykinesia, postural instability, and resting tremor. These symptoms are primarily due to loss of dopaminergic neurons in the substantia nigra (SN), an area of the brain critical to executing motor control. Current therapies address symptomatic control; there is currently no therapeutic intervention that prevents neurodegeneration in PD patients.

First-line treatments for PD center on dopamine replacement. The precursor molecule L-3,4-dihydroxyphenylalanine (e.g. L-dopa or levodopa) is usually paired with a peripheral dopamine decarboxylase inhibitor (e.g. carbidopa) or a catechol-o-methyltransferase (COMT) inhibitor (e.g. entacapone), to prevent degradation of L-dopa before it crosses the blood-brain barrier (**Figure 1**). Dopamine agonists that bind and activate dopamine receptors (e.g. pramipexole, ropinirole, bromocriptine, rotigotine) may also be employed (Stayte & Vissel, 2014). Lastly, anticholinergic options (e.g. trihexyphenidyl, benztropine) and monoamine oxidase B inhibitors (e.g. selegiline and rasagiline) have also

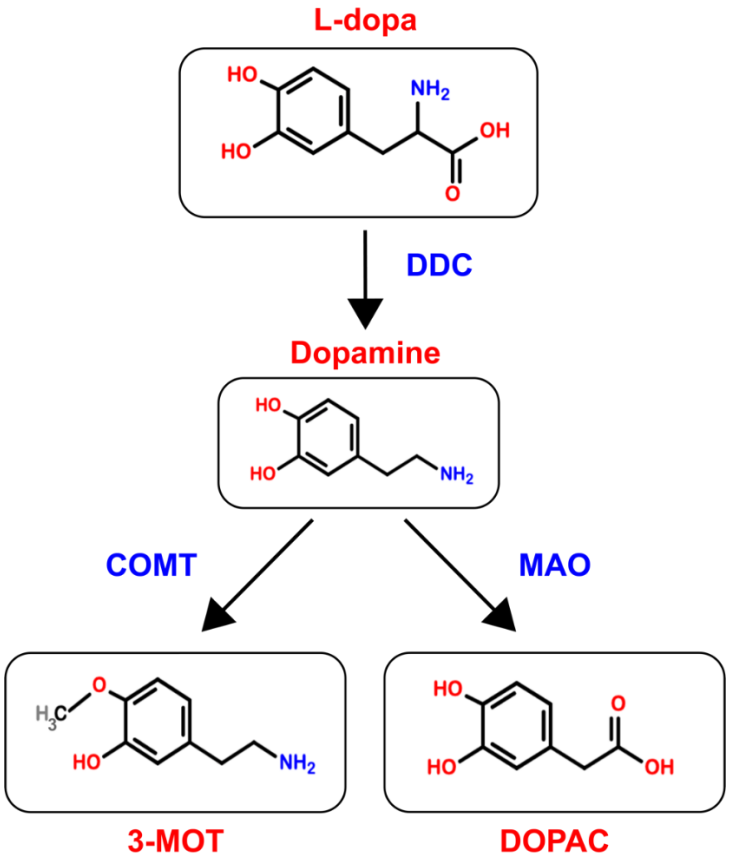

Figure 1. Dopamine biosynthetic pathway.

Dopamine is produced from the decarboxylation of L-dopa by DOPA decarboxylase (DDC). Dopamine can be broken down by catechol-O-methyltransferase (COMT) or by monoamine oxidase (MAO).

been indicated for use in PD (Stayte & Vissel, 2014). All of these therapeutics work to correct the imbalance in neurotransmitters as a result of the loss of neurons in the substantia nigra, however they do not stop or reverse dopaminergic neurodegeneration. At first diagnosis of PD, it is estimated that 50-80% of substantia nigra pars reticulata (SNpc) dopaminergic neurons have already been lost, with remaining neurons regularly displaying Lewy body pathology - aggregates containing the protein α-synuclein often observed in PD brains (Gómez-Benito et al., 2020). How exactly Lewy bodies may result in cell death remains an active area of research.

Inherited Forms of Parkinson's Disease

Most PD cases are idiopathic, however 5-10% have a clear genetic association (Islam & Moore, 2017). The first identified genetic link was discovered in 1997 for the gene *SNCA* (encoding α-synuclein) (Polymeropoulos et al., 1997) identifying duplication/triplication of *SNCA* segregating with early onset PD (Singleton et al., 2003). Since then, over 20 genes (via genome-wide association studies for idiopathic PD or direct single gene phenotype-genotype relationships for inherited PD) have been found that may predispose, or directly cause, people to develop PD (Abeliovich & Gitler, 2016). The most common inherited disease-causing gene for PD are rare variants in *LRRK2*. Interestingly, *LRRK2*, and indeed many of the genes that can cause inherited PD, function in

various steps of intracellular trafficking (**Figure 2**) implying that PD may be due to an inability of neurons to properly sort, import, or secrete vesicles required for neuronal function and/or survival.

SNCA Mediated Parkinson's Disease

SNCA encodes the protein α-synuclein, a major component of Lewy bodies whose aggregation is thought to be a pathogenic event for PD. α-synuclein is abundantly expressed in presynaptic terminals in the central nervous system (CNS) (Usmani et al., 2021). Its precise function is still unclear, but it is believed to play a role in synaptic vesicle recycling, with evidence suggesting a role in maintaining soluble N-ethylmaleimide-sensitive factor (NSF) attachment protein receptor (SNARE) architecture (Benskey et al., 2016; Huang et al., 2019). α-synuclein, a small protein of only 140 amino acids, displays conformational plasticity with a dynamic equilibrium maintained between unfolded monomers and α-helically folded tetramers (Nuber et al., 2018). α-synuclein is intrinsically disordered and forms a partial α-helix upon interaction with membranes through an amphipathic motif at its N-terminus (Gómez-Benito et al., 2020). The ability of α-synuclein to contribute to the formation of Lewy bodies is due to its ability to form soluble pre-fibrillar oligomers, leading to insoluble fibrillar aggregates with cross β-sheet formation and Lewy body formation (Mehra et al., 2019). The process(es) that predispose α-synuclein to the formation of insoluble aggregates

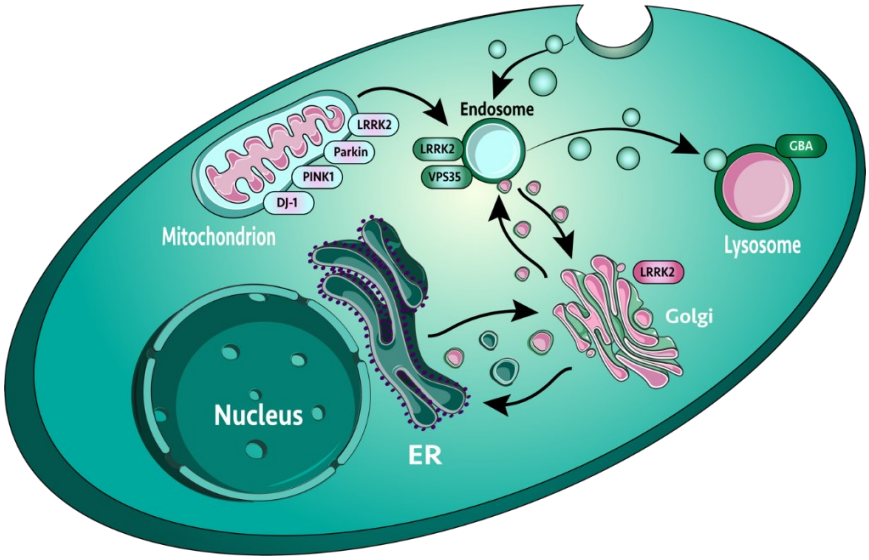

Figure 2. Role of proteins whose genes predispose to Parkinson's disease.

Several genetic rare variants have been linked to the development of PD. The association of PD with *GBA1*, encoding for glucocerebrosidase, has been speculated to be due to perturbed localization or stabilization of α-synuclein, the aggregating protein accumulating in PD patients. PINK1 and Parkin, as a kinase and E3 ubiquitin ligase pair, leads to mitophagy and energy depletion. Rare variant alleles of *VPS35*, a component of retromer, disrupt trafficking to the lysosome. The exact association of PD with DJ1, a molecular chaperone with many interactions, is unclear. Rare variants of *LRRK2,* encoding a large protein with a kinase and GTPase domain, represent the majority of genetic inheritance of PD. LRRK2 function regulates membrane trafficking and mitochondrial activity, with the precise mechanism yet to be determined.

is unclear. PD predisposing variants are either *SNCA* missense mutations or duplication/triplication of the *SNCA* gene (Usmani et al., 2021). The point mutations A53T/V, E46K and H50Q have been shown to increase SNCA fibrillation, although this has only been observed in vitro (Mehra et al., 2019). Larger fibril aggregates can “spread” in a prion-like fashion based on experiments in tissue culture where cells overexpressing α-synuclein secrete exosomes that contain α-synuclein which can transfect neighbouring cells and co-aggregate with native α-synuclein (Bae et al., 2015). It is thought that α-synuclein PD causing variants, and/or increased *SNCA* dose, may promote α-synuclein aggregation due to impaired vesicular trafficking of α-synuclein into lysosomes, implicating another PD predisposing gene, *GBA1*, in a shared process.

Parkinson’s Disease Due to GBA Variants

Patients with PD *GBA1* variants often display an increased level of α-synuclein aggregation. *GBA1* encodes the lysosomal enzyme glucocerebrosidase, or GCase, which hydrolyzes glucose moieties from the glycosphingolipids glucocerebroside and glucosylsphingosine (Blumenreich et al., 2020). A role for *GBA1* in human disease was first determined due to variants in *GBA1* being identified as causal for the rare autosomal dominant lipid storage disorder Gaucher disease. Fourteen years ago, it was discovered that Gaucher

disease patients and their relatives had 25% incidence of PD (Behl et al., 2021). Variants in *GBA1* have been identified that preferentially segregate with PD, with 130 variants identified to date. The *GBA1* encoded GCase is a 497 amino acid protein synthesized in the ER, glycosylated in the Golgi, and trafficked to lysosomes by a LIMP2-dependent pathway where its enzymatic activity is activated by the acidic environment of the lysosome (Do et al., 2019). PD associated *GBA1* variants have been demonstrated to have reduced enzymatic function, are mistrafficked and do not end up in the lysosome, or are degraded due to improper folding of the GCase protein (Gündner et al., 2019). How loss of GCase localization or enzymatic activity results in increased α-synuclein aggregation is still unclear. One hypothesis is that GCase and α-synuclein can directly interact at the pH (pH 5.5) found in lysosomes (Yap et al., 2011). Using fluorescence and NMR spectroscopy, the C-terminus of α-synuclein interacted with three His residues in the GCase C-terminal β sheet domain adjacent to the GCase active site (Mazzulli et al., 2011). It was suggested that the interaction of α-synuclein with GCase promotes lysosomal degradation of α-synuclein. However, evidence for this α-synuclein-GCase interaction only exists in vitro. Very little is known regarding the proposed GCase-α-synuclein complex in cells and how it could then affect α-synuclein stability and aggregation.

A second link between GCase function and α-synuclein stability was the observation that the GCase substrate glucosylceramide stabilized α-synuclein oligomeric intermediates that are known to lead to the formation of α-synuclein

fibrils (Yap et al., 2011). Again, this process has only been determined to occur in vitro. It appears that trafficking and import of α-synuclein into lysosomes is required to maintain normal α-synuclein level and prevent its aggregation, although how this is regulated and the precise mechanism by which GCase contributes to the maintenance of α-synuclein stability requires further research.

The lysosome is no longer thought of as just an organelle that degrades excess cellular material, the cell's garbage disposal unit. The lysosome is now recognized as an organelle interconnected with the cell via vesicular trafficking pathways and is required to monitor nutrient status and to recycle cellular nutrients and macromolecules (due to it containing more than 60 acidic hydrolases, such as the *GBA1*-encoded GCase). This role for the lysosome is most obvious during autophagy, the orderly degradation and recycling of cellular components, as well as the removal of dysfunctional components, both of which require vesicular trafficking machinery.

VPS35 Variants as a Cause of Parkinson's Disease

VPS35 is a component of the cellular vesicular trafficking machinery and *VPS35* variants were identified as predisposing for PD in 2008 (Vilariño-Güell et al., 2011). VPS35 is a subunit of the vesicle coat of the retromer complex, a heterotrimeric complex of VPS35 along with VPS26 and VPS29 (Usmani et al., 2021). The retromer complex functions in vesicular transport from endosomes to

the trans-Golgi network (TGN), which in turn is critical for trafficking proteins to the lysosome via endosomes (Inoshita et al., 2017). VPS35 is 796 amino acids in length and harbours one clearly verified PD variant, D620N, resulting in autosomal dominant familial PD (Williams et al., 2017). As retromer function is essential, one possibility is that the PD-causing VPS35 variant does not affect all retromer functions, but rather only that of select cargo (Williams et al., 2017). Indeed, it was found that the *VPS35* D620N variant resulted in the mistrafficking of a protein required for autophagy induction, ATG9. ATG9 normally moves between the trans-Golgi network, the plasma membrane, and recycling endosomes. However, in VPS35 D620N expressing cells ATG9 was trapped in a perinuclear location and was unable to traffic to autophagic structures. Interestingly, defective ATG9 trafficking was also observed in cells in which *SCNA* encoded α-synuclein was over-expressed. The ability of cells to recycle and/or dispose of components through the lysosome (including autophagy) is beginning to emerge as a common theme linking PD causing genes (Lin et al., 2019; Tang et al., 2015).

Defective PINK1 and PARK2 Imply a Mitochondrial Role in Parkinson's Disease

Two genes where rare variants have been observed to cause PD in a homozygous or compound heterozygous (recessive) manner are *PINK1* and *PARK2* (also referred to as *PRKN* and most often referred to as *Parkin*). *PINK1*

encodes a protein kinase and Parkin is a E3 ubiquitin ligase (Malpartida et al., 2020; Sekine, 2020; Yoboue & Valente, 2020). *PINK1* and *Parkin* are often discussed in tandem, given their intertwined roles (Abeliovich & Gitler, 2016). PINK1 and Parkin function to remove damaged mitochondria via mitophagy, the selective degradation of mitochondria via lysosome mediated autophagy. *PINK1* is a nucleus-encoded mitochondrial kinase that is translated with a mitochondrial targeting sequence, which allows it to translocate across the mitochondrial outer membrane (MOM) and subsequently the mitochondrial inner membrane (MIM). The targeting sequence is cleaved upon entry into the mitochondria and the 63 kDa PINK1 is processed into its 52 kDa active form (Yoboue & Valente, 2020). In healthy mitochondria the pool of PINK1 on the MOM is very small, however, when mitochondria are damaged (i.e. start to become depolarized) PINK1 is recruited to the MOM. At the MOM, PINK1 phosphorylates Parkin. Phosphorylation of Parkin by PINK1 recruits Parkin to the MOM and increases its enzymatic activity, resulting in the decoration of the MOM by ubiquitin chains. This positive feedback cycle tags mitochondria for degradation by mitophagy resulting in damaged mitochondrion being engulfed by autophagosomes-lysosomes for degradation consistent with lysosomal vesicular trafficking playing an important role in the genetic causes of PD.

LRRK2 Variants are the Most Common Cause of Congenital Parkinson's Disease

The most common cause of inherited PD is the result of rare variants in *LRRK2*, responsible for 5% of familial cases worldwide (Nguyen & Moore, 2017) and up to 40% of genetic PD cases attributed in African Berber and Ashkenazi Jewish patients (Berwick et al., 2019). LRRK2 is a large multi-domain protein whose function has been implicated in various vesicular trafficking pathways. The first PD-linked variant of *LRRK2* patients was identified in 2004 (Paisán-Ruíz et al., 2004; Smith et al., 2006; Zimprich et al., 2004). Several *LRRK2* missense variants, all shown or predicted to increase LRRK2 kinase activity, have been identified in inherited PD patients (Erb & Moore, 2020; Nalls et al., 2014). Increased levels of LRRK2 protein have also been identified in the brains of some patients with idiopathic PD, implying that increased kinase activity of LRRK2 could cause PD.

The identification of small molecules that can inhibit the function of a major regulator of LRRK2, ArfGAP1, is the major subject of this thesis work. A more in-depth description of LRRK2 and ArfGAP1 structure and function, followed by their proposed roles in PD, is below.

LRRK2 Structure, Function, and Biology

LRRK2 Domain Organization and Enzyme Activity

LRRK2 is a large multi-domain protein comprised of 2527 amino acids (MWt of 280 kDa) that can form homodimers. At its N- and C-termini are domains involved in protein-protein interactions while the central region of the protein contains two enzymatic motifs (**Figure 3**). At the N-terminus are an armadillo domain, ankyrin repeats, and a leucine-rich repeat region while at the C-terminus there is a string of WD40 repeats. The two central enzymatic domains of LRRK2 are a GTPase and a protein kinase domain separate by a COR (C-terminus of Roc) region (Alessi & Sammler, 2018). Most of the prevalent variants that cause inherited PD are found in the GTPase and kinase domains. Of the known *LRRK2* pathogenic variants, two are found in the kinase domain: G2019S (the most common *LRRK2* PD disease causing variant) and I2020T (Berwick et al., 2019). The GTPase domain of LRRK2 has similarity to the Ras of complex (RoC) GTPase domain. Similar to small monomeric GTPases of the Ras superfamily, the GTPase domain of LRRK2 is capable of binding GTP and hydrolyzing it to GDP at a low level (Bosgraaf & Van Haastert, 2003). There are seven prevalent PD variants in the LRRK2 GTPase and COR domains: N1437H, R1441C/H/G, R1629P, and Y1699C/G.

Several interesting features of the LRRK2 kinase domain have been determined. The activation loop contains a DYG motif rather than the normal DFG motif found in most kinases (Schmidt et al. 2019). The Tyr within the

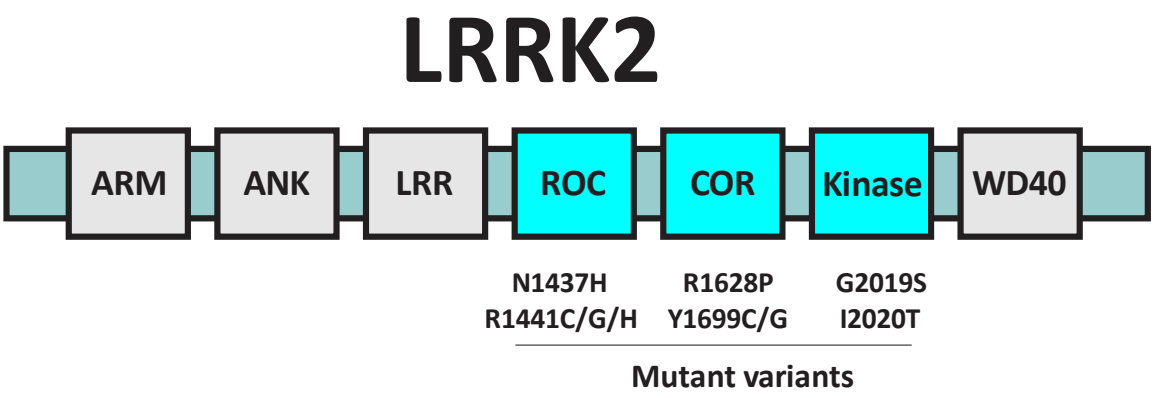

Figure 3. Domain structure of human LRRK2.

The armadillo (ARM), ankyrin (ANK), leucine-rich region (LRR), and WD40 domains are involved in protein-protein interactions. The majority of PD causing variants are located within the kinase domain, a Ras of complex proteins (ROC) GTPase domain, or the COR (C-terminus of Roc) region.

LRRK2 DYG motif works as a brake by decreasing substrate access and favoring an inactive kinase at resting state. Mutating the Tyr residue to a Phe in the DYG/DFG kinase site motif results in a LRRK2 with increased kinase activity. In general, LRRK2 prefers to phosphorylate Thr resides versus Ser residues in vitro and in vivo.

The LRRK2 GTPase domain uses a standard phosphate binding P-loop motif to bind GTP and GDP (Myasnikov et al., 2021). GTP binding by LRRK2 appears to be necessary to activate its kinase activity (Stafa et al., 2012). Point mutations that result in a form of LRRK2 that cannot bind GTP results in a LRRK2 that has no kinase activity. This crosstalk between the kinase and GTPase domains of LRRK2 appears to be modulated via two mechanisms: intramolecular interactions and LRRK2 homodimerization. LRRK2 dimerizes via interactions between the COR domain and the C-terminal WD40 domains. Cryo-electron tomography revealed a J-like structure that facilitated intramolecular interactions in which the COR and GTPase domains turn back toward the kinase domain enabling the kinase and GTPase domains to closely interact and thus are proposed to modulate the activity of each other (Sejwal et al., 2017).

Cellular substrates for LRRK2 include an autophosphorylation site on LRRK2 at S1292 and several Rab proteins (Sheng et al., 2012). All characterized PD-causing LRRK2 variants increase the kinase activity of LRRK2 (Reynolds et al., 2014). PD-causing variants in the kinase domain, G2019S and I2020T, increase resting state catalytic activity. The N1437H variant appears to be unique

in that it appears to lock LRRK2 into a GTP-bound state by stabilizing a dimerized form of LRRK2 that has increased affinity for GTP (Huang et al., 2019).

The increased kinase activity in familial forms of PD, coupled with increased levels of LRRK2 protein observed in some idiopathic PD patients, prompted the search for LRRK2 kinase inhibitors as a potential treatment for PD. Highly selective LRRK2 active site kinase inhibitors that occupy the ATP binding pocket (DYG motif region) were synthesized by several pharmaceutical companies (Zhao & Dzamko, 2019). Treatment of animal models from mice to nonhuman primates resulted in several issues including kidney and lung pathologies similar to those observed in *LRRK2* knockout mice (Tolosa et al., 2020). Interestingly, all of these LRRK2 kinase inhibitors resulted in LRRK2 being localized to microtubules where it was ubiquitinated and degraded by the proteasomal system. Thus, it is unclear if the systemic issues due to administration of these LRRK2 kinase inhibitors are due to LRRK2 kinase inhibition itself or decreased LRRK2 protein level. Differentiation of these mechanisms could result in potential new LRRK2 inhibitor kinase designs if it can be proven that kinase inhibition itself can ameliorate LRRK2-mediated PD.

LRRK2 Subcellular Location and Cell Biological Roles

In cell models, LRRK2 has been localized in the cytoplasm and at numerous vesicular membranes (e.g. Golgi, multivesicular bodies and autophagic vesicles).

Biologically active LRRK2 is thought to be at membranes as well as the cytoskeleton. LRRK2 has been implicated in processes related to vesicular trafficking including endocytosis, autophagy, and lysosomal function (Alessi & Sammler, 2018). LRRK2 has also been found to directly bind tubulin raising the possibility that LRRK2 dysfunction may impair transport along microtubules (Deniston et al., 2020).

Membrane bound LRRK2 can phosphorylate members of the Rab small GTPase family of proteins (Tang, 2017). A family of over 60 Rabs is known with most serving as regulators of membrane trafficking via their GTP-bound membrane state and GDP-bound cytoplasmic state. LRRK2 has been determined to phosphorylate conserved Thr/Ser residues on 16 different Rab proteins in the switch II effector domain resulting in disruption of Rab binding to Rab GDP dissociation inhibitors (GDIs) causing Rabs to preferentially bind GTP and associate with membranes (Steger et al., 2016). The best-studied LRRK2-Rab interaction is with Rab29 (Erb & Moore, 2020). Beyond Rab29 being a substrate for LRRK2 phosphorylation for activation of Rab29 membrane trafficking function, Rab29 can also activate LRRK2 function. Rab29 appears to activate LRRK2 by recruiting LRRK2 to the trans-Golgi (MacLeod et al., 2013). Increased localization of LRRK2 to the trans-Golgi results in Golgi fragmentation, and this is enhanced by the PD causing G2019S LRRK2 variant. Interestingly, *RAB29* is located within the *PARK16* locus identified has a high-risk region for the development of PD in idiopathic PD patients (Tang, 2017).

At the trans-Golgi LRRK2 appears to have a role in retromer function (Erb & Moore, 2020). The retromer complex recycles membrane proteins from endosomes to the trans-Golgi to enable further rounds of secretion from the trans-Golgi. The retromer core is comprised of cargo-binding vacuolar protein sorting proteins VPS35, VPS29, and VPS26. As noted earlier in this thesis, rare variants in *VPS35* cause inherited PD suggesting that defective retromer function may drive PD. A connection between LRRK2, Rab29, and VPS35 is beginning to emerge. Increased expression of VPS35 can rescue trans-Golgi-retromer mediated defects due to the presence of LRRK2 G2019S or Rab29 knockdown (Williams et al., 2017). However, more insight into the mechanisms by which LRRK2, VPS35, and Rab29 regulate trans-Golgi-retromer function is needed to determine how defects in the function of these proteins result in predisposition to PD.

LRRK2 also appears to regulate vesicular trafficking to the lysosome including roles in both mitophagy and autophagy. The role of LRRK2 in regulating autophagy is unclear. It is known that when lysosomal transport is inhibited LRRK2 translocates to endolysosomal membranes and the phosphorylation of the LRRK2 substrates Rab10 and Rab8a is increased (Gitler et al., 2008; Ito et al., 2016). The phosphorylation of these Rab proteins is thought to be a compensatory effect in an attempt by the cell to prevent defective lysosomal transport. Mitophagy, the transport of defective mitochondria to lysosomes for their destruction, uses some of the same vesicular trafficking components as autophagy. The full role of LRRK2 in the regulation of mitophagy

is still being explored but evidence suggests its role in mitophagy is kinase dependent (Malpartida et al., 2020). LRRK2 G2019S increases phosphorylation of Rab10 and inhibits mitophagy resulting in damaged mitochondria accumulation. Recently it was shown that the LRRK2 kinase substrate Rab10 is driven to the mitochondria by PINK1 and Parkin, whose gene variants also cause inherited PD (Wauters et al. 2020). A kinase-dependent role for LRRK2 has also been implicated in mitochondrial tethering to the ER via ER-mitochondria contact sites (Yoboue & Valente, 2020). It has been demonstrated that LRRK2 can interact with the mitochondrial outer membrane protein Miro, with PD causing LRRK2 G2019S preventing proteasomal degradation of Miro decreasing the ability of a cell to perform mitophagy resulting in an accumulation of damaged mitochondria (Yoboue & Valente, 2020).

Beyond LRRK2 translocation to membranes, LRRK2 can also bind directly to microtubules (Leschziner & Reck-Peterson, 2021). A recent cryo-electron tomography structure of LRRK2 determined that it oligomerizes as a right-handed helix around microtubules, and that PD causing LRRK2 variants can form this structure at microtubules better than wild type LRRK2 (Watanabe et al., 2020). Microtubule association of pathogenic LRRK2 variants was disrupted by active site kinase inhibitors and by GTP binding site inhibitors demonstrating that both kinase and GTPase functions of LRRK2 mediate microtubule binding. LRRK2 bound to microtubules is regulated by the ubiquitin E3 ligase TRIM1 (Stormo et al., 2020). TRIM interacts with microtubule-bound LRRK2 and causes its ubiquitination and degradation by the proteasome, whereas knockdown of

TRIM1 can rescue neurite survival outgrowth due to overexpression of LRRK2 G2019S. LRRK2 binding to microtubules, and how this fits with the role of LRRK2 in regulating various membrane trafficking pathways, is unclear but intriguing.

A Role for LRRK2 in Neurons and Inherited Parkinson's Disease

How LRRK2 PD causing variants interfere with dopaminergic neuron function and eventually cause death for neurons of the substantia nigra is not clear. However, it is known that endolysosomal, mitochondrial, and cytoskeletal functions are in high demand in neurons. Dopaminergic neurons have a high energy requirement and their widely branched, long, and unmyelinated axons require exquisite control of microtubule and endolysosomal functions (Hang et al., 2015). If energy requirements are not sufficient, oxidative stress and other stressors that disrupt mitochondrial activity appear to be particularly damaging to substantia nigra neurons. The necessity of LRRK2 in the regulation of damaged mitochondrial removal via mitophagy, and LRRK2 PD causing variants decreasing damaged mitochondrial turnover, could be one process that contributes to preferential loss of substantia nigra neurons.

Highly branched and long dopaminergic neurons require robust microtubule and vesicular trafficking activity, and a role for LRRK2 in their function has been explored via its regulation of endolysosomal vesicular trafficking and its intersection with synaptic vesicle fusion. Recent work

determined that LRRK2 can phosphorylate endophilin A, synaptojanin, and auxilin in various models (Vidyadhara et al., 2019). For example, in *Drosophila* expression of human LRRK2-G2019S increases phosphorylation of endophilin A and this inhibited synaptic vesicle endocytosis (Matta et al., 2012). In human iPSC models of LRRK2 PD-causing variants abnormal synaptic vesicle endocytosis was also observed, along with the accumulation of neurotoxic oxidized dopamine, potentially helping to explain the selective neurotoxicity of PD causing versions of LRRK2 for neurons of the substantia nigra (Li et al., 2018).

Much progress has been made in understanding the functions of LRRK2 in general and in dopaminergic neurons in particular. However, more work is required to determine how altered LRRK2 function leads to PD pathogenesis. Phosphorylation of Rab proteins by LRRK2 to regulate numerous aspects of vesicular trafficking is clear. However, roles of the numerous Rab substrates upon phosphorylation by LRRK2 have yet to be elucidated, and how these could be altered by the multiple disease-causing variants of LRRK2 is also not clear. The co-regulation of vesicular trafficking with microtubule dynamics by LRRK2 PD causing also requires further elucidation. Finally, the intersection of LRRK2 with the other PD causing variants in other genes requires further exploration and explanation.

A LRRK2-ArfGAP1 Connection in Parkinson's Disease

A Yeast Genetics Screen Determines that Loss of ArfGAP1 Activity Decreases LRRK2 Toxicity

The first link between LRRK2 and the GTPase ArfGAP1 was from studies performed in yeast cells (Xiong et al., 2010). It was found that expression of the region of human LRRK2 containing the GTPase and protein kinase domains resulted in a decrease in yeast cell growth. The expression of full-length human LRRK2 was unable to recapitulate this phenotype as it was found to localize to insoluble cytoplasmic inclusion bodies.

To identify modifiers of human LRRK2 (GTPase and protein kinase domains) inhibition of yeast cell growth, a high-throughput screen against the non-essential yeast gene deletion set was performed. Specifically, a human LRRK2 GTPase-kinase region expressing yeast query strain was crossed to a collection of 4,800 yeast strains each with an individual non-essential yeast gene genetically inactivated. Scoring the strains for alterations to the growth defect due to LRRK2 GTPase-kinase expression led to identification of nine 'hit' yeast genes, two of which increased toxicity and seven which mitigated the growth defect. Of the seven gene-knockout strains that prevented LRRK2 mediated toxicity in yeast, two have human homologs: Slt2, a MAP kinase in the protein kinase C signalling pathway, and Gcs1, an ADP-ribosylation factor GTPase activating protein 1 (ArfGAP1) that functions in transport to and from the Golgi.

Since LRRK2 contains a GTPase domain, it was postulated that an active Gcs1 may promote toxicity by increasing the GTPase activity of LRRK2.

Human Cell Culture Experiments and In Vitro Assays Further Validate a Role for ArfGAP1 in the Regulation of LRRK2 Activity

To support the hypothesis that ArfGAP1 increases LRRK2 GTPase activity, subsequent studies determined that in HEK293 cells human ArfGAP1 and LRRK2 co-localized and co-immunoprecipitated (Stafa et al., 2012). The same study also showed that purified ArfGAP1 increased GAP activity for the GTPase domain of purified LRRK2 in vitro, and ArfGAP1 also increased the kinase activity of LRRK2 in vitro. Additionally, it was determined that ArfGAP1 is required for LRRK2 toxicity in cultured primary neurons, as siRNA knockdown of ArfGAP1 mitigated the neurite-shortening and cell death phenotypes observed upon expression of PD-causing LRRK2-G2019S. Taken together, these results are consistent with the theory that ArfGAP1 promotes LRRK2 toxicity by activating its GTPase domain, which in turn increases LRRK protein phosphorylation activity by the kinase domain. Inhibition of ArfGAP1 may be a useful strategy to prevent LRRK2-mediated PD.

ArfGAP1 Structure and Proposed Functions

ArfGAP1 Structure and Function

ArfGAP1 is a member of a larger family of ArfGAP proteins (Cukierman et al., 1995). There is little research on ArfGAP1 and its role in cell and organismal biology and much needs to be learned.

ArfGAP1 has two other members in its subfamily, ArfGAP2 and ArfGAP3. ArfGAP1 is 45 kDa in size and contains a GAP domain at its N-terminus which comprises the first 130 amino acids of the protein. The GAP domain contains a Zn^{2+}-binding motif and an invariant arginine in a motif characteristic of GAP domains (CxxC...CxxC...R) (Kahn et al., 2008) (**Figure 4**). The Zn^{2+}-binding motif plays a structural role, positioning the arginine finger that in turn stabilizes the transition state during ArfGAP1 mediated hydrolysis of GTP to GDP (Spang, Shiba, and Randazzo 2010).The C-terminus of ArfGAP1 is largely unstructured aside from two amphipathic lipid packing sensing (ALPS) motifs that fold into helices to enable interaction with highly curved membranes (Bigay et al., 2005). ArfGAP1 is the only member of the ArfGAP family to contain an ALPS motif. The two ALPS motifs increase binding of ArfGAP1 to smaller (endosome-sized) vesicles and the binding of ArfGAP1 to highly curved membranes increases its ArfGAP1 enzymatic activity (Drin et al., 2009). The best characterized substrate for ArfGAP1 is the small GTPase ADP-ribosylation factor 1 (Arf1), although LRRK2 has also been determined to be a direct substrate for ArfGAP1.

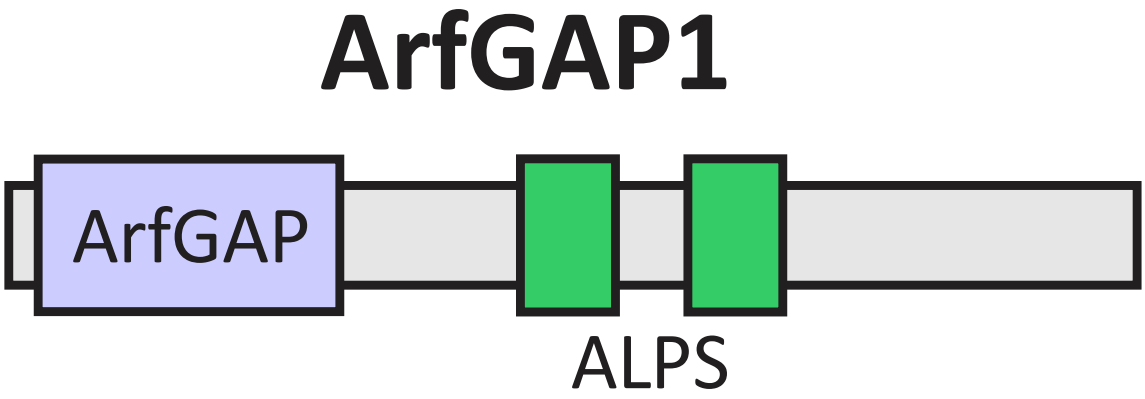

Figure 4. Domain structure of human ArfGAP1.

An ArfGAP domain, which activates GTPase activity in select proteins, is present in all ArfGAP proteins. Amphipathic Lipid Packing Sensor Domains (green boxes) target protein localization to highly curved membranes increasing the enzymatic activity of the ArfGAP domain.

Proposed Cell Biological Roles for ArfGAP1

Arf proteins, key regulators in the trafficking of material intracellularly, are members of the Ras superfamily of small monomeric GTPases. Arfs bind GTP in the “active” form and have innate, albeit low, ability to hydrolyze GTP to GDP to transition to an “inactive” form. Humans have five Arfs divided into three groups, all localized to different sites in the cell (Kahn et al., 2008). The best characterized is Arf1 and its role at the cis-Golgi. GTP-bound Arf1 localizes to Golgi membrane and recruits a complex of coatomer proteins for the COPI coat of a vesicle destined for retrograde transport to the ER (Drin et al., 2009). Retrograde transport primarily serves to recycle vesicular trafficking machinery from the Golgi to the ER to enable further rounds of vesicular trafficking between these two organelles. Arf1, typical of members of the Ras family, requires an activating protein to aid in the hydrolysis of GTP. After the initiation of COPI coat polymerization to enable vesicle budding, ArfGAP1 hydrolyzes Arf-bound GTP to GDP and Arf then dissociates from the budding vesicle. ArfGAP1 may regulate COP1 vesicle coat polymerization in a cargo-dependent manner. For example, the cargo protein p24 inhibits ArfGAP1 activity. In the absence of this cargo protein, Arf1-ArfGAP1 will hydrolyze GTP, preventing formation of an empty vesicle. Interestingly, the three ArfGAP1 subfamily members all increase GTP hydrolysis by Arf1 and thus may have overlapping functions at the Golgi in their regulation of COPI function.

In addition to retrograde transport from the cis-Golgi to the ER via regulation of assembly of the coat protein complex COPI, ArfGAP1 has been determined to function in endocytosis to the trans-Golgi via the clathrin-AP2 (adapter protein 2) coat complex (Bai et al., 2011). Depletion of ArfGAP1 by siRNA prevents endocytosis of select cargo from the plasma membrane (e.g. the transferrin receptor but not the EGF or LDL receptors). ArfGAP1 was demonstrated to directly interact with AP-2 as well as internalization/sorting signals on the transferrin receptor itself. Thus, ArfGAP1 is required for endocytosis of select cargo by directly binding to cargo and AP-2. Similar to what was observed in COPI trafficking, ArfGAP enzymatic activity was required for ArfGAP1 to promote AP-2 dependent endocytosis implying an Arf substrate in this process. Human Arf6 was known to be required for AP-2 dependent endocytosis and Arf6 was determined to be a substrate for ArfGAP1. It is not known if other ArfGAPs also participate in the regulation of AP-2 dependent plasma membrane-derived endocytosis. ArfGAP1 regulation of plasma membrane-derived vesicular trafficking was independent of its regulation of Golgi-derived vesicular trafficking.

A recent study determined that ArfGAP1 can interact directly with mammalian target of rapamycin complex 1 (mTORC1) (Meng et al., 2021). mTORC is a master regulator of cellular nutrient status via an amino acid sensing process. Amino acid accumulation promotes mTORC1 localization, via vesicular trafficking, to lysosomes. Interaction of mTORC1 with ArfGAP1 prevents mTORC1 lysosomal localization, with the ALPS motif of ArfGAP1 required for

this interaction. Interestingly, the GAP activity of ArfGAP1 does not appear to be required to promote mTORC1 lysosomal localization. This directly links ArfGAP1 function with cellular nutrient status sensing via the endolysosomal system in a manner independent of its ArfGAP1 enzymatic activity.

Unanswered questions regarding the role of ArfGAP1 in vesicular trafficking include determining the full range of substrates for ArfGAP1, and the overlapping versus specific functions for each ArfGAP family member. For ArfGAP1, roles in regulating vesicular trafficking involving the Golgi, the plasma membrane, and the lysosome have been determined but it is not known if this represents the entirety of its function. The non-GAP mediated regulation of mTORC1 vesicular trafficking to the lysosome has recently been determined and requires further research. It is also clear that LRRK2 is a substrate for ArfGAP1, and that inhibition of ArfGAP1 function can prevent LRRK2 mediated cellular toxicity; it is unclear how ArfGAP1 does so.

Model Organisms and their Capacity to Increase the Understanding of Inherited Diseases

Overview of Inherited Disease and the Use of Model Organisms for their Study

It is predicted that there are ~7,000 single-gene inherited disorders, with disease-causing variants in over 5,500 causal genes identified thus far (Online Mendelian Inheritance in Man (OMIM)). For human inherited disease discovery,

pedigrees aid in determining if a potential gene variation causes the disease, especially if genes within the same pathway are known to cause the same, or a similar, disease. In cases where the genotype-phenotype connection is unknown or unclear, model organisms have served a critical role in determining if identified gene variants can affect the function of the encoded protein at the subcellular, cellular, and organismal level (Lehner, 2013).

Inherited disease research has mainly focused on identifying causal variants(s) in affected individuals. These diagnostic efforts are important and ongoing, with model organisms having an instrumental role in validating genotype with phenotype (Foley, 2015; Lehner, 2013). However, 95% of inherited diseases have no effective treatment (Boycott et al., 2014; Dodge et al., 2011). Model organism researchers can also apply genetic and chemical-genetic approaches to determine novel human disease-specific genotype-phenotype correlations with the aim of identifying novel drug targets, and drugs/drug-like molecules, as a starting point toward increasing treatment options for patients with genetic diseases.

Model organisms ranging from *Saccharomyces cerevisiae* (yeast) to *Caenorhabditis elegans* (worm), to *Drosophila melanogaster* (fly), to *Danio rerio* (zebrafish) to *Mus musculus* (mouse) are important and useful tools to determine gene function, delineate genotype-phenotype correlations, and identify potential therapeutic avenues for genetic diseases (Guernsey et al., 2009, 2011; Lehner, 2013). The genomes of all of these organisms have been sequenced, increasing their usefulness in the study of genetic disease.

Yeast are single-celled eukaryotes that allow for relatively quick genome-wide genetic and chemical genetic analysis. Much of the functionality of yeast genetics is due to the ability of yeast to grow as both haploid and diploid cells, enabling second-site mutations to be introduced into diploid cells in a heterozygous state and subsequently testing the effect by isolating haploid cells with both the causal mutation and the second-site mutation (Boone et al., 2007; Costanzo et al., 2010, 2016; Enserink, 2012; Hillenmeyer et al., 2008; van Leeuwen et al., 2016). However, as a single-celled organism, yeast do not offer insights into differentiated cell types and whole organs.

The short life cycle and transparency of *C. elegans*, coupled with assays that rely on fluorescence and observable defects in cellular function, make it ideal for organismal analysis. The fact that all 302 of its neurons have been precisely mapped is also a major attraction of this model (Hobert, 2016; Lemieux & Ashrafi, 2015). However, of the multi-cellular models, *C. elegans* has fewer mammalian homologs and is missing key organs present in fly, zebrafish, and mouse models (*e.g.* no heart and no centralized brain).

Drosophila is an efficient, well-defined genetic model organism. Overall protein sequence homology between the fly and mammals is 40%, with 80-90% homology in conserved domains (Ugur et al., 2016). Furthermore, 75% of genes associated with human disease have functional orthologs in the fly. A wide range of genetic tools developed for the fly can be applied to the study of genetic disease including the Gal4/UAS system, CRISPR technology, and transgenic approaches (Millburn et al., 2016). The fly also offers opportunities for rapid

phenotypic screening such as locomotion and behavior (Boutros et al., 2004; Jaiswal et al., 2012).

Zebrafish represents a powerful model system for studying genetic disease (Howe et al., 2017). Zebrafish have a high level of genetic conservation with humans, 71% of human proteins have a clear zebrafish homologue and 82% of all human disease-causing genes have a zebrafish homologue (Howe et al., 2017). Conservation extends genomically to syntenic regions that have been preserved through evolution from fish to man (Woods et al., 2000). In addition, as a vertebrate, zebrafish provides substantial genetic complexity over simpler model organisms. Zebrafish are closer to humans in genetic homology compared to flies and have many organs similar to mammals. This latter feature is important for establishing functional significance as well as for evaluating drug metabolism and toxicity. Higher order models such as mouse or rat can serve as a critical segue between preliminary investigations performed in simpler organisms. As their genetic manipulation is much more complex, expensive, and time-consuming, their use is often reserved for deep phenotyping of inherited disease once a clear genotype-phenotype relationship for a gene variant has been determined from studies in other model organisms (Zon, 2016).

Animal Models of *LRRK2* Mediated Parkinson's Disease

Pros and Cons of Inherited Parkinson's Disease Models

A major limitation in the field of PD research is the fact that no single model of the disease recapitulates the cellular and behavioural deficiencies that are present in the human condition (Bezard & Przedborski, 2011). Cells in culture, and numerous model organisms, have all been used to further our understanding of PD. As model organisms were used in this thesis work, here I describe the various model organisms that are commonly used to study inherited PD, with a focus on *LRRK2*-mediated disease.

Inadvertently, the first animal model of PD was human. In 1982, four young and previously healthy users of illicit drugs injected heroin contaminated with 1-methyl-4-phenyl-1,2,3,6-tetrahydropyridine (MPTP) and within one week presented with symptoms of acute Parkinsonism (Langston et al., 1983). All the patients responded well to L-dopa treatment, and post-mortem analysis of the brain of one of the patients confirmed damage to the substantia nigra, albeit without the Lewy body pathology that is characteristic of PD (Langston, 2017). A primate model of MPTP followed soon after and helped establish new therapies for patients, specifically dopamine agonism (Fox & Brotchie, 2010). However, rodent models using MPTP are of limited use as rats and mice metabolize MPTP differently from primates and are less susceptible to its toxicity (Manning-Bog & Langston, 2007).

Rodent Models of LRRK2 Mediated Parkinson's Disease

The first attempts to study *LRRK2*-mediated PD in mice were through global knockout of the single mouse *Lrrk2* gene (Xu et al., 2012). Several groups did so, however there was no clear DA neurodegeneration, no obvious locomotor defects, and no altered sensitivity to MPTP-induced toxicity (Andres-Mateos et al., 2009; Ramonet et al., 2011; Y. Tong et al., 2010). Thus, it was suggested that PD *LRRK2* patient-derived mutations cause disease via a dominant gain-of-function mechanism. Many groups have generated mouse models where wild type or PD disease causing *LRRK2* alleles have been expressed, including in a neuronal specific manner. Very few of these models resulted in either loss of DA neurons or clear locomotor defects (Volta & Melrose, 2017). Only two studies have reported loss of DA neurons (20-50%) but neither resulted in locomotor defects, both of these studies over-expressed LRRK2 G2019S in neurons in mice using the *Pdgf-b* promoter (Chen et al., 2012; Chou et al., 2014). Researchers have also used viral vectors, such as AAV, injected directly into brain regions such as the substantia nigra to increase expression of human or mouse *LRRK2/Lrrk2* and PD disease causing variants. Over-expression was achieved, and in some cases resulted in 20-40% loss of DA neurons but again locomotion defects were not observed (Bae et al., 2018; Nguyen et al., 2018). It is unclear why over-expression of PD-causing *LRRK2* alleles in mice do not result in the degree of loss of DA substantia nigra observed in humans with PD,

however this may explain why there is a lack of locomotion defects observed in these mouse models.

As mouse models were unable to recapitulate the PD phenotypes observed due to the presence of PD causing *LRRK2* alleles, the rat model was explored. Similar to the mouse, inactivation of the rat *Lrrk2* gene did not result in DA neurodegeneration or locomotor defects. In addition, over-expression of human LRRK2, or the G2019S or R1441G variants, did not show signs of neurodegeneration and the rats did not develop locomotor defects (Dusonchet et al., 2011).

Rodent models of *LRRK2*-mediated PD have met with limited success when attempting to recapitulate LRRK2 mediated PD. They may be useful for assessing DA neuron loss but do not appear to be useful when determining locomotion defects and their amelioration.

Zebrafish as a LRRK2 Model of Parkinson's Disease

Danio rerio is often utilized as a vertebrate model for human disease. In addition to well-characterized neural networks and conservation of neurobiochemical mechanisms, it also has the advantage of optical transparency allowing for in vivo and real-time imaging. There is one human homologue of *LRRK2* in zebrafish, lrrk2 (Seegobin et al., 2020). Zebrafish *lrrk2* models are not well studied. From the limited studies of zebrafish *lrrk2*, two studies using morpholinos to knock down its expression reported conflicting results. One

reported loss of DA neurons and locomotion defects (Sheng et al., 2010), while the other did not observe DA neuron loss or locomotion defects (Ren et al., 2011). A more refined study generated a zebrafish *lrrk2* allelic series predicted to encode lrrk2 proteins that lacked various domains including, the kinase domain, the GTPase domains, and both of these domains (Wint & Sirotkin, 2020). All three *lrrk2* variants were viable, morphologically normal, and displayed normal locomotion. To date, the study of zebrafish *lrrk2* has not resulted in the development of a model that enables study of PD phenotypes. To that end, *D. rerio* has been used for chemically-induced models of PD. Treating fish with MPTP showed a similar deleterious effect on neurons in an area of the brain analogous to the human midbrain (where the substantia nigra is found) (Vaz et al., 2018). Subclinical doses of MPTP showed changes in mitochondrial transport along axons, before diminishment of neuron count or deficits in behaviour were observed (Dukes et al., 2016). Quantifying antero- and retrograde transport in the live animals supported the hypothesis that disruption of processes at the presynaptic terminal results in the compensatory transport of compromised mitochondria back to the cell body. Chemically induced PD in zebrafish results in similar phenotypes to those observed in primates, however, genetic models to further probe *LRRK2*-mediated disease are still in progress and have yet to yield conclusive results.

Caenorhabditis elegans as a LRRK2 Model of Parkinson's Disease

The worm *Caenorhabditis elegans* is a simple organism that lends itself well to studying neurological diseases. The 900-cell nematode's nervous system consists of 300 neurons in total, eight of which are DA neurons (Chia et al., 2020). Their short generation time and genetic tractability have also been useful in studying PD mechanisms (Dung & Thao, 2018). *C. elegan*s have most PD-causing gene loci, but not *SNCA* (α-synuclein) (Caldwell et al., 2020). Over-expression of human *LRRK2*, including the PD-disease causing alleles G2019S and R1441C, in DA neurons in *C. elegans* caused age-dependent DA loss and locomotor defects that were accompanied by a reduction in dopamine level in vivo (Saha et al., 2009). Several studies suggested that the increased expression of human *LRRK2* PD causing variants resulted in enhanced vulnerability to mitochondrial dysfunction and autophagy inhibition (Liu et al., 2011; Sämann et al., 2009; Senchuk et al., 2021). Co-expression of a GTPase-defective LRRK2 mutant prevented DA neurotoxicity and locomotor defects, as did LRRK2 kinase inhibitor small molecules (Yao et al., 2013). These studies suggest both the kinase and GTPase domains of LRRK2 have crucial roles in LRRK2-mediated DA neurodegeneration in *C. elegans*. These aberrant phenotypes due to expression of human *LRRK2* in *C. elegans* were enhanced if human α-synuclein was co-expressed (Prabhudesai et al., 2016). Indeed, expression of α-synuclein itself was toxic to DA neurons in an age-dependent manner and resulted in locomotion defects. This worm model of α-synuclein showed a role for dopamine

in formation of α-synuclein oligomers and appears to be an effective model for the study of PD causing *LRRK2* variants (Mor et al., 2017).

The *C. elegans* phenotypes due to expression of human LRRK2 or α-synuclein have been exploited for potential drug discovery. As proof of concept, and to verify the *C. elegans* model for PD drug discovery, small molecules identified from a high-throughput yeast screen (expressing toxic levels of human α-synuclein in yeast) protected worm DA neurons from human α-synuclein over-expression (Caldwell et al., 2020). These studies lend credence to the use of model organisms in the discovery of potential PD therapeutics (Liu et al., 2011).

Drosophila melanogaster as a Model to Increase Knowledge of LRRK2 Mediated Parkinson's Disease

The fruit fly *Drosophila* possesses 70% of disease-associated gene homologues that are known to cause inherited disease in humans, including one homologue of human *LRRK2* (Szabo et al., 2017). Other human PD causing orthologous genes are also present in *Drosophila,* with the exception of *SNCA* (α-synuclein). The first attempts to study inherited PD in *Drosophila* were via inactivation of the endogenous *Lrrk2* gene (Lee et al., 2007). Homozygous *Lrrk2* knockout flies developed normally and contained a normal number of DA neurons, and indeed the majority of studies determined that *Lrrk2* is dispensable for survival of flies (Seegobin et al., 2020). This led to the consensus that the *LRRK2* mutations observed in PD patients likely resulted in a toxic gain-of-

function mechanism. This is consistent with the observation that variants in the kinase domain of LRRK2 that are known to predispose patients to PD result in an increase in LRRK2 protein kinase activity. More recent *Drosophila* models have expressed human *LRRK2* and *LRRK2* PD-causing pathogenic variants in DA neurons of *Drosophila*. These led to reductions in locomotor activity and loss of DA neurons, with pathogenic variants generally leading to more severe phenotypes (Godena et al., 2014; Hindle et al., 2013; Lin et al., 2010; Ng et al., 2009; Venderova et al., 2009). The *Drosophila* model appears to be one of the more complete when it comes to recapitulating the phenotypes observed in *LRRK2* dependent PD in humans.

When expressing human genes in *Drosophila*, there are drivers (promoters) that can be used for inducible tissue or cell type specific expression, such as expression in DA neurons as was used for human *LRRK2*. The most common employs the *GAL4*/upstream activation sequence (UAS) system. The system has two parts, the yeast *GAL4* gene which encodes the yeast transcriptional activator protein Gal4, and the UAS which is the promoter to which Gal4 binds to activate transcription. An inducible system is preferred as it prevents adaptions over time for flies expressing a gene that is deleterious. Using the *GAL4* system in *Drosophila*, the yeast *GAL4* gene is placed under control of a fly promoter that has the desired expression pattern for the gene under study. As an example, for expression specific to DA neurons the *ddc* promoter (*ddc* itself encodes dopa decarboxylase) is often employed and has been the main driver (*ddc-GAL4*) used to study expression of human *LRRK2* in

Drosophila DA neurons (Seegobin et al., 2020). A separate strain is produced whereby the UAS that is bound by the Gal4 protein to drive gene transcription is upstream of the human gene under study (e.g. UAS_{GAL4}-*LRRK2*). To express human LRRK in DA neurons, the *ddc-GAL4* strain is bred with a UAS_{GAL4}-*LRRK2* strain resulting in progeny that express human *LRRK2* in a *ddc* promoter dependent manner; that is human *LRRK2* would be expressed in fly DA neurons.

Expression of various human *LRRK2* PD-causing variants in DA neurons in *Drosophila* is starting to enable differentiation of function and possible pathogenic mechanisms for each variant. For example, expression of LRRK2 G2019S, which results in a constitutive increase in LRRK2 protein kinase activity, resulted in DA neuron apoptosis similar to that observed in DA in PD patients and was dependent on the kinase activity of LRRK2 (Imai et al., 2008). Expression of LRRK2 variants in the GTPase domain (R1441C or Y1699C) resulted in the expected locomotor defects, with these versions of LRRK2 preferentially associating with microtubules and inhibiting axonal transport (Godena et al., 2014). These microtubule defects were not observed with the LRRK2 G2019S mutant. This implies that the pathogenic kinase and GTPase variants in LRRK2 may act through distinct mechanisms to affect LRRK2 function resulting in the observed neurodegeneration and subsequent pathology.

Using these ‘humanized’ *Drosophila LRRK2* models genetic screens have revealed genetic interactions with other PD causing genes (or risk factors) including *Vps35*, *Rab7l*, *parkin*, and *pink1* (Hsieh et al., 2016; Huang et al., 2012;

Inoshita et al., 2017; MacLeod et al., 2013; Ng et al., 2009). Genetic interactions between *LRRK2* alleles with *Vps35* and *Rab7l* are consistent with LRRK2 functioning in retromer and endolysosomal vesicular trafficking pathways, while the *parkin* and *pink1* genetic interactions are consistent with LRRK2 functioning in the regulation of the regulation of mitophagy.

Studies of *Drosophila* Lrrk2 itself have revealed multiple roles in vesicle trafficking including synaptic vesicle endocytosis and endolysosomal pathways (Aryal & Lee, 2019). *Drosophila* Lrrk2 was observed to localize to membranes of late endosomes and lysosomes and directly interacted with Rab7, a major regulator of late endosomal-lysosomal transport (Dodson et al., 2012). Rabs have been determined to be direct phosphorylation substrates of human LRRK2, although it has yet to be determined or *Drosophila* Lrrk2 can directly phosphorylate Rab7. *Drosophila* Lrrk2 has been determined to phosphorylate endophilin A and mediate synaptic vesicle endocytosis at neuromuscular junctions.

Drosophila appears to be one of the better model organisms for the study of LRRK2 mediated PD. The *Drosophila* LRRK2 mediated PD models display the expected locomotion defects, loss of DA neurons, genetic interactions between known PD causing genes, and neuronal subcellular vesicular trafficking defects consistent with those observed in PD models for human cells in culture.

Yeast as a Model to Increase Knowledge of Inherited Disease

Overview of Genome-wide Yeast Genetic Screens

The yeast *Saccharomyces cerevisiae* has been widely used to perform near genome-wide searches for suppressors of genetic mutations (most often single gene mutations). A foundation of this approach is referred to as synthetic genetic array (SGA), or synthetic genetic enhancement, analysis (Boone et al., 2007; Costanzo et al., 2010, 2016; Dixon et al., 2009; A. H. Tong et al., 2001; A. H. Y. Tong et al., 2004; van Leeuwen et al., 2016). The SGA approach was enabled by the construction of a barcoded yeast single-gene knockout collection whereby each yeast gene was singularly inactivated in a diploid cell flanked by two unique 20 base pair sequences that serve as gene identifiers. The creation of the single-gene knockout collection (some of which have human homologues that can cause inherited disease) itself revealed some interesting data. Interestingly, only ~20% of yeast genes were essential for survival when yeast were grown under normal laboratory conditions (Boone et al., 2007; Costanzo et al., 2010; Dixon et al., 2009). This underscores the buffering capacity of the genome to deal with gene inactivation at a single node.

Much of SGA analysis has been used to identify synthetic lethal pairs of genes, basically two genes whose inactivation alone has very little or no phenotype but their combined inactivation results in a severe phenotype. This is most often measured as a defect in growth (synthetic lethality), but can be any

phenotype that can be easily determined, and has been used to assign phenotypes to genes of no known function based on a similar set of genetic interactions to genes of known function, and to connect what were thought to be disparate biological processes together to uncover previously unknown biochemical or metabolic networks (Costanzo et al., 2010; Curwin et al., 2009; Dowell et al., 2010; Fairn et al., 2007; Gaspard & McMaster, 2015; Mattiazzi Usaj et al., 2016).

As opposed to synthetic lethality, mutations that ameliorate a growth or biochemical defect associated with an inherited genetic disease may be a viable approach to identify pathways that could be a target for their treatment (McLornan et al., 2014). As the identification of human disease-causing genes is now rapidly expanding, it may be interesting to apply SGA approaches to query human disease-causing variants where a similar mutation in a yeast gene, or the analogous human disease-causing allele expressed in yeast, results in a phenotype that can be monitored at a genome-wide level. These screens have not been performed in depth as they require specific mutant versions of genes and often a defect in a cell based assay that is specific to the gene/process under study.

Chemical Genetics to Search for Small Molecule Modifiers of Inherited Disease Phenotypes

Cell Based Drug Screening

There has been a resurgence in cell or organism-based drug discovery, referred to as the outside-in approach, versus target-based drug screening efforts referred to as the inside-out approach. A major driver of interest in the outside-in approach was an analysis of first-in-class FDA approved drugs between 1999 and 2008 which revealed that 62% were discovered using cell or organisms based screens, despite the fact that only a small subset of drug screens used this method (Eder et al., 2014; Moffat et al., 2017; Schirle & Jenkins, 2016). Several reasons are thought to contribute to the better track record of the outside in approach to drug screens. Outside in based screens take into account drug uptake by cells/organisms and can often combine screening and counter screening (***e.g.*** against toxicity in cells or a whole organism) enabling compounds that are both efficacious and non-toxic to be discovered using the same screen (Wagner, 2016). Phenotypic screens can also uncover compounds or drugs that are ameliorative in the absence of a validated drug target (**Figures 5 and 6**).

The nature of the drug or small molecule library is an important aspect when considering screening for potential therapeutics. There has been considerable interest in repurposing known drugs (Cha et al., 2018; Corsello et al., 2017). Drug repurposing focuses on identifying drugs that are approved for

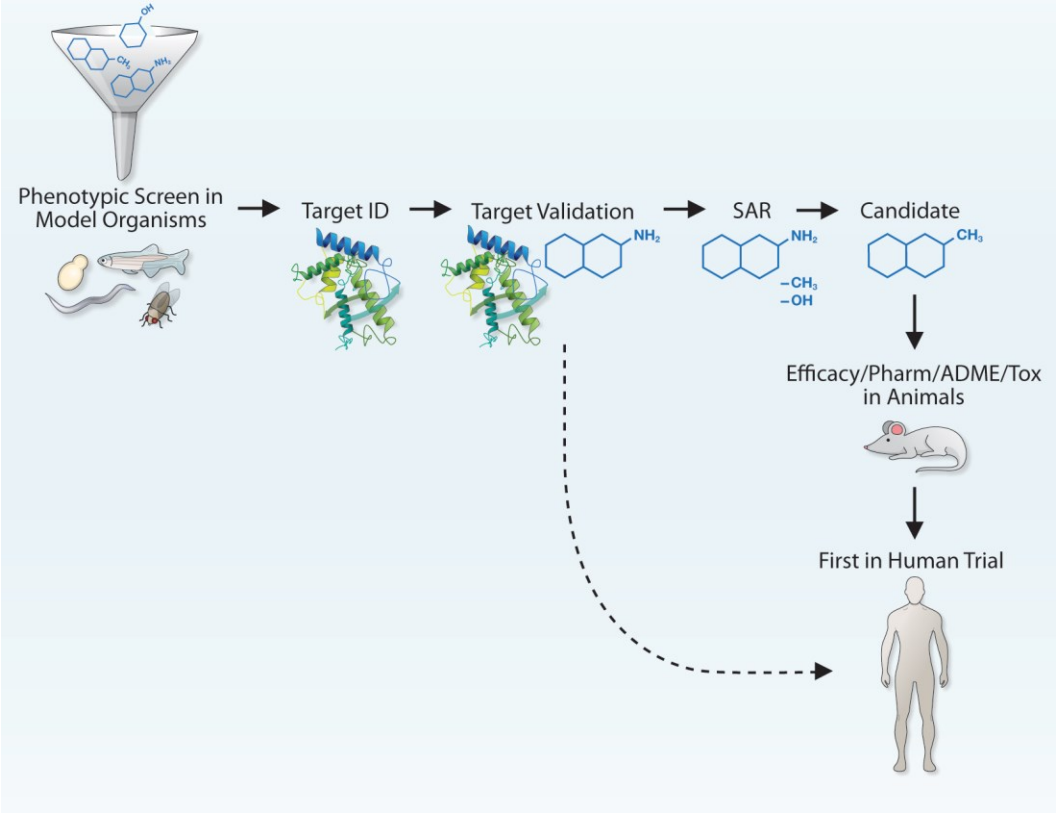

Figure 5. Outside-in approach to drug discovery.

Outside-in screens start with a small molecule screen versus a cellular model or organism model of a genetic disease, followed by target identification (ID), validation, building an expanded library of small molecules based on structure activity relationships (SAR) and declaring a candidate drug for in vitro and in vivo pharmacokinetic/pharmacodynamic (pharm), absorption/distribution/metabolism/excretion (ADME), and toxicology (tox) studies in animals subsequent to a first in human trial. Figure reproduced from Strynatka et al (Genetics 208, 833-851 (2018)) with permission form the Genetics Society of America.

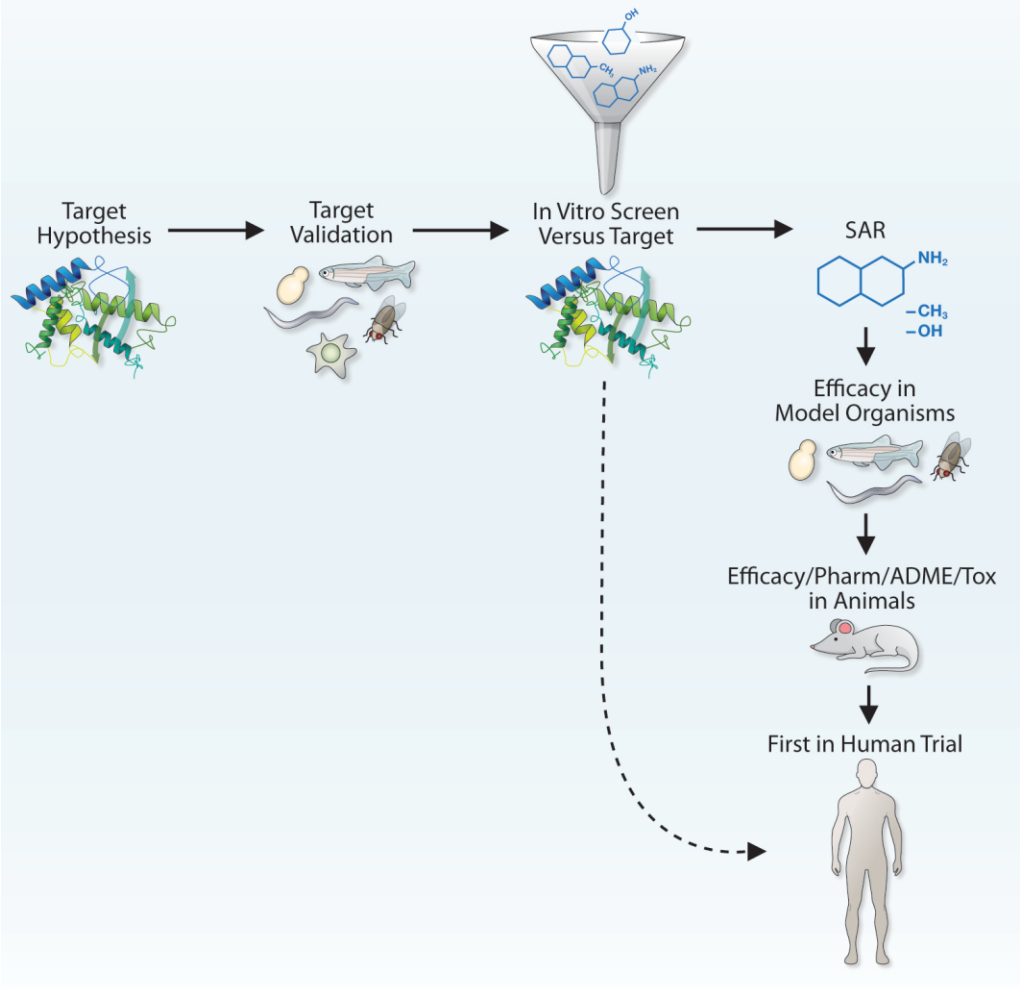

Figure 6. Inside-out approach to drug discovery.

Inside-out screens start with a large chemical entity screen for inhibition (normally) of a purified drug target (e.g. protein) hypothesized to be able to ameliorate the genetic disease under study, building an expanded library of small molecules based on structure activity relationships (SAR), and determining the efficacy of lead compounds in model organisms and declaration of a candidate drug for in vitro and in vivo pharmacokinetic/pharmacodynamic (pharm), absorption/distribution/metabolism/excretion (ADME), and toxicology (tox)

(Figure 6 legend continued)

prior to a first in human trial. Figure reproduced from Strynatka et al (Genetics 208, 833-851 (2018)) with permission form the Genetics Society of America.

use in humans. On-target effects of these drugs, or off-target effects on other processes that are as yet unknown, may prove efficacious for disease treatment. The main advantage of drug repurposing is that the drug can often be tested directly in the clinic for utility. For inherited orphan diseases, efficacy of a known drug in a model organism can allow for a human clinical trial in as few as 5-10 patients, with success supporting subsequent drug approval for use in humans (Bronstein & Kakkis, 2016; Ekins, 2017; Joppi et al., 2016). This is of a cost and scale that can be performed by academic centers and small biotechnology companies.

A major caveat to drug repurposing for inherited disease is that there are only ~1,500 FDA-approved drugs (Eder et al., 2014) with many in a similar chemical space (e.g. different versions of statins). If we consider only Mendelian diseases there are an estimated ~7,000 distinct diseases (Boycott et al., 2014). If a small molecule therapy approach is to be considered for an inherited disease, most inherited diseases will not be ameliorated by a known drug and instead will likely require the screening large new chemical entity libraries, and new chemical entity development, to find an effective treatment.

Yeast Chemical Genetic Methods to Identify Potential Therapies

In yeast, similar approaches to SGA have been taken with respect to chemical-genetic analysis (Enserink, 2012; Fairn & McMaster, 2005; Fletcher et al., 2021; Hillenmeyer et al., 2008; Lehner, 2013; A. M. Smith et al., 2010; Wong

et al., 2016). In chemical genetics, how a drug/compound affects the growth of the entire yeast knockout collection is assessed. Popular yeast chemical-genetics methods are comparing synthetic lethal gene pairs in yeast to chemical-genetic results to determine potential drug targets (**Figure 7**). Popular yeast chemical-genetic screens include drug-induced haploinsufficiency profiling (HIP) and homozygous profiling (HOP), and multi-copy suppressor screens (Giaever et al., 1999; Lee et al., 2014).

With respect to the potential to discover new drugs, HIP screening versus the diploid heterozygous yeast gene deletion set is thought to be more useful when trying to determine a drug target (**Figure 8**). The theory is that the loss of one allele of a drug target will result in a yeast strain that is more sensitive to the drug compared to other strains within the yeast deletion collection. As an example, a HIP chemical-genetic screen identified yeast *DFR1* haploinsufficient yeast, encoding dihydrofolate reductase, as being sensitive to methotrexate (Giaever et al., 1999, 2004). Methotrexate competitively inhibits human dihydrofolate reductase that is used to treat certain types of leukemia, as well as cancers of the breast, skin, bone, ling, and head and neck. In contrast, HOP profiling uses the haploid non-essential yeast gene deletion collection and most often identifies genes/processes that buffer against the drug (Ho et al., 2011). Another approach that has been employed is multi-copy suppression, where individual genes are individually over-expressed in separate yeast cells and this strain set is used to identify genes that increase or decrease sensitivity to a particular drug or compound (Ho et al., 2011). In many cases an over-expressed

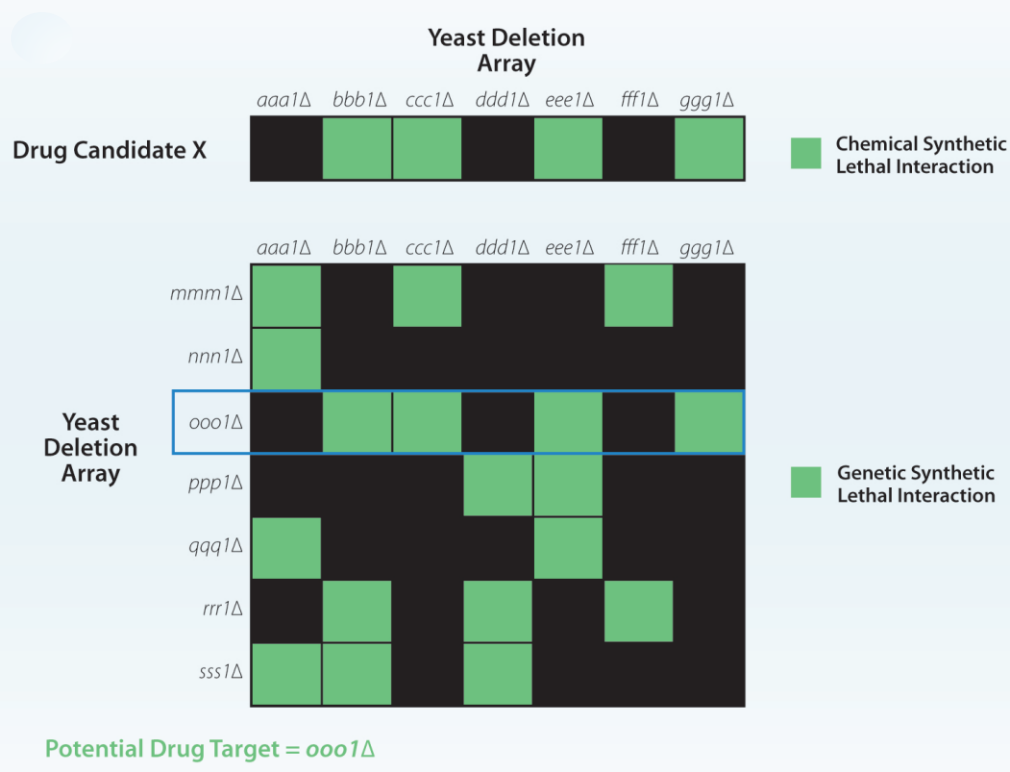

Figure 7. Combined chemical-genetic and synthetic lethal screens to determine potential drug targets.

A small molecule (drug) is screened versus the ~4,800 separate non-essential yeast gene deletion set and is compared to the known yeast deletion array synthetic lethal genetic interactions. The yeast gene deletion(s) with a similar set of interactors to the small molecule can point to the pathway or gene/protein targeted by the small molecule. Figure reproduced from Strynatka et al (Genetics 208, 833-851 (2018)) with permission form the Genetics Society of America.

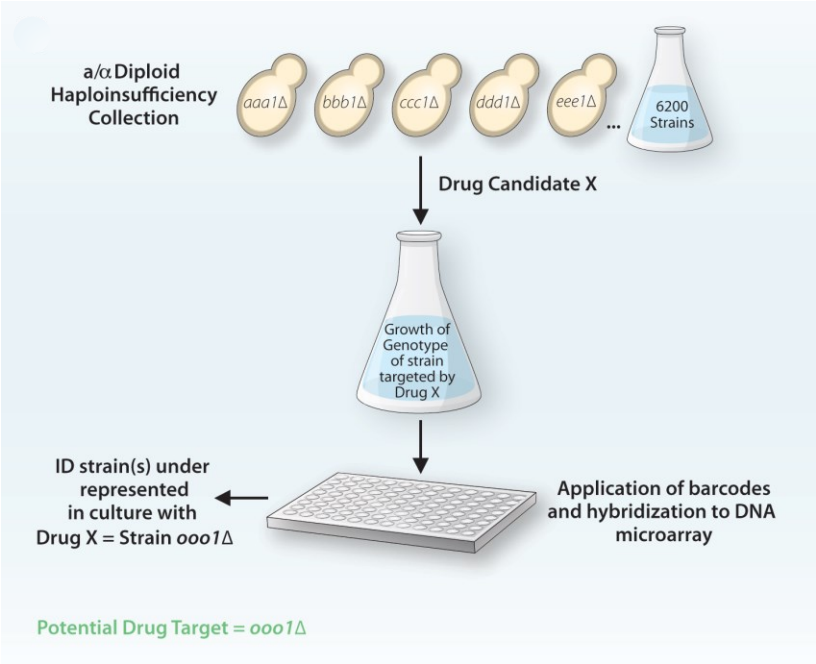

Figure 8. Haploinsufficiency profiling to determine potential drug targets.

HIP profiling makes use of the diploid haploinsufficiency collection of all yeast genes. The entire collection is exposed to a small molecule and the culture is allowed to grow. Using barcoding technology the yeast strain(s) whose growth is decreased (or increased) compared to a no drug control can be identified. A potential small molecule drug target should show decreased growth in a strain that is haploinsufficent for its target compared to the other strains. Figure reproduced from Strynatka et al (Genetics 208, 833-851 (2018)) with permission from the Genetics Society of America.

gene is the drug target, but genes that inactivate the drug or result in its export from the cell can also be identified.

Yeast chemical-genetics has primarily focused on decreased cell growth as the major phenotypic readout. Decreased cell growth is amenable to finding potential new drugs for diseases such as cancers (Albrecht et al., 2016; Sekigawa et al., 2010). However, yeast chemical genetics could also be used to identify compounds or drugs that ameliorate growth of a yeast strain that contains a mimic of a genetic variant within a human inherited disease-causing gene. These types of screens have not been routinely performed in high throughput as often they require non-standard growth conditions to be used and/or a specific yeast strain/gene allele to be engineered. It will be interesting to see if the successes in chemical-genetics synthetic lethality in yeast can be recapitulated for drugs/small molecules that ameliorate growth as potential treatments for inherited diseases.

The identification of gene knockouts, or drugs/metabolites, in 'humanized' yeast could serve as a jumping off point for experiments in higher order organisms to determine if the potential drug target (inactivated gene) or drug could be of potential use in individuals with that disease-causing genetic mutation. All yeast genetic and chemical-genetic interactions, and human homologs of yeast genes including functional complementation relationships are constantly archived and updated. These can be browsed or queried through the *Saccharomyces* Genome Database (Chatr-Aryamontri et al., 2017) (www.yeastgenome.org).

Using 'Humanized' Yeast to Identify Compounds and Drugs to Treat Human Disease

Introducing mutations within yeast genes that correspond to the analogous variants that cause human disease has been a common practice in assessing if the corresponding mutation affects protein function. A second approach is to 'humanize' yeast via expression of the human open reading frame (ORF) in a yeast cell (often in a strain where the corresponding yeast gene has been genetically inactivated) and then determine to what extent the human ORF (or human ORF variant) can complement loss of function of the analogous yeast gene (Sun et al., 2016). This can take place in haploid yeast cells containing a null allele of a non-essential gene, or in the case of essential genes through the use of regulatable promoters, mRNA degrons, conditional alleles (*e.g.* temperature sensitive strains), or through the use of a diploid heterozygous strain and subsequent isolation of haploid progeny lacking the yeast gene which can express the human ORF (**Figure 9**) (Kachroo et al., 2015; Steinmetz et al., 2002).

An important aspect of these large-scale studies is the use of constitutive or regulatable promoters that remove both temporal and gene dose from consideration (*e.g.* cell cycle genes) and thus may under-estimate the capacity of yeast to be successfully complemented by their human counterparts. A large

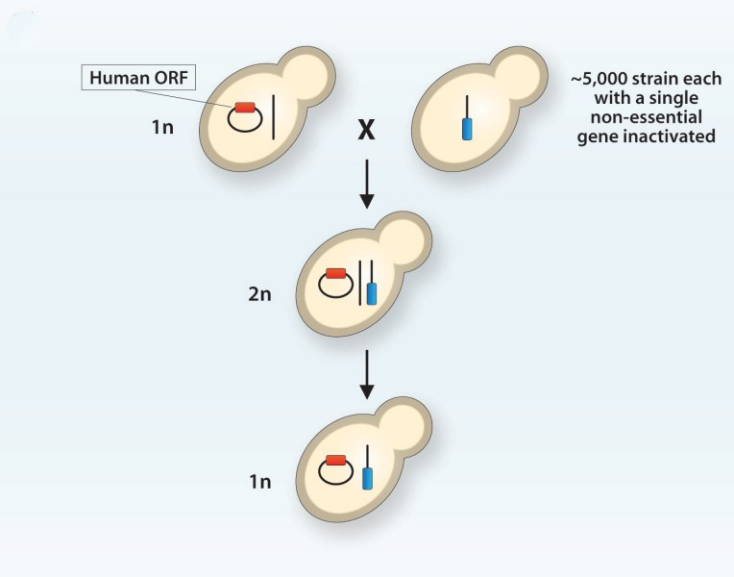

Figure 9. Multi-copy suppression to determine potential drug targets.

The principle is based on the observation that inducible over-expression of a human open reading frame in yeast can result in an easily measurable phenotype (often growth inhibition). The yeast strain containing the human open reading frame (uninduced) can be mated to each of the ~4,800 non-essential yeast gene deletion strains and through a series of strain selection steps can result in the isolation of haploid yeast strains each containing the human open reading frame under control of an inducible promoter in each of the ~4,800 individual yeast gene deletion strains. Expression of the human protein can be induced and yeast gene deletion strains that prevent its toxicity point to potential drug targets whose inhibition could prevent the toxicity of the human protein. Inducible over-expression of a human open reading frame in yeast can also be

(Figure 9 legend continued)

used to screen drug libraries to directly search for drugs that ameliorate the growth defect in the presence of an over-expressed gene. Preventing a decrease in cell growth due to over-expression of a specific gene in the presence of a drug could point to the encoded protein being a target of the drug. Figure reproduced from Strynatka et al (Genetics 208, 833-851 (2018)) with permission from the Genetics Society of America.

scale 'yeast humanization' project, where each potential human ORF ortholog is placed within the yeast genome at its cognate gene site such that dose and temporal issues are controlled for would be a useful resource to assess function and complementarity of normal human ORFs, as well as how variations in these genes could result in a phenotype(s) associated with a human disease.

Using Yeast to Increase Knowledge of Inherited Human Neurological Diseases

A neurodegenerative disease that has been effectively studied in yeast is Alzheimer disease (AD). In AD, plaques of β-amyloid are found in neurons (Chartier-Harlin et al., 1991; Citron et al., 1992; Mawuenyega et al., 2010; Mullan et al., 1992; Qiang et al., 2017) that are derived from amyloid β precursor protein (encoded by the *APP* gene), which is cleaved to an Aβ-42 form that is aggregation-prone and toxic (Tcw & Goate, 2017). Yeast do not contain an APP gene orthologue, so to create a yeast model of Aβ-42 toxicity the open reading frame for the Aβ-42 peptide was fused to an ER-targeting signal and this construct was expressed in yeast. Expression of ER-targeted Aβ-42 in yeast was found to be toxic to yeast cells. A genetic screen was performed looking for modifiers of this toxicity (Matlack et al., 2014; Treusch et al., 2011). The screen identified the yeast homolog of the endocytic factor phosphatidylinositol binding clathrin assembly protein (*PICALM*), as well as several other endocytic factors

whose relationship to Aβ-42 toxicity was not known, as being able to alter Aβ-42 toxicity. Genes identified in yeast to that were found to decrease Aβ-42 toxicity were found to also decrease Aβ-42 toxicity in glutamatergic neurons of *C. elegans* and in primary rat cortical neurons suggesting that there was relevance of these genes to AD. The yeast model was used to perform a chemical screen of 140,000 compounds looking for drugs that reversed Aβ-42 toxicity. From this screen 30 compounds were identified with half belonging to the hydroxyquinoline family. A subset of these compounds was found to be efficacious in *C. elegans* and mouse AD models (Matlack et al., 2014).

The above studies show that the expression of human genes in yeast that do not have yeast homologues can increase knowledge of their function. These types of studies have been successfully used to learn about mechanisms of disease and to identify potential. The expression of α-synuclein and LRRK2 in yeast to study PD are other examples.

Using Yeast to Increase Understanding of Parkinson's Disease

The yeast *Saccharomyces cerevisiae* does not contain a homologue of either α-synuclein or LRRK2, but contains many of the remaining genes where human gene variants have been observed to predispose people to PD. Duplication and triplication, as well as specific variants, of *SNCA* (which encodes α-synuclein) are causal for PD (Polymeropoulos et al., 1997; Singleton et al., 2003). Yeast was first used as a model for a PD causing gene in 2003 when α-

synuclein was heterologously expressed (Outeiro & Lindquist, 2003). Inducible expression of human α-synuclein in yeast resulted in α-synuclein first being localized to the plasma membrane followed by its internalization and its formation into cytoplasmic inclusions. Similar to what is observed in human cells, increasing the dose of α-synuclein in yeast cells increased the level of α-synuclein cytoplasmic inclusion formation and inhibited cell growth. This inhibition of cell growth by α-synuclein (as well as the PD causing variant A53T) was accompanied by decreased endocytosis and decreased ER to Golgi vesicular trafficking (Outeiro & Lindquist, 2003). A screen for yeast genes whose over-expression could prevent α-synuclein mediated toxicity resulted in the identification of the yeast Rab Ypt1, whose over-expression prevented the decreased cell growth phenotype as well as the defect in ER to Golgi vesicular transport (Cooper et al., 2006). The over-expression of Rab1 also prevented the loss of DA neurons in *Drosophila* and *C. elegans* models of α-synuclein mediated PD, as well as the α-synuclein mediated death of mammalian primary neurons grown in culture (Cooper et al., 2006; Gitler et al., 2008; Winslow et al., 2010). This work occurred prior to Rabs being identified as substrates for the protein kinase function of LRRK2, and points to a conserved function across many cell types for known genes that cause PD.

Similar to expression of α-synuclein in yeast, expression of a LRRK2 fragment containing its two enzymatic domains (the GTPase domain and the kinase domain) resulted in toxicity to yeast (Xiong et al., 2010). A genetic screen of all the non-essential yeast genes identified seven gene deletions that reversed

the toxicity of LRRK2 expression. Two of these genes had human homologues, one of which (*GCS1*) was the yeast homologue of human *ARFGAP1*. Studies in cultured neurons confirmed that ArfGAP1 is required for the toxic phenotypes of the major pathogenic version of LRRK2 as RNAi mediated knockdown of ArfGAP1 in neuronal cells expressing pathogenic versions of LRRK2 prevented LRRK2 mediated toxicity (Stafa et al., 2012; Xiong et al., 2012). Further biochemical studies determined that ArfGAP1 accelerated GTP hydrolysis by LRRK2 demonstrating a direct relationship between LRRK2 and ArfGAP1 function.

Yeast models of PD have also been used to identify potential small molecules (drugs or drug leads) based on their ability to reverse the growth and vesicular trafficking defects. A small molecule screen in yeast determined that N-aryl benzimidazole was protective against α-synuclein mediated toxicity in yeast, and also *C. elegans* and primary neuron models of α-synuclein mediated PD (Tardiff et al., 2014). This compound promotes endosomal transport via the E3 ubiquitin ligase Rps5/Nedd4 and it alleviated both the defective ER to Golgi as well as endocytic defects observed due to increased α-synuclein.

In this thesis work, we performed a chemical genetic screen in the yeast *Saccharomyces cerevisiae* to identify small molecule inhibitors of human ArfGAP1, a mediator of *LRRK2* induced toxicity.

HYPOTHESIS AND OBJECTIVES

Hypothesis

Small molecule inhibition of human ArfGAP1 will provide a tool for insight into ArfGAP1 and *LRRK2* biology, and could point to a potential therapeutic route for the treatment of *LRRK2* mediated PD.

Main Objectives

- Develop a high throughput screen to identify small molecule inhibitors of human ArfGAP1
- Identify potential ArfGAP1 small molecule inhibitors. Verify direct binding of identified small molecules to human ArfGAP1
- Determine if small molecule inhibition ArfGAP1 can prevent LRRK2, and LRRK2-G2019S, mediated cell death
- Test identified compounds for efficacy in an animal model of LRRK2, and LRRK2-G2019S, mediated PD

MATERIALS AND METHODS

Plasmids Used and Molecular Biology Techniques

Plasmids used in this study are described in Table 1 and primers in Table 2. To construct plasmid pKS3:9 for the expression of human ArfGAP1 (ArfGAP1) tagged with the GFP variant mEmerald for expression in yeast the Gibson Assembly kit (New England Biolabs) was used. The ArfGAP1 template cDNA was obtained from Dharmacon (now Horizon) and the mEmerald template DNA source was plasmid pIND4-Km-RSP_627-mEmerald, a kind gift from Sergio Muñoz-Gómez (Dalhousie University). ArfGAP1 was amplified by PCR using primers OKS2:147-1_F and OKS2:147-1_R, and mEmerald was amplified using OKS2:147-2_F and OKS2:147-2_R. The resulting amplicons were then ligated into the plasmid pESC-LEU, which had been linearized with restriction enzymes SalI-HF and XhoI (NEB). Successful insertion was confirmed by Sanger sequencing. The resulting plasmid was human ArfGAP1 fused to mEmerald in the yeast expression plasmid pESC-LEU enabling expression of this fusion protein from the yeast *GAL1* promoter.

Table 1. Plasmids used in this study.

Name	ORF	Backbone	Description	Source
pPP16:141-18	Galactose-inducible full-length human ArfGAP1	pESC-LEU		Pak Poon
pPP18:45	Galactose-inducible truncated human LRRK2	pESC-URA		Pak Poon
pESC-LEU	-	pESC-LEU	multi-copy *LEU2* with *GAL1* promoter	Agilent Technologies
pESC-URA	-	pESC-URA3	multi-copy *URA3* with *GAL1* promoter	Agilent Technologies
pKS3:9	Galactose-inducible full-length human ArfGAP1-GFP fusion	pESC-LEU		This study
pPP18:49-22	IPTG-inducible full-length human ArfGAP1	pET16b		Pak Poon
pET-Arf1	IPTG-inducible full-length yeast Arf1	pET21b		Poon et al. 1996
pACY177/ET3d/yNMT	IPTG-inducible full-length yeast N-myristoyl transferase 1	pET3d		Haun et al. 1993

Table 2. Primers used in this study.

Name	Sequence
OKS2:147-1_F	5'tacgactcactatagggcccgggcgtcgacatggccagcccaagaacc3'
OKS2:147-1_R	5'cctccagaacctcctccaccccagttctggttgtcccagc3'
OKS2:147-2_F	5'gctgggacaaccagaactggggtggaggaggttctggagg3'
OKS2:147-2_R	5'tagctagccgcggtaccaagcttactcgagctacttgtacagctcgtccatgc3'
OKS2:151-1F	5’ccagcccaagaaccaggaa 3’
OKS2:151-1R	5’ccttcttggtgccctccc 3’
OKS2:151-2F	5’cagtggggtctctcagttgg 3’
OKS2:151-2R	5’cttgtacagctcgtccatgc3’

Yeast Strains and Yeast Cell Transformation

Yeast strains used are described in Table 3. Yeast cells were grown in synthetic growth media which consisted of 0.5% ammonium sulfate (ThermoFisher), 0.17% yeast nitrogen base (Sunrise), 0.004% required amino acids (Sunrise), and 0.002% each of adenine and uracil. The carbon source was either 2% galactose, 2% glucose (ThermoFisher), or 3% glycerol/2% ethanol (ThermoFisher).

Yeast cells were transformed with plasmids using a standard lithium acetate/polyethylene glycol protocol (Gietz & Schiestl 2007). Cells were retrieved from glycerol stocks maintained at -80°C and streaked onto an agar plate for single colonies. After 3 days of incubation at 30°C, a single colony was inoculated into 5 mL of liquid media and grown overnight in an orbital shaker at 30°C. The next day, the culture was back-inoculated with 45mL liquid media and grown with shaking at 30°C for approximately 5 hours to ensure that the cells were in logarithmic phase. Cells were harvested by centrifugation at 3000 *g* for 5 min and washed twice in sterile water before being resuspended in transformation mix (23% polyethylene glycol 3350, 0.1M LiAc, 5 μg sonicated herring sperm DNA). Plasmid DNA was then added and the sample was subjected to heat shock at 42°C for 1 hour before being washed with water and plated on agar plates containing the appropriate selective media required for plasmid maintenance. Plates were incubated at 30°C for 3 days until single colonies appeared.

Table 3. Yeast strains used in this study.

Name	Genotype	Source
W303-1a	MAT**a** *leu2–3 112 ura3-1 his3–11 15 trp1–1 ade2-1 can1–100*	Thermo Fisher
JBY3	W303 MAT**a** *gcs1*::*natMX6*	(Benjamin 2011)
PPY17:50f-3b	W303 MAT**a** *gcs1*::*natMX6 pdr5::HIS3 snq2::TRP1*	Pak Poon

Determination of Yeast Cell Growth

Yeast strains expressing a human open reading frame (ORF) under the galactose-inducible *GAL1* promoter were first grown in transcription repressing media (synthetic complete with 2% glucose) overnight at 30°C before being transferred to media containing 3% glycerol/2% ethanol as a transitional carbon source. ORF expression was induced by transferring yeast cells into 2% galactose containing media.

To assess cell growth on solid media, yeast cells were grown in selective liquid media with 3% glycerol/2% ethanol as carbon source and lacking uracil and leucine for plasmid maintenance. Cell density was determined by reading optical density at 600 nm (OD 600) and cell cultures were diluted to a uniform density (OD 600 = 0.4) before being spotted on solid agar media. Each sample was spotted as tenfold serial dilutions on sets of plates containing media with either 2% glucose or 2% galactose as carbon source and incubated at 30°C for 3 days. Yeast plates were imaged using a Bio-Rad VersaDoc.

To assess cell growth in liquid media, cell density was determined by OD 600 and after cells were grown in liquid media with 3% glycerol/2% ethanol as carbon source the cultures were diluted to equal cell number. Cells were transferred to medium containing 2% galactose as carbon source and OD 600 was measured over time.

Yeast Screen to Identify Potential ArfGAP1 Small Molecule Inhibitors

The high-throughput screen was conducted in collaboration with the lab of Michel Roberge at the University of British Columbia, and the Centre for Drug Research and Development. PPY17:50f-3b yeast cells were transformed with plasmid pPP18:49-22 for inducible expression of human ArfGAP1 from the *GAL1* promoter in yeast cells lacking its endogenous ArfGAP1 (*gcs1*$^{-}$). Yeast cells were seeded in 96-well plates at an OD 600 of 0.05. A BioRobotics TAS1 robot equipped with an FP3 96-pin tool was used to dispense chemical compounds to yeast cells. Libraries screened included the Prestwick FDA-approved therapeutics library, Sigma LOPAC 1280, Chembridge DiverSet, and proprietary libraries for a total of just over 100,000 compounds. Plates were incubated at 30°C for 40 hours and cell density was measured using a Dynex Opsys Microplate Reader at 600 nm. Potential hits were identified as compounds that restored growth >2-fold over no-compound controls. Fresh stocks of hit compounds (termed compounds 4, 5, 8, 9, 10, 11, 12 and 13) were ordered from ChemBridge and were tested again for their ability to restore growth using the same assay.

To further confirm the inhibitors identified in the high throughput screen a secondary screen was performed. JBY3 yeast cells expressing either human ArfGAP1, LRRK2, both together under control of a galactose inducible promoter, or carrying an empty vector, were seeded in 96-well plate (OD 600 = 0.01) in 2% galactose containing media. Compounds 4, 8, 11, 12, and 13 (resuspended in

DMSO), or DMSO-only control, were added to cells at two different final concentrations (10 μM and 50 μM). Plates were incubated at 30°C. At regular time points, plates were vortexed gently and OD 600 was recorded spectrophotometrically using a Multiskan Ascent 96-well plate reader to determine cell growth.

Western Blotting

Yeast cells were lysed at 4°C in lysis buffer (20 mM Tris-HCl pH 7.5 and 10% glycerol, containing pepstatin A and Roche complete protease inhibitor cocktail (1/50 v/v) and subjected to mechanical disruption with equal volume 0.45 mm acid-washed glass beads in a bead beater for 3 rounds of 1 min each. The cell lysate was clarified by centrifugation, mixed with Laemmli buffer (2% SDS, 10% glycerol, 5% 2-mercaptoethanol, 0.02% bromophenol blue and 30 mM Tris HCl, pH 6.8) and incubated at 90°C for 5 min prior to resolution by SDS-PAGE. Protein quantitation was performed using Coomassie reagent (BioRad) and compared to a set of bovine serum albumin standards of known concentration. Cell lysates were subjected to electrophoretic separation using 10% bis/acrylamide gels, alongside the Page Ruler prestained protein ladder (ThermoFisher). Using a wet transfer system, proteins were transferred to a PVDF membrane (GE Healthcare) in 25 mM Tris-HCl, 200 mM glycine, 1% SDS, 20% methanol overnight at 20 V. Membranes were stained with Ponceau-Red to ensure even protein loading and transfer before being blocked with Odyssey

blocking buffer (1:4 dilution in TBST, Li-Cor) for 1 hr at room temperature. The primary antibodies, mouse anti-myc, (clone 9B11, Cell Signaling) and (anti-Pgk1, Molecular Biosystems) were diluted in Odyssey blocking solution (Li-Cor) at a concentration of 1:1000 and incubated with the membrane at either at room temperature for 1 hour, or overnight at 4°C. The membrane was washed with TBST three times for 5 min each. The secondary antibody, goat anti-mouse conjugated to the fluorophore IRDye 800CW (Li-Cor) was diluted in Odyssey blocking buffer to a final concentration of 1:5000 and incubated with the membrane for 30 minutes at room temp before being subjected to washes, as before, and imaged using a Li-Cor Odyssey scanner.

Recombinant Protein Expression and Purification

Bacterial strains used are described in Table 4. To express recombinant His-ArfGAP1, a 1 L culture of BL21(DE3)-Rosetta2 *E. coli* cells transformed with plasmid pPP18:49-22 was grown to mid-log phase in LB medium supplemented with 100 μg/mL ampicillin (Sigma) and 34 μg/mL chloramphenicol (Sigma). Protein expression was induced by the addition of isopropyl β-D-1-thiogalactopyranoside to at a final concentration of 0.4 mM. Cells were then grown at 21°C for 6 hours, harvested by centrifugation at 4000 *g* for 30 min at 4°C, resuspended in lysis buffer (20mM Tris pH 8/600 mM NaCl/15 mM imidazole/Roche complete protease inhibitors without EDTA) and frozen at -80°C. To purify polyhistidine-tagged human ArfGAP1 from *E. coli*, cells were

lysed by mechanical disruption by four passes through a French press. The lysate was clarified by centrifugation at 20,000 *g* for 30 min at 4°C. The soluble fraction was subjected to incubation with pre-equilibrated Ni-NTA agarose beads (Qiagen) with gentle rocking for 1 hour at 4°C. The slurry was transferred to a disposable PolyPrep column (Bio-Rad) and the beads were stringently washed by gravity flow with lysis buffer before the 10xHis-ArfGAP1 was eluted from the beads with fractions of elution buffer with increasing concentrations of imidazole (25 mM, 50mM, 75mM, 150mM and 250mM). Dithiothreitol to final concentration of 1mM was added post-elution. To improve purity of ArfGAP1 and to remove imidazole that may interfere with downstream assays, eluted fractions containing ArfGAP1 were then pooled and concentrated using an Amicon Ultra Centrifugal Filter (Millipore Sigma) with a 10 kDa MWt cut-off. The concentrated sample was subjected to gel filtration using the ÄKTA Pure Fast Protein Liquid Chromatography system (GE Life Sciences) equipped with the size-exclusion column Superdex 200 Increase 10/30 using the buffer 50mM NaH_2PO_4 pH 7.4/150 mM NaCl. UNICORN software (GE Life Sciences) was used to identify fractions that contained protein corresponding to the expected size of ArfGAP1. The purity of the ArfGAP1-containing fractions was determined by SDS-PAGE and subsequent staining with Coomassie R-250. Mass spectrometry of the 45 kDa band confirmed that the product was ArfGAP1. Final protein conc was determined using absorbance at 280 nm with the NanoDrop spectrophotometer and the theoretical extinction coefficient of pure ArfGAP1 (calculated using ExPASY Prot Param). For aliquots of ArfGAP1 to be used in downstream MST,

the protein was snap-frozen with liquid nitrogen and stored at -80°C. For aliquots to be used in the in vitro GTPase assays, glycerol was added to a final concentration of 40% prior to snap-freezing and storage at -80°C.

To express recombinant yeast 6xHis-Arf1, a 1L culture of BL21(DE3) *E. coli* cells transformed with plasmids pET-Arf1 and pACY177/ET3d/yNMT and was grown to mid-log phase in LB supplemented with 100 μg/mL ampicillin and 50 μg/mL kanamycin. The pACY177/ET3d/yNMT plasmid expresses a myristoyltransferase which adds the 14 carbon myrisotyl fatty acid to Arf1 as it is being expressed in *E. coli*. This post-translational modification is essential for Arf1 activity. Sodium myristate pH 9.0 was solubilized in BSA and added to the culture at a final concentration of 10 μM. The culture was further incubated at 37°C before being induced with isopropyl β-d-1-thiogalactopyranoside at a final concentration of 0.1 mM. Induction proceeded for 14.5 hours at 22°C before cells were harvested at 4,000 *g* for 30 min at 4°C, resuspended in lysis buffer (20mM Tris pH 8/600mM NaCl/15 mM imidazole/Roche complete protease inhibitors without EDTA) and frozen at -80°C. Purification of 6xHis-Arf1 was achieved with the same Ni-NTA protocol as ArfGAP1. To remove excess imidazole from Arf1, the protein was dialyzed overnight at 4°C using dialysis tubing in 20mM Tris-HCl 8.0/100 mM NaCl/ 1mM DTT/1 mM $MgCl_2$ with three buffer changes of 300 mL each. The dialyzed sample was concentrated using an Amicon Ultra Centrifugal Filter (Millipore Sigma) with a 3 KDa MWt cut-off and protein purity was assessed

by SDS-PAGE. The protein was quantified using Abs 280 nm and then snap-frozen and stored at -80°C.

Table 4. *E. coli* strains used in this study.

Name	Genotype	Source
DH5α	*F- endA1 glnV44 thi-1 recA1 relA1 gyrA96 deoR nupG purB20 φ80dlacZΔM15 Δ(lacZYA-argF)U169, hsdR17(rK–mK+), λ–*	New England Biolabs
Rosetta2(DE3)	*F- ompT gal dcm lon? hsdSB(rB–mB–) λ(DE3 [lacI lacUV5-T7p07 ind1 sam7 nin5]) [malB+]K-12(λS) pLysSRARE[T7p20 ileX argU thrU tyrU glyT thrT argW metT leuW proL orip15A](CmR)*	Novagen
BL21(DE3)	*F- ompT gal dcm lon hsdSB(rB–mB–) λ(DE3 [lacI lacUV5-T7p07 ind1 sam7 nin5]) [malB+]K-12(λS)*	New England Biolabs

Microscale Thermophoresis to Determine Direct Binding of Compounds to Human ArfGAP1

To determine if the small molecule compounds isolated in the yeast cell-based screen for human ArfGAP1 inhibitors directly bound ArfGAP1 two separate microscale thermophoresis (MST) technologies were tested, a label-free version that uses intrinsic tryptophan fluorescence as well as a fluorescent dye-based version.

Monolith systems were used for MST analysis. In these systems, a laser detects movement of a target molecule (in our case the protein ArfGAP1) along a thermal gradient in an aqueous environment contained in a glass capillary. To induce a thermal gradient, an infrared laser applies heat to the end of a capillary and if a ligand (eg: small molecule) binds to the target, one of several molecular parameters will change (size, charge, conformation), altering the pattern of movement as compared to unbound target. A fluorescent detector assesses target movement. A curve of the movement over time is generated, and as unbound compound moves faster, the drop in fluorescence is more rapid. At a single time point, determining the thermophoresis signal expressed as normalized fluorescence versus the concentration of the ligand can generate a binding curve, from which the K_d (dissociation constant, concentration at which half of the compound is associated with the target) may be determined.

Label-free MST was performed using Monolith NT.LabelFree capillaries (Nanotemper) loaded with 10 mM PIPES pH 7.4/150 mM $NaCl_2$, increasing

concentrations of each compound under study, 50 nM purified 10xHis-ArfGAP1 and measured in Monolith NT.LabelFree at Abs 280 nm as per manufacturer's instructions. The detection laser excitation power was set to 40% and the infrared laser was used on the medium setting. Graphs of fluorescence changes were generated using MO.Control software (Nanotemper).

Dye-based MST was performed using purified 10xHis-ArfGAP1 labelled with His-tag NTA dye (Nanotemper) according to manufacturer's instructions. Using the red-dye channel of the Monolith NT.115 the detection laser excitation power was set to 20% and the infrared laser was used on the high setting. For binding checks, capillaries were loaded in triplicate, and maximum conc of drug was tested against drug-free DMSO-matched control with either 50 nM or 100 nM dye-labelled 10xHis-ArfGAP1. For quantitative binding assays, a 1:2 serial dilution of drug was prepared and constant conc (100 nM) of fluorescently labelled 10xHis-ArfGAP1 was added to each tube. For affinity binding determinations, Monolith NT.115 capillaries were filled with 10xHis-ArfGAP1 and increasing concentrations of each compound, loaded into the Monolith NT.115 and subjected to MST analysis.

Human ArfGAP1 Enzyme Assay

The ArfGAP1 protein needs to bind to curved membranes to be active. In addition, the myristoyl group of the ArfGAP1 substrate Arf1 needs to insert into

membranes for Arf1 to be active. To facilitate these processes, mixed-composition liposomes were prepared to test in the ArfGAP1 enzyme assay.

A mixed phospholipid liposome preparation was made from chloroform stocks of each lipid by mixing each in the following molar ratio: 5% egg phosphatidylserine (PS); 50% egg phosphatidylcholine (PC); 19% bovine phosphatidylethanolamine (PE); 10% bovine phosphatidylinositol (PI), 1% porcine phosphatidylinositol-4,5-bisphosphate (PIP_2), and 15% cholesterol. This mixture seeks to mimic a normal endoplasmic reticulum/Golgi membrane composition. The lipid stocks were combined, dried under a nitrogen stream for 1 hr, and then further dried under vacuum overnight. The dried lipid film was resuspended in buffer (100 mM KCl/25 mM MOPS pH 7.4) and subjected to five rapid freeze-thaw cycles using liquid nitrogen and a 40°C water bath. The lipid mixture was then sonicated in a room-temperature water bath for 10 min and subjected to stepwise extrusion through Whatman polycarbonate filters of decreasing pore size (200nm, 100nm, 50nm, 30nm). Extruded liposomes were prepared immediately prior to the assay being performed and were used at a final concentration of 400 μM.

Two ArfGAP1 enzyme assays were used; one was a colourimetric malachite-green assay and the other was a radiolabelled γ-[^{32}P]-based assay. Both assays measure the release of free phosphate from GTP.

The malachite-green colourimetric assay (Innova Biosciences) was performed to assess the GTPase activity of yeast Arf1 as stimulated by ArfGAP1.

The reactions were performed in a 96-well plate in volumes of 200 μL each. Arf1 (final concentration 0.1 μM) was assayed with and without the presence of ArfGAP1 (final concentration 1 μM). Arf1 in assay buffer (25 mM MOPS pH 7.4/ 50 nM NaCl/ 1 mM $MgCl_2$) was first loaded with GTP (final concentration 250 μM) in the presence of liposomes and incubated at room temp for 12 min. To start the reaction, ArfGAP1 was added and the mixture was incubated for 2 hr at room temp. To stop the reaction, Pi ColorLock dye was added as per manufacturer's recommendations, and incubated for 2 min before stabilizing buffer was added. Colour was left to develop for 30 min prior to being read in a BioTek Synergy LX spectrophotometer at 595 nm. Values were compared to a standard phosphate curve. Background only controls lacking Arf1 were subtracted to account for non-enzymatic hydrolysis of GTP or contamination of the GTP stock with phosphorous. Averages from triplicate reactions were determined with error bars representing standard deviation.

For the radiolabelled ArfGAP1 assay, Arf1 was loaded with GTP in a volume of 150 μL at a concentration of 10 μM Arf1 with 400 μM mixed-composition liposomes in GTP-exchange buffer (25 mM HEPES pH 7.4/1 mM EDTA pH 8/0.5 mM $MgCl_2$/100 mM NaCl). A mix of GTP (final concentration of 25 μM and [γ-^{32}P]-GTP (20 μCi) was added and the GTP loading reaction was incubated for 90 min at 30°C. To stop the loading reaction, $MgCl_2$ was added to a final concentration of 2 mM and the solution was chilled to 4°C. To separate Arf1-GTP from unloaded GTP, the sample was loaded onto a Sephadex G-25 spin

column and centrifuged at 1,500 *g* for 2 min at 4°C. Aliquots of the Arf1-containing eluant were set aside to be counted and compared to post-reaction counts. To determine ArfGAP1 activity, ArfGAP1 (final concentration of 0.5 μM) was added to the Arf1-GTP (final concentration of 1.5 μM) preparation. Samples were incubated for 12 min at room temperature before 20 μL (out of the 25 μL reaction) of the reaction was added to 980 μL of a 5% charcoal solution in 20 mM Na_2HPO_4, mixed, and chilled. Quenched samples were centrifuged at 3,000 *g* for 10 min at 4°C, then 750 μL of the supernatant was removed and mixed with scintillation fluid and counted in a Beckman Coulter LS6500 Liquid Scintillation Counter. Scintillation counts were converted to disintegrations per minute (dpm) and the averages of triplicate reactions were determined with error bars representing sample standard deviation.

Drosophila Maintenance and Strain Construction

Drosophila lines used in this study are tabulated in Table 5. Flies were maintained on standard cornmeal-agar-molasses medium and kept on a 12 hr light/dark (L/D) cycle at 25°C. Dopaminergic driver lines *ddc-Gal4* were obtained from the Bloomington *Drosophila* Stock Center and the *UAS-LRRK2* lines were a kind gift from the lab of Kah-Leong Lim (Duke-NUS). All experiments used McMaster lab-specific stocks where flies from outside sources were back-crossed eight times to the reference line iso31 (a kind gift of Amita Sehgal,

Table 5. *Drosophila* strains used in this study.

Name	Genotype	Reference
ddc-Gal4	w[1118]; +; P{w[+mC]=Ddc-GAL4.L}Lmpt[4.36]	BDSC #7009
UAS-LRRK2-WT10	w[*]; P{w[+mC]=UAS-LRRK2-WT}; +	(Ng et al. 2009)
UAS-LRRK2-G2019S	w[*]; P{w[+mC]=UAS-LRRK2-G2019S}; +	(Ng et al. 2009)
iso31	w[*]; +; +	(Zhang et al. 2018)

UPenn). To express human LRRK2 in a tissue-specific manner, P_1 females carrying a *UAS-LRRK2* variant (wild-type LRRK2 or LRRK2 G2019S) were isolated from peers shortly after eclosion and housed separately to ensure virginity. After five days of no progeny, females were deemed virgins and crossed to P_1 male flies carrying either a *ddc-Gal4* driver (**Figure 10**). The resulting F_1 progeny were collected after eclosion and used in the behavioural experiments.

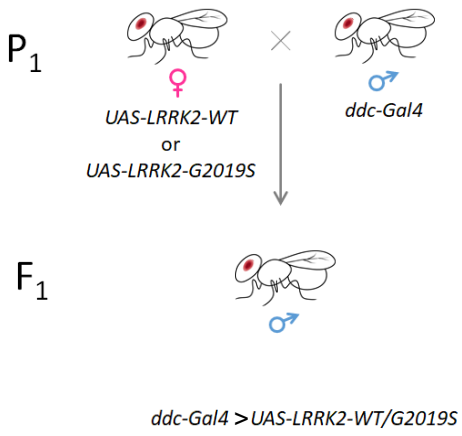

Figure 10. Mating schemes to generate Drosophila strains used in this study.

Virgin female *UAS-LRRK2* (wild-type or variant G2019S) flies were crossed to male *ddc-Gal4* flies to generate progeny that expressed LRRK2 in dopaminergic neurons. Progeny were collected post-eclosion, aged up to 55 days and studied using a locomotion assay.

Maximum Tolerated Dose Assay

Three groups of 30 iso31 flies of various ages and both sexes were transferred to standard fly food, with either compound 4, 12, 13 or a DMSO-matched concentration mixed in. Each compound was tested at maximum concentration achievable, given solubility limitations and a maximum DMSO final concentration of 0.5% (compound 4 at 620 μM, compound 12 at 123 μM , compound 13 at 366 μM). Additionally, three dilutions (1/5, 1/25, and 1/125) of the maximum soluble concentration were tested for each individual compound. The flies were maintained on regular food, compound-containing food, or 0.5% DMSO food for 7 days and survival was scored at the end of the assay. Rates of survival were determined with error bars representing the sample standard deviation of the triplicate experiments.

Drosophila Locomotion Assay

Flies expressing *ddc* only, *ddc-GAL4;UAS-LRRK2*-WT or *ddc-GAL4;UAS-LRRK2* (henceforth referred to as *ddc>LRRK-WT* and *ddc>LRRK-GS)* were selected and aged for 25 days on standard cornmeal-agar food at 25°C, with a 12 hour light/dark cycle. At d25 post-eclosion, flies were transferred to cornmeal-agar medium containing the maximum dissolvable concentration of compound 4, 12, or 13, or DMSO-matched food. Flies continued to be incubated at 25°C, with food/drug changes 3x/week, for a further 30 days.

Locomotion assays were performed on F_1 flies at end of life (day 50 or 55). Locomotion was recorded using activity monitors (DAM 5 TriKinetics). Individual flies were loaded into a capillary with a diameter that permits the fly to walk but not fly. Food was loaded at one end and the capillary closed with a cotton plug. Flies were given 24 hr for acclimatization to the new environment at 25°C with a 12 hr light/dark cycle. Post-entrainment, for an additional 48 hours DAMSystem3 software recorded fly movement as the number of times laser beams bisecting the capillaries were broken by movement of the fly. The counts were binned into 30 min intervals by a custom Python code, averaged to show a representative 24h day from 48 hours of data, and graphed as a function of time. Late-evening peaks in movement were compared across genotypes as bar graphs depicting the total average movement recorded for that 30 min interval, with error bars representing standard deviation. Dead flies, defined as flies that showed no recorded movement for >12 consecutive hours, were excluded from analysis. Flies were randomly selected from their cohort for experiments. For aged flies, all surviving flies were assayed and as such the number of flies for each genotype/condition ranged from 8 to 26.

RESULTS

Yeast Based Screen to Identify Potential Human ArfGAP1 Small Molecule Inhibitors

Given that (i) genetic inactivation/knockdown of ArfGAP1 expression in yeast and mammalian cells, including neurons, can prevent the toxicity caused by over-expression of LRRK2 and LRRK2-G2019S, (ii) ArfGAP1 directly binds to LRRK2 and increases its GAP activity, (iii) GAP activity drives LRRK2 kinase activity, (iv) PD-causing LRRK2 variants have increased LRRK2 kinase activity, and (v) many idiopathic PD patients have an increased level of LRRK2 in their brains, we hypothesized that the identification of small molecule inhibitors of ArfGAP1 may prove to (i) be useful probes to further understand the role of ArfGAP1 in cell and organismal biology, (ii) inform on the regulation of LRRK2 and pathogenic forms of LRRK2 by ArfGAP1, and (iii) be a potential starting point to develop therapeutic compounds for the treatment of LRRK2 mediated PD. To find such small molecules, we performed a cell-based high-throughput screen (HTS) for human ArfGAP1 inhibitors.

The budding yeast *Saccharomyces cerevisiae* has been previously used as a cell-based model for small molecule/drug screening. To use yeast in our HTS for human ArfGAP1 inhibitors, we sought to use an overt, easy-to-read phenotype. One of the simplest to observe is growth, which in yeast can be monitored by determining optical density at 600 nm using a spectrophotometer or

plate reader. To perform a high-throughput screen for human ArfGAP1 inhibitors, a yeast strain (*gcs1*Δ *pdr5*Δ *snq2*Δ) lacking the gene encoding the endogenous yeast homologue of ArfGAP1 (*GCS1*) in addition to two ABC transporters known to be effective drug efflux pumps, was transfected with a high-copy plasmid that can express human ArfGAP1 from a galactose-inducible promoter. Yeast cells were seeded at low density in 96-well plates and the expression of ArfGAP1 was induced by the addition of galactose to the medium. The addition of galactose resulted in inhibition of cell growth in cells containing the human ArfGAP1 expressing plasmid compared to empty vector control (**Figure 11**). To identify potential small molecule inhibitors of human ArfGAP1, an HTS of a library of small molecules to identify those that that could reverse ArfGAP1 mediated growth inhibition was performed.

The HTS for human ArfGAP1 small molecule inhibitors was initiated by seeding yeast cells in 96-well plates in the presence of galactose as a carbon source to induce human ArfGAP1 expression. A robotic system supplied compounds at 40 μM from a set of compound libraries comprised of the Prestwick FDA-approved therapeutics library, the Sigma LOPAC 1280 library, the Chembridge DiverSet, and a set of proprietary libraries for a total of just over 100,000 compounds. Each compound was tested at one single concentration and without replicates, due to technical limitations. The optical density at 600 nm was determined after 40 hours of incubation at 30°C to identify compounds that prevented ArfGAP1 mediated cell growth inhibition. Compounds that restored growth >2-fold in

human ArfGAP1-expressing yeast cells over no-compound control were determined. This initial screen identified 14 compounds (**Figure 11**). Comparison of chemical structures of these compounds revealed that seven compounds (compounds 4, 5, 8, 9, 10, 11, and 12) had similar piperazine core structures, suggesting that a specific class of compounds that may inhibit ArfGAP1 toxicity in yeast.

To verify results from the initial drug screen, the growth restoration assay was repeated with eight of the 14 small molecules identified (**Figure 12**) (six were not retested due to lack of compound availability). Three concentrations of each compound were tested (3, 15 and 40 μM). As per the initial HTS, human ArfGAP1-expressing yeast cells were seeded in 96-well plates, and compounds or a DMSO-matched control were added to the wells, with each condition tested once, without replicates, due to limitation of compound availability. After an incubation for 40 hours at 30°C, cell growth was assessed by determining absorbance at 600 nm. Compound 11 showed the maximum restoration of growth at the lowest concentration (3 μM), however most compounds showed maximal activity at 15 μM. Compound 13 showed highest restoration of growth, with a maximum increase of 3.79-fold over DMSO-matched control. Compound 5 showed weakest activity out of the compounds assayed with a maximum growth restoration of 1.87-fold.

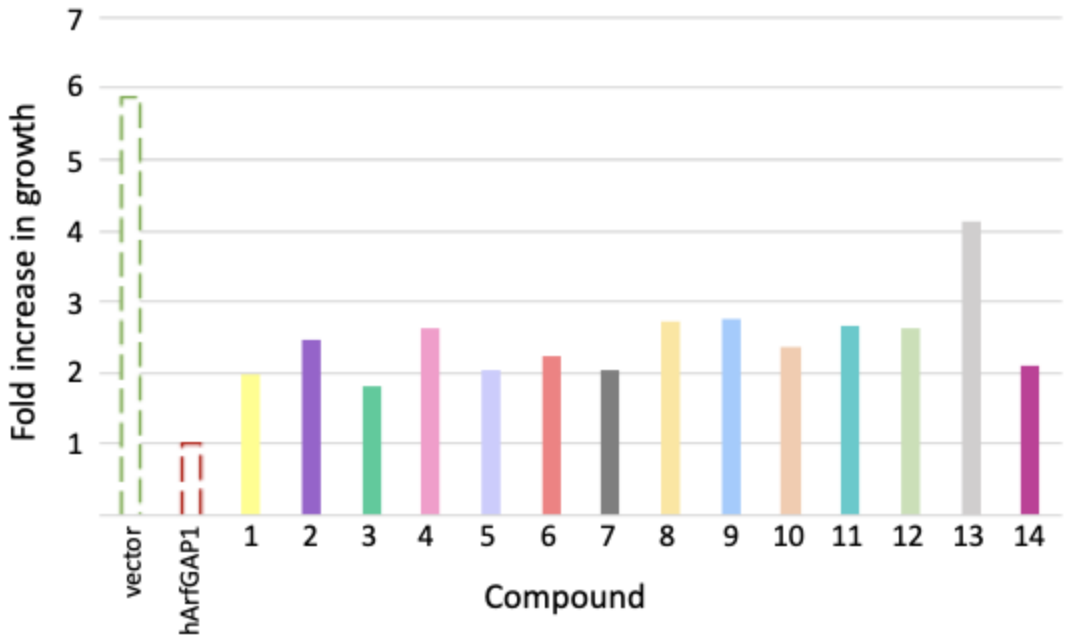

Figure 11. Fourteen compounds were identified from a HTS that decreased human ArfGAP1 growth inhibition in yeast.

Human ArfGAP1-expressing yeast cells in 96-well plates underwent a high-throughput screen for compounds that ameliorated ArfGAP1 toxicity. A series of compound/drug libraries comprising over 100,000 molecules were delivered to yeast at 40 μM and cell growth was determined after a 40 hr incubation at 30°C spectrophotometrically by absorbance at 600 nm. Fourteen compounds that restored growth to cells >2-fold over untreated cells were identified. This initial screen was performed once over the entire set of compound/drug libraries, without technical replicates.

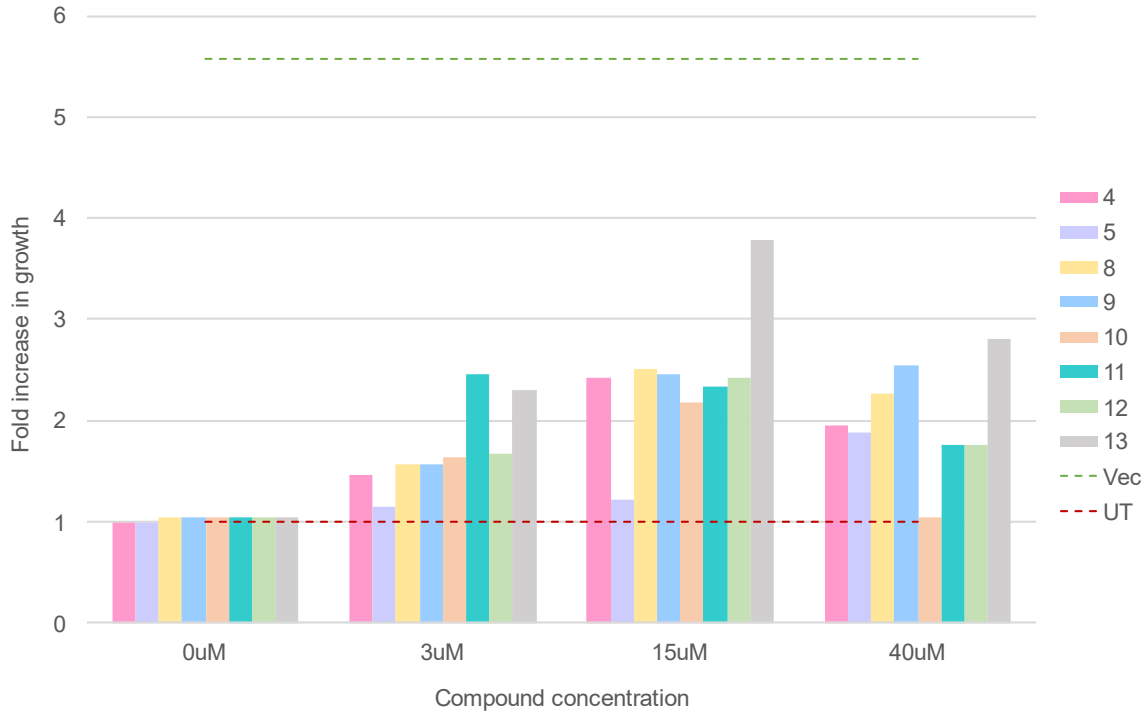

Figure 12. Confirmation of yeast growth rescue with putative ArfGAP1 inhibitors.

Eight compounds from the initial high-throughput screen that ameliorated a growth defect due to human ArfGAP1 expression in yeast cells were re-tested at 3, 15, and 40 μM. and compared to DMSO-matched control strains. Cells were seeded in 96-well plates in a galactose-containing medium in the presence of the indicated compounds for 40 hours at 25°C and cell density was determined spectrophotometrically at 600 nm. Restoration of growth is reported as the fold increase in growth as compared to untreated controls. The green dotted line represents the growth of yeast transformed with an empty vector (Vec) in the absence of compound. The red dotted line is growth of untreated (UT) human ArfGAP1 expressing yeast cells. This secondary screen was performed once, without technical replicates.

Six compounds were reordered from the manufacturer (based on availability) and tested for their capacity to ameliorate the growth defect due to human ArfGAP1 expressed in yeast cells at concentrations from 0 – 25 μM (**Figure 13)**. Compounds 4, 8, 9, 11 and 12 are from a family of structurally related (piperazine-based) small molecules and compound 13 has a unique structure (**Figure 14, Table 6**). All six compounds increased the growth of human ArfGAP1 expressing yeast.

The HTS and follow-up studies imply that a subset of small molecules appear to prevent the growth inhibition caused by expression of human ArfGAP1 in yeast. From these high-throughput proof of concept experiments, I moved on to study in greater depth the role of these compounds in human ArfGAP1 and human LRRK2 mediated growth defects in the yeast system.

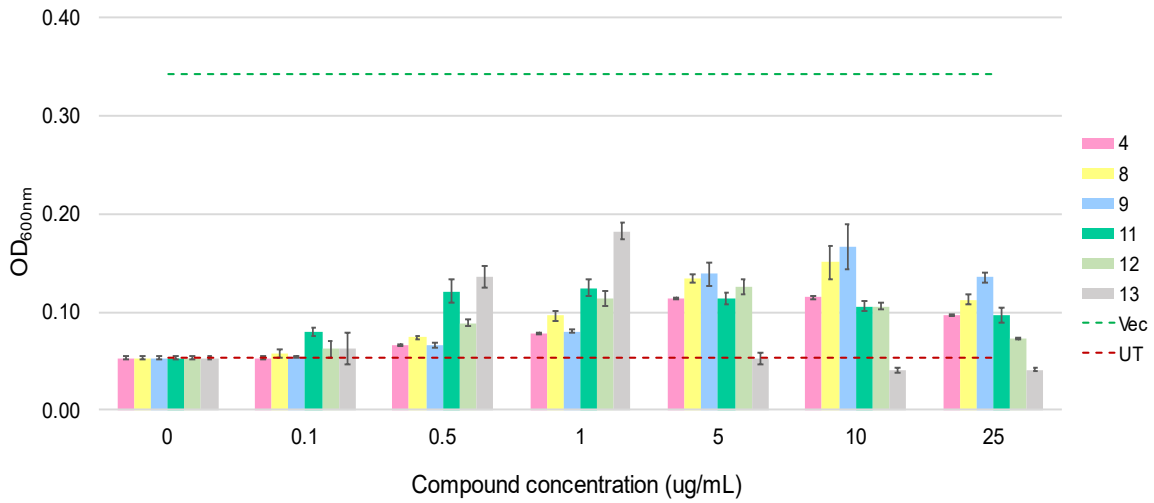

Figure 13. Confirmation of yeast growth rescue with newly purchased putative ArfGAP1 inhibitors.

Newly ordered compounds were re-tested in human ArfGAP1 expressing yeast cells. Cells were seeded in 96-well plates in a galactose-containing medium and incubated with compounds (at either 0, 0.1, 0.5, 1, 5, 10 or 25 µg/mL) for 40 hours at 25°C. Culture density was measured spectrophotometrically at 600 nm after 40 hours. Averages of triplicate wells were plotted as a grouped bar graph, with error bars representing standard deviation. The green dotted line represents the growth of yeast transformed with an empty vector (Vec) in the absence of compound. The red dotted line (UT, untreated) is the growth of yeast cells expressing human ArfGAP1.

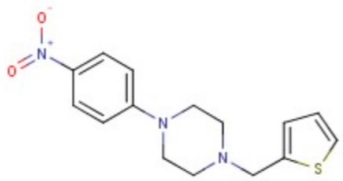

Compound 4

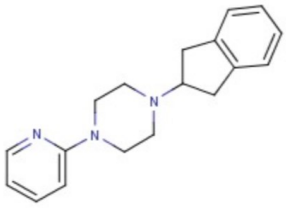

Compound 8

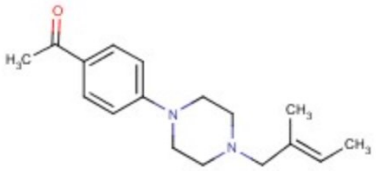

Compound 9

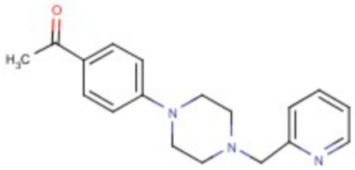

Compound 11

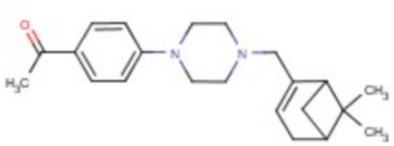

Compound 12

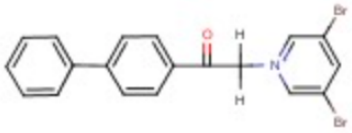

Compound 13

Figure 14. Structure of the six small molecules that prevent toxicity due to human ArfGAP1 expression in yeast.

The compounds are from the Chembridge compound (hit2lead) library.

Table 6. Chemical information for the identified potential ArfGAP1 inhibitors

Compound	Chembridge ID	Formula	M Wt	Chemical name
4	5261344	C15H17N3O2S	303	1-(4-nitrophenyl)-4-(2-thienylmethyl)piperazine oxalate
8	5459804	C18H21N3	279	1-(2,3-dihydro-1H-inden-2-yl)-4-(2-pyridinyl)piperazine
9	5423076	C18H21N3O	295	1-{4-[4-(2-pyridinylmethyl)-1-piperazynyl]phenyl}ethanone
11	5431942	C17H24N2O	272	1-{4-[4-(2-methyl-2-buten-1-yl)-1-piperazinyl]phenyl}ethanone
12	5429814	C22H30N2O	338	1-(4-{4-{(6,6-dimethylbicyclo[3.1.1]hept-2-en-2-yl)methyl]-1-piperazinyl}phenyl)ethanone oxalate
13	5468123	C19H14Br2NO	432	1-[2-(4-biphenylyl)-2-oxoethyl]-3,5-dibromopyridinium

Confirmation of Small Molecule Amelioration of ArfGAP1 and LRRK2 Mediated Cell Growth Defect

A major goal of this research was to prevent LRRK2 toxicity to cells via inhibition of ArfGAP1. We next sought to test the compounds that prevented human ArfGAP1 toxicity to yeast in a yeast model co-expressing human ArfGAP1 and a version of human LRRK2 that had previously been proven to be toxic to yeast cells. This version of LRRK2 contains the region harbouring the GTPase and kinase domains (**Figure 3**) (Xiong et al., 2010).

A yeast strain (*gcs1*Δ *pdr5*Δ *snq2*Δ) lacking the endogenous yeast homologue of ArfGAP1 (*GCS1*), and the two major drug efflux pumps was transfected with multi-copy plasmids that allow for galactose-inducible expression of either human ArfGAP1, human LRRK2 (the GTPase and kinase domain region), or co-expression of both together. Cells were grown in glucose and transferred to galactose-containing medium to induce expression of ArfGAP1 and/or LRRK2 and grown at 30°C. Growth was recorded at regular time points by reading optical density at 600 nm. The growth of strains expressing either ArfGAP1, or LRRK2, or both together is significantly decreased, as compared to the vector-only control strain (**Figure 15**). Assessing the slope of the growth curves, expression of human ArfGAP1 decreased growth to 72% of the control group, LRRK2 to 76% of control, and expression of both to 15% of control. This suggests that the co-expression of ArfGAP1 and LRRK2 has an additive effect

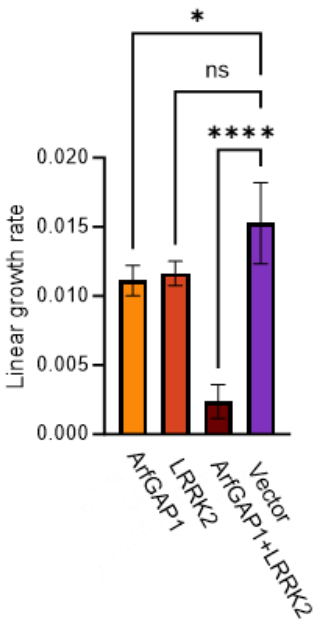

Figure 15. Growth rate of yeast cells expressing human ArfGAP1, human LRRK2 GTPase plus protein kinase domains, or both.

Yeast cells expressing ArfGAP1 or LRRK2, co-expressing ArfGAP1 + LRRK2, or carrying an empty vector were seeded in 96-well plates and incubated for 54 h at 30°C. At regular intervals, the plates were read at 600 nm to score for culture density. Using data from three repetitions of the experiment, slopes were calculated from the linear portion of a growth curve for each genotype (from hour 27 to hour 45) by linear regression using Prism 9 software and plotted as a bar graph. Data is reported as mean +/- standard error of the mean from at least three experiments performed in triplicate. P values were determined using a one-way ANOVA, comparing each genotype to cells expressing empty vector control (*$p \leq 0.05$).

on growth inhibition of yeast cells. Western blot analysis probing for the myc tag on both constructs showed single bands corresponding to expected sizes of ArfGAP1 and the GTPase-protein kinase region of LRRK2 (**Figure 16**). From these data, we can conclude that ArfGAP1 and LRRK2 have been successfully expressed in yeast, and that expression of human ArfGAP1 and LRRK together inhibit yeast cell growth more than either expressed alone. This suggests that yeast may be a suitable system for further exploration of the interplay between human ArfGAP1 and LRRK2.

To determine if the compounds identified in the HTS for potential human ArfGAP1 inhibitors also prevented growth of yeast cells expressing both ArfGAP1 and LRRK2, five compounds from the HTS (4, 8, 11, 12, and 13) were tested at 10 and 50 μM and compared to DMSO-matched controls (compound 9 was no longer available from the vendor). Compounds were also tested on cells carrying an empty vector and found not to affect growth. Out of the five compounds tested four compounds (4, 11, 12, and 13) were found to prevent ArfGAP1-LRRK2 mediated toxicity (**Figure 17**). None of these compounds affected expression of either human ArfGAP1 or LRRK2 in yeast implying that their ability to enable cell growth is not due to decreased gene expression of ArfGAP1 or LRRK2.

Based on an initial HTS of over 100,000 compounds containing known drugs and novel compounds, and subsequent subscreens, four compounds were identified that mitigate the toxic effect of expression of human ArfGAP1, and the additive growth inhibition of human ArfGAP1 plus LRRK2 co-expression, in

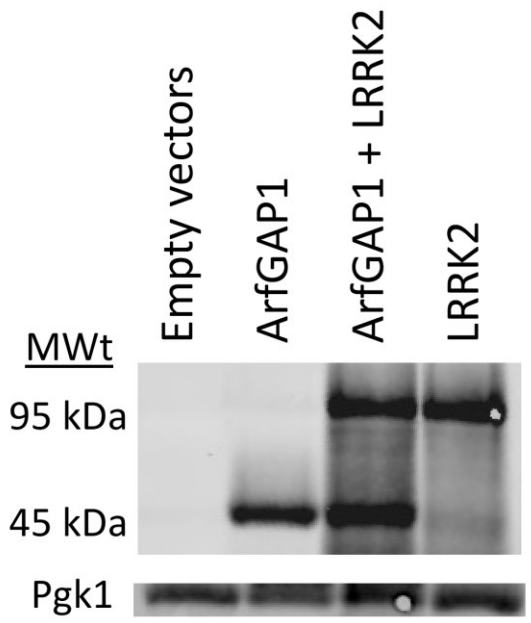

Figure 16. myc-ArfGAP1 and myc-LRRK2 are expressed in yeast.

Yeast cells carrying plasmids expressing human ArfGAP1, truncated LRRK2 (GTPase and protein kinase domains), both, or empty vectors were induced in a galactose medium for 14 hours at 30°C before being lysed by mechanical disruption. Lysates were resolved on a 10% bis-acrylamide gel, transferred to a nitrocellulose membrane, and probed with an anti-myc antibody for tagged hArfAGP1/LRRK2 detection, and anti-Pgk1 as a control for even loading and transfer. Blots were imaged with the LiCor Odyssey scanner, detecting fluorophore-conjugated secondary antibodies.

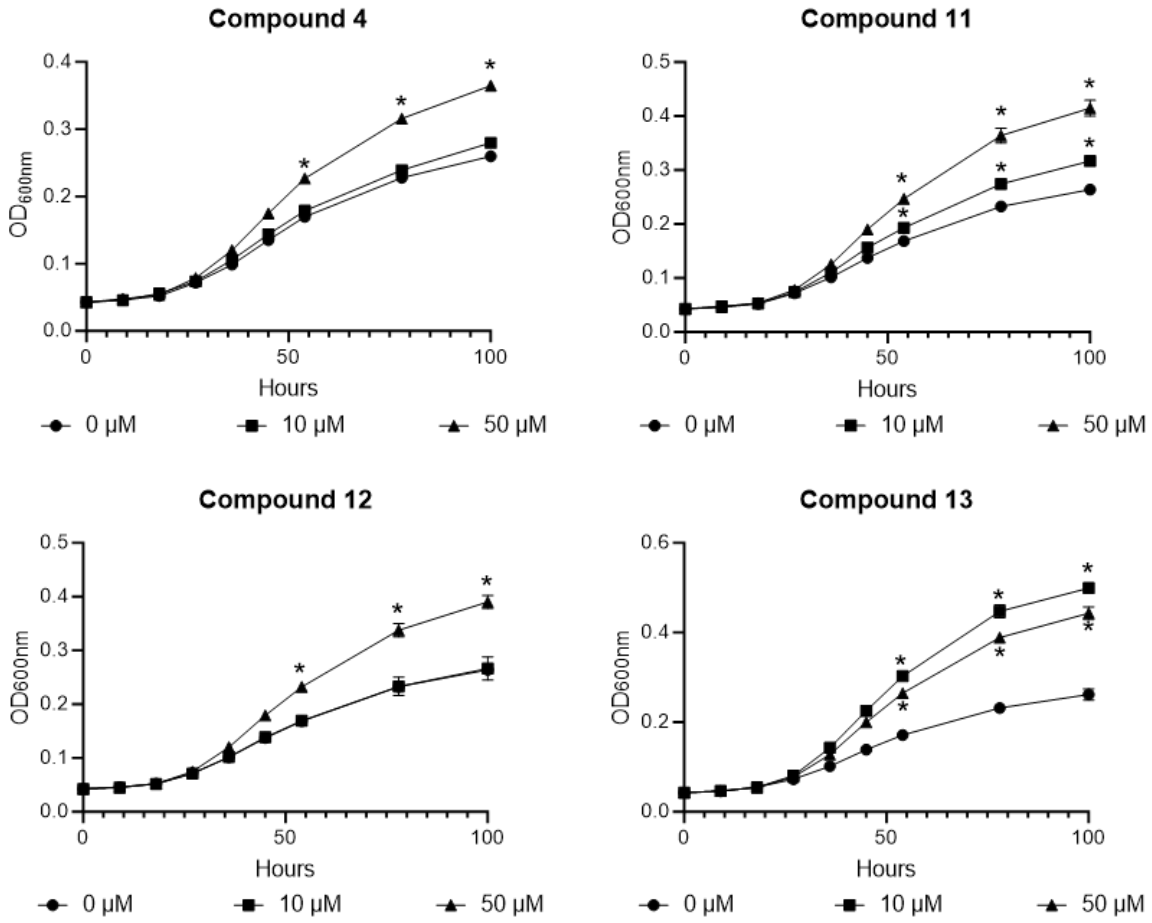

Figure 17. Four compounds restored growth to yeast cells co-expressing ArfGAP1 and LRRK2.

Yeast cells co-expressing ArfGAP1 and LRRK2 were seeded in 96-well plates, treated with one of of the putative ArfGAP1 inhibitors resuspended in DMSO at two different concentration or only DMSO as a control, and incubated for 100 h at 30°C. At regular intervals, the plates were read at 600 nm to score for culture density. Line graphs were generated with mean OD600nm values plotted as a function of time and error bars indicating the standard deviation of triplicate wells.

(Figure 17 legend continues)

A one-way ANOVA was performed comparing the mean growth of compound-treated strains (at t=54, t=78, and t=100) to DMSO-only control (*$p \leq 0.05$).

yeast. As this is a cell-based model we cannot definitively conclude that the four compounds identified directly interact with human ArfGAP1, versus impacting a tangential pathway that may enable yeast to be more fit in the presence of these compounds. We next sought to address if these compounds could directly interact with human ArfGAP1.

Expression and Purification of Human ArfGAP1

We identified putative human ArfGAP1 inhibitors based on their ability to decrease toxicity due to over-expression of ArfGAP1, or ArfGAP1 plus LRRK2, in yeast cells. These compounds could decrease toxicity of ArfGAP1 or ArfGAP1-LRRK2 over-expression indirectly by altering a yeast cell function, or by directly binding to ArfGAP1 and preventing its toxicity directly. To determine if the compounds bind ArfGAP1 directly, microscale thermophoresis (MST) was utilized.

MST to identify protein-compound interactions works best when using purified protein. Mammalian ArfGAP1 has previously proved difficult to express and purify, and a truncated version of the first 257 amino acids of the rat homologue has been routinely used. We sought to purify full-length human ArfGAP1 as we were unsure if the compounds were binding ArfGAP1 in its active site or elsewhere on the protein. The ArfGAP1 open reading frame was subcloned into the pET-16b plasmid, which adds a 10xHis tag to the C-terminus of the encoded protein, and enables IPTG-inducible expression in *E. coli* and purification using a Ni^{2+} resin.

The ArfGAP1 expressing plasmid was transformed into the *E. coli* strain Rosetta2, a BL21(DE3) derivative that carries human rare-codon tRNA plasmids to enable increased expression of human proteins in *E. coli*. Several growth temperatures and IPTG concentrations were used to determine optimal ArfGAP1 expression. Highest expression was obtained using a moderate concentration of IPTG (0.4 mM), a temperature of 20°C during IPTG induction, and an expression time of 4-6 hrs.

Subsequent to cell lysis under non-denaturing conditions, the lysate was separated into soluble and insoluble fractions by centrifugation and purified using Ni^{2+} affinity chromatography. The insoluble fraction was then denatured while the soluble *E. coli* lysate was maintained in non-denaturing conditions. Both fractions were applied to a Ni-NTA column. The column was washed with buffer (25mM Tris pH 8/ 300mM NaCl/ 15 mM imidazole/ protease inhibitors) and ArfGAP1 protein was eluted with 250 mM imidazole. Fractions from the Ni-NTA column were separated by SDS-PAGE and stained with Coomassie blue to determine those that contained ArfGAP1 protein and to determine the level of protein purity. A 45 kDa band at the correct molecular weight of ArfGAP1 was present, however, other contaminating protein bands were also apparent (**Figure 18**), necessitating further purification prior to downstream use in in vitro assays. Approximately 50% of total ArfGAP1 was found in the soluble fraction. Using the soluble fraction for further purification avoids refolding the protein, a process which may not guarantee proper folding into the native conformation, therefore it

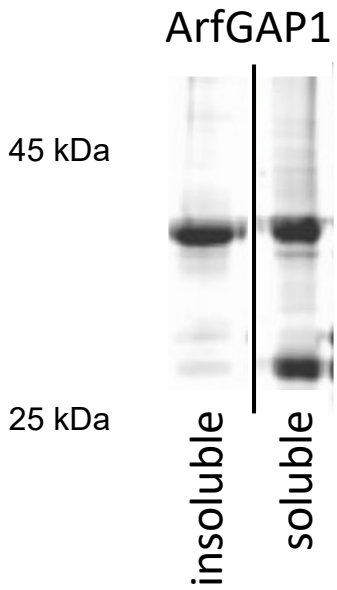

Figure 18. Partitioning of human ArfGAP1 into soluble versus insoluble fractions isolated from E. coli.

To explore whether recombinant ArfGAP1 could be isolated in its native conformation, human ArfGAP1 expression was induced in Rosetta-2 (DE3) *E. coli* using 0.4 mM IPTG for 6 hr at 20°C. Cells were lysed by mechanical disruption and centrifuged at 20,000 *g* for 30 min at 4°C to separate soluble and insoluble fractions. Both fractions were purified using Ni^{2+} affinity chromatography prior to resolution by SDS-PAGE and staining with Coomassie blue. ArfGAP1 is present as a 45 kDa band, however a contaminating band is also present in the preparation purified from the soluble fraction. Here a representative preparation is shown.

was decided that only the soluble fraction from *E. coli* would be used, under non-denaturing conditions, and with additional steps to maximize protein purity and yield.

To improve the purity of ArfGAP1, a modified approach that used several stepwise gradients of increasing amounts of imidazole to elute the proteins bound to the Ni-NTA resin was used. The highest purity was achieved using stepwise elutions of 25 mM, 50 mM, 75 mM, 150 mM, and 250 mM imidazole (**Figure 19**). The ArfGAP1 protein samples were purer than the single 250 mM elution method but did contain a small number of weak contaminating proteins. Fraction were selectively pooled (fractions eluted with 75 mM and 150 mM imidazole), with fractions containing high amounts of contaminating bands excluded from the mix, to maximize ArfGAP1 purity.

To further purify ArfGAP1 from contaminating proteins, and to simultaneously remove the high level of imidazole from the protein preparation, size-exclusion chromatography was employed. This approach has the added flexibility of buffer exchange to remove imidazole from the sample, as well exchanging the buffering component from a Tris to a phosphate buffer. Phosphate buffers are preferable for downstream MST, given that the thermal coefficient of Tris is 10-fold higher than that of phosphate, and thus the buffering capacity of Tris could vary across a thermal gradient. For size-exclusion chromatography, an ÄKTA Pure Fast Protein Liquid Chromatography (FPLC)

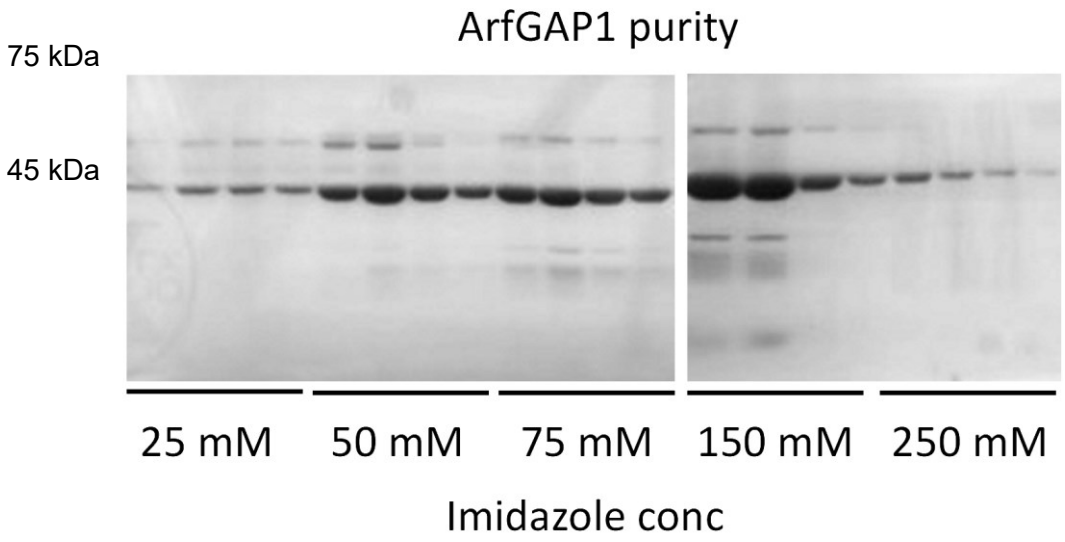

Figure 19. Stepwise elution of His10x-ArfGAP1 increases sample purity.

Rosetta-2 *E. coli* cells expressing human ArfGAP1 were lysed by mechanical disruption and the resulting lysate subjected to purification with Ni-NTA beads. A stepwise elution of increasing concentrations of imidazole (25 mM, 50 mM, 75mM, 150 mM, 250 mM) was employed and fraction individually collected. To evaluate the presence and quantity of contaminating proteins in the eluent, fractions were resolved by SDS-PAGE followed by staining with Coomassie. A representative preparation is shown here with ArfGAP1 as the major species at 45 kDa; highest purity and yield was obtained upon elution with 75 mM imidazole.

system equipped with a Superdex 200 Increase 10/30 column was used. Fractions from the imidazole elution were pooled and concentrated with an Amicon spin filter to 500 μL. The sample was injected into the FPLC system and proteins were eluted using 25 mM NaH_2PO_4/50 mM NaCl buffer, pH 7.4. A UV detector enabled detection of eluted proteins into specific fractions. Fractions containing the highest amount of protein were analyzed by SDS-PAGE (**Figure 20**). There was enrichment of ArfGAP1 protein (eg: fractions 20 and 21) based on the major species being a 45 kDa band. The identity of this band as human ArfGAP1 was confirmed by LC-MS/MS.

Microscale Thermophoresis to Detect Interaction Between Human ArfGAP1 and Proposed Small Molecule Inhibitors

MST assesses binding of a ligand to a target molecule by measuring the change in movement of a protein along a thermal gradient induced by an infrared laser. There are two main MST platforms with protein movement tracked using a detection laser through either intrinsic protein (tryptophan, Trp) fluorescence or by fluorescent labelling of the protein. Each has specific requirements that must be met for a protein to be considered amenable to MST analysis; for example, the intrinsic Trp fluorescence method requires protein that is purified to near homogeneity. I used MST to determine if human ArfGAP1 can directly bind to three of the putative ArfGAP1 small molecule inhibitors identified in our high-

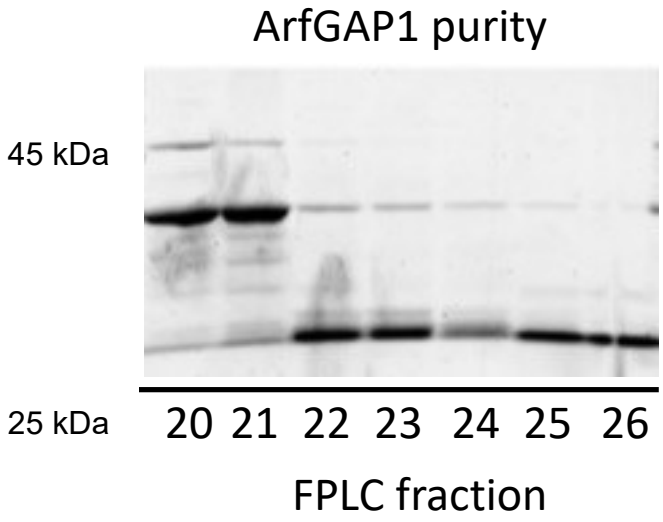

Figure 20. Size-exclusion chromatography increases purity of full-length ArfGAP1.

Fractions of $Ni2^{+}$-purified human 10x-His ArfGAP1 eluted with 75 mM imidazole were pooled and subjected to size-exclusion chromatography as a second step of purification. The sample was injected into a Superdex 200 Increase 10/30 column operated by the ÄKTA Pure Fast Protein Liquid Chromatography system. Fractions were eluted based on size and analyzed by SDS-PAGE and Coomassie staining to identify fractions yielding full-length ArfGAP1 (fractions 20 and 21).

throughput screen (compounds 4, 12, and 13). I utilized both the intrinsic ArfGAP1 fluorescence method, and labelling of ArfGAP1 with a fluorescent tag, to determine the best MST method to detect small molecule binding to ArfGAP1. Intrinsic human ArfGAP1 fluorescence (label-free MST) detects Trp residues present in proteins via detection at 280 nm. Human ArfGAP1 contains eleven Trp residues and thus may offer enough intrinsic fluorescence to not require fluorescent labelling of the protein. To test this, I performed a pre-MST quality check by measuring Abs_{280} of 50 nM ArfGAP1 against a buffer-only control. At this concentration, 10xHis-ArfGAP1 showed fluorescence within an optimal range of detection (**Figure 21**). Pre- and post- assay peaks showed no major decrease in fluorescence magnitude indicating that the infrared laser used to induce the thermal gradient did not compromise the structure of ArfGAP1 to the extent where its Trp fluorescence was altered. The shapes of the fluorescent peaks do not indicate aggregation of the protein within solution or adsorption to the capillary wall (e.g. bimodal peaks or scattered peaks). These data suggest that ArfGAP1 would be an appropriate target for label-free MST.

Having verified that purified human 10xHis-ArfGAP1 may be suitable for label-free MST, I then checked the buffer and putative ArfGAP1 inhibitors to determine if background autofluorescence might interfere. Capillaries contained buffer alone, or 100 μM of compound 4, compound 12, or compound 13 and a fluorescence check was performed (**Figure 22**). Compound 4 displayed

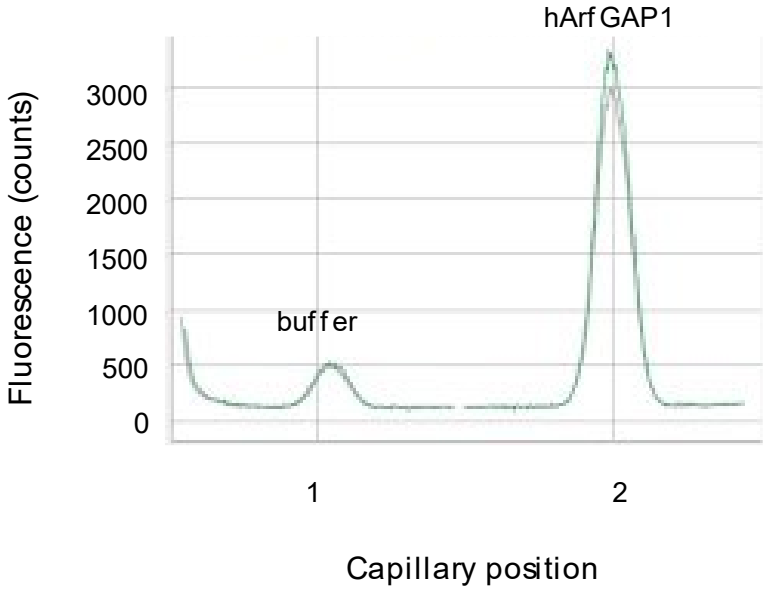

Figure 21. Intrinsic ArfGAP1 fluorescence is detectable with label-free MST.

A solution of 50 nM human ArfGAP1 in 10mM PIPES pH 7.4/150 mM $NaCl_2$, or buffer-only (no protein) control, was read in the Monolith NT.LabelFree at 280 nm. The graph depicts single-capillary readings at 280 nm, prior to induction of the thermal gradient (green line) and post (grey line). Fluorescence checks shown here fall within the detectable range using 40% excitation power of the detecting laser and the medium setting of the infrared laser. No appreciable loss of fluorescence signal was observed post-MST, suggesting protein stability within the thermal gradient.

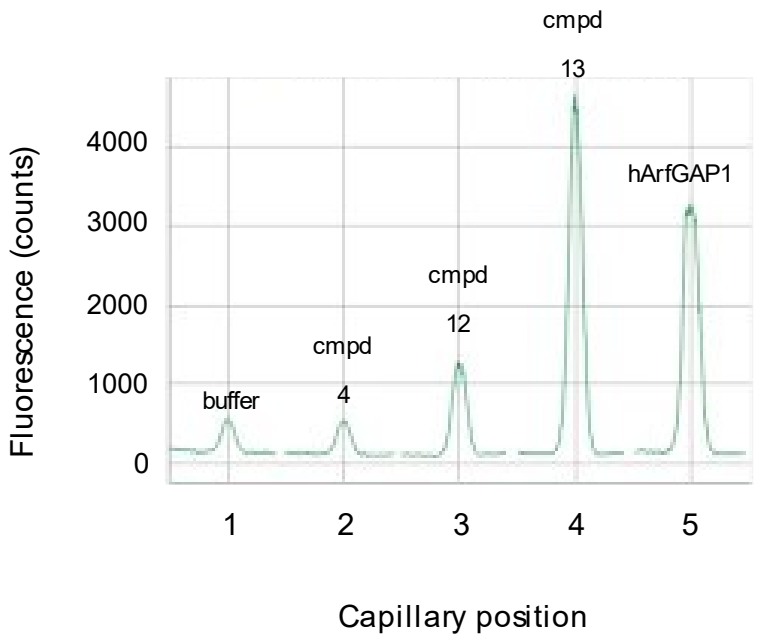

Figure 22. Compound 13 displays high autofluorescence at 280 nm.

Compounds 4, 12, and 13 were tested for autofluorescence at 280 nm by loading capillaries with a buffer-only control for compound 4, compound 12, or compound 13 at 100 μM, or ArfGAP1 at 50 nM, in 10 mM PIPES pH 7.4/150 mM $NaCl_2$. Capillaries were read in the Monolith NT LabelFree at 280 nm using 40% excitation power of the detecting laser and the medium setting of the infrared laser. Compound 13, displaying higher fluorescence than ArfGAP1, was found to be incompatible for downstream binding assays due to this high intrinsic fluorescence at 280 nm.

approximately the same minimal level background fluorescence as buffer alone while the fluorescence of compound 12 was about one third the level of that of ArfGAP1, which is a high but acceptable level of background. However, compound 13, the small molecule from the screen that does not structurally resemble the others, displayed 1.3 times the fluorescence of ArfGAP1. Therefore compound 13 would be unsuitable for testing using label-free MST with human ArfGAP1.

Given that compound 4 passed pre-MST background checks on the Monolith NT LabelFree, I performed a preliminary MST assay testing two concentrations of compound 4 (36.5 μM and 1.88 μM) with a constant concentration of ArfGAP1. **Figure 23** shows the fluorescence peaks as compared to compound-free and protein-free controls. At both concentrations, the total fluorescence of ArfGAP1 is reduced to approximately half of the ArfGAP1-only control. This loss of fluorescence signal surpasses the recommended range for variation in fluorescence across capillaries, which is 10%. Therefore, the detection laser at Abs 280 does not seem suitable to assess interaction between compound 4 and ArfGAP1. It was thus decided to try an alternative MST approach by labelling ArfGAP1 with a fluorophore and using the red channel of a Monolith NT.115 at 650 nm.

Purified 10xHis-ArfGAP1 was labelled with a red NTA dye as per manufacturer's (Monolith) protocol and tested for fluorescence in the NT.115. The protein was detectable within the readable range for the Monolith NT.115 at

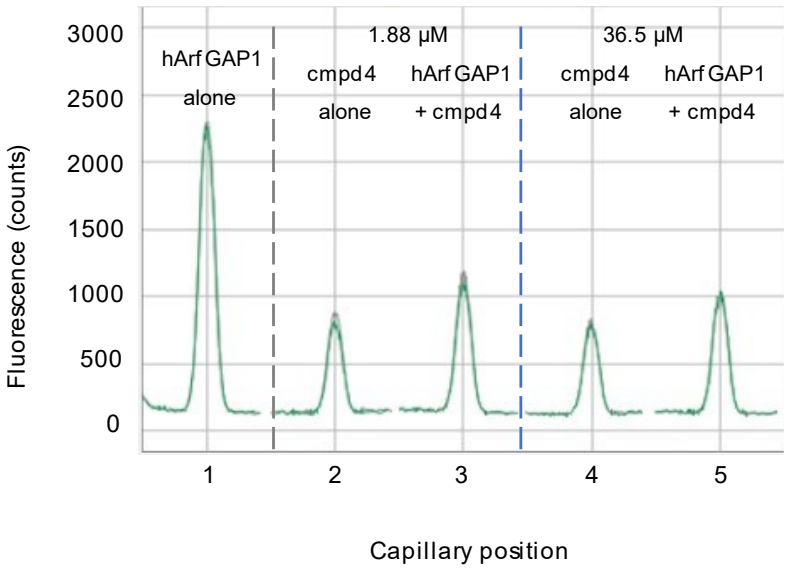

Figure 23. Compound 4 decreases ArfGAP1 intrinsic fluorescence by half.

Compound 4 was assessed for fluorescence alone and with 50nM ArfGAP1 at two different concentrations (1.88 µM and 36.5 µM) in 10mM PIPES pH 7.4/150mM $NaCl_2$. Capillaries (one per condition) were read in the Monolith NT LabelFree at 280nm using 40% excitation power of the detecting laser and the medium setting of the infrared laser. The fluorescence of ArfGAP1 was substantially decreased upon addition of compound 4, surpassing the limit recommended by the manufacturer for variation in fluorescence between samples. Compound 4 was thus deemed incompatible for a binding assay with the Monolith NT Label Free and an alternative approach was warranted.

650 nm (200 to 1500 fluorescence counts) at the tested concentration of 50 nM ArfGAP1. The protocol appropriately dye-labelled ArfGAP1. I performed binding check assays with three compounds (4, 12, and 13) assessing binding at one concentration of each drug in quadruplicate capillaries (**Figure 24**). Monolith (MO.Control) software recorded the movement of ArfGAP1 before, during, and after the induction of the thermal gradient, recording a baseline value prior to induction of the gradient (termed "F_{cold}") and a value after the MST laser is turned on (termed "F_{hot}"). The F_{hot} values were compared, measuring the difference between F_{hot} values of ArfGAP1 alone versus ArfGAP1 incubated with a compound undergoing testing for binding. A difference in fluorescence readings between ArfGAP1 alone and ArfGAP1 + compound is consistent with altered protein mobility along the thermal gradient in the aqueous environment of the capillary, thus suggesting that a binding activity between ArfGAP1 and the compound may be taking place that affects the hydrodynamic movement of the protein. Readings between quadruplicate capillaries of each condition were taken and a "noise" value was calculated by MO.Control software. The signal-to-noise ratio was then determined. A signal to noise ratio greater than 5 suggests an acceptable assay and greater than 12 is considered excellent, as per the manufacturer's guidelines. Each tested at a concentration of 500 μM, compound 4 yielded a ratio of 12.8, compound 12 gave a ratio of 15.5, and compound 13 resulted in a ratio of 31.3. These results suggest that all three compounds directly bind purified ArfGAP1.

A

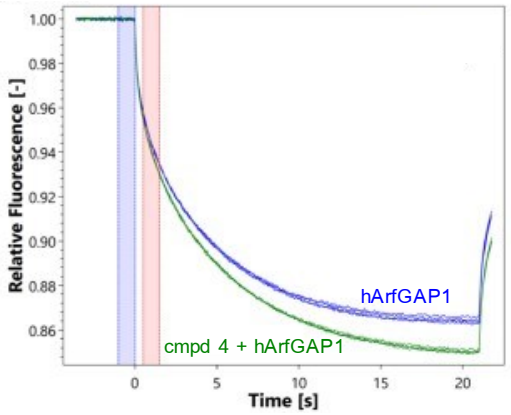

At t = 1 sec:

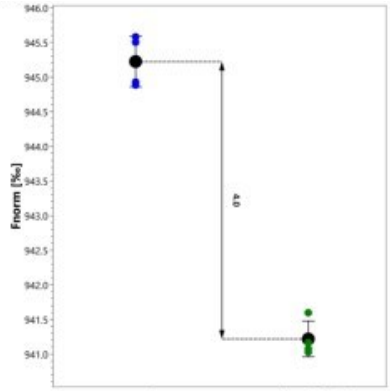

	hArfGAP1	Compound 4 + hArfGAP1
Response	945	941
Noise	0.4	0.3
Response amplitude	4.0	
Signal : noise	12.8	

B

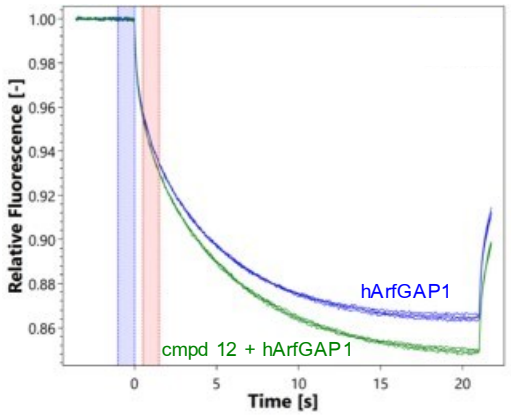

At t = 1 sec:

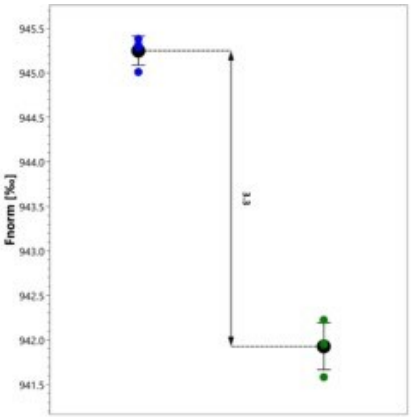

	hArfGAP1	Compound 12 + hArfGAP1
Response	945	942
Noise	0.2	0.3
Response amplitude	3.3	
Signal : noise	15.5	

C

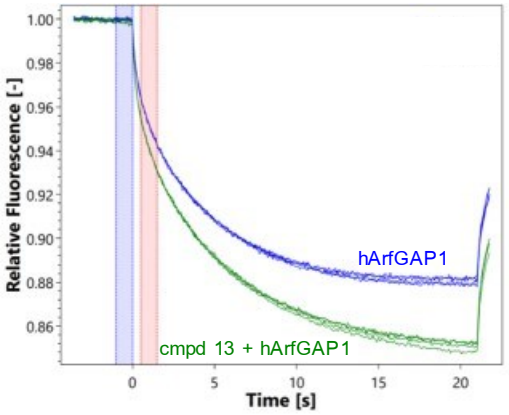

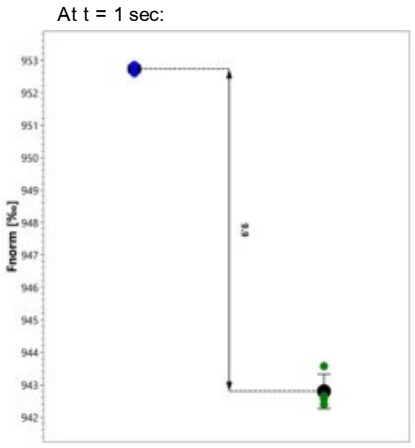

	hArfGAP1	Compound 13 + hArfGAP1
Response	953	943
Noise	0.1	0.5
Response amplitude	9.9	
Signal : noise	31.1	

Figure 24. Compounds 4, 12 and 13 bind ArfGAP1 in vitro.

To determine whether ArfGAP1 binds any of the three compounds tested, binding checks were performed using the Monolith NT.115 with one concentration (0.5 mM) of compound 4 (**A**), compound 12 (**B**) or compound 13 (**C**) and fluorescently-labelled human ArfGAP1 using the red channel. Compounds were incubated with either 100 nM labelled ArfGAP1 (compounds 4 and 12) or 50 nM labelled ArfGAP1 (compound 13) in PBS + 0.05% Tween-20. For 50 nM ArfGAP1, capillaries were read using 40% excitation power of the detecting laser and the medium setting of the infrared laser; for 100 nM ArfGAP1, capillaries were read using 20% excitation power of the detecting laser and the

(Figure 24 legend continued)

medium setting of the infrared laser. Quadruplicate capillaries were read for each condition to assess the signal-to-noise ratio. MO.Control software (provided by the manufacturer) plotted movement of the protein, as a loss of fluorescence signal as a function of time, with each individual line representing a single capillary. Prior to induction of the thermal gradient, baseline readings of fluorescence were found to be stable and a baseline value (F_{cold}, blue shaded area) was recorded. At t = 0 sec, the MST laser was turned on and the system selected an F_{hot} (red shaded area) value at t = 1 sec for each assay, to compare to baseline. The system then calculated the signal (mean fluorescence) to noise (standard deviation) ratio, comparing the F_{hot} values of ArfGAP1-only capillaries to the capillaries containing ArfGAP1 and a compound. Binding is considered likely when a signal to noise ratio exceeds 5.

In addition to determining whether or not a small molecule binds to a protein, MST can also provide a quantitative estimate of K_d, a measure of binding affinity. For this experiment, a serial dilution of drug is prepared and a constant concentration of labelled ArfGAP1 is added to each capillary (**Figure 25**). Similar to the binding checks, MO.Control software measures the difference between F_{hot} and F_{cold} (F_{norm}) values of each capillary representing a single replicate, and plots the dose-response data to fits a sigmoidal curve to estimate the K_d value. For all three compounds tested, solubility issues prevented higher concentration to be used and thus a K_d value was unable to be determined. However, as a dose response curve was apparent, these results lend further credence to compounds, 4, 12, and 13 directly binding to human ArfGAP1.

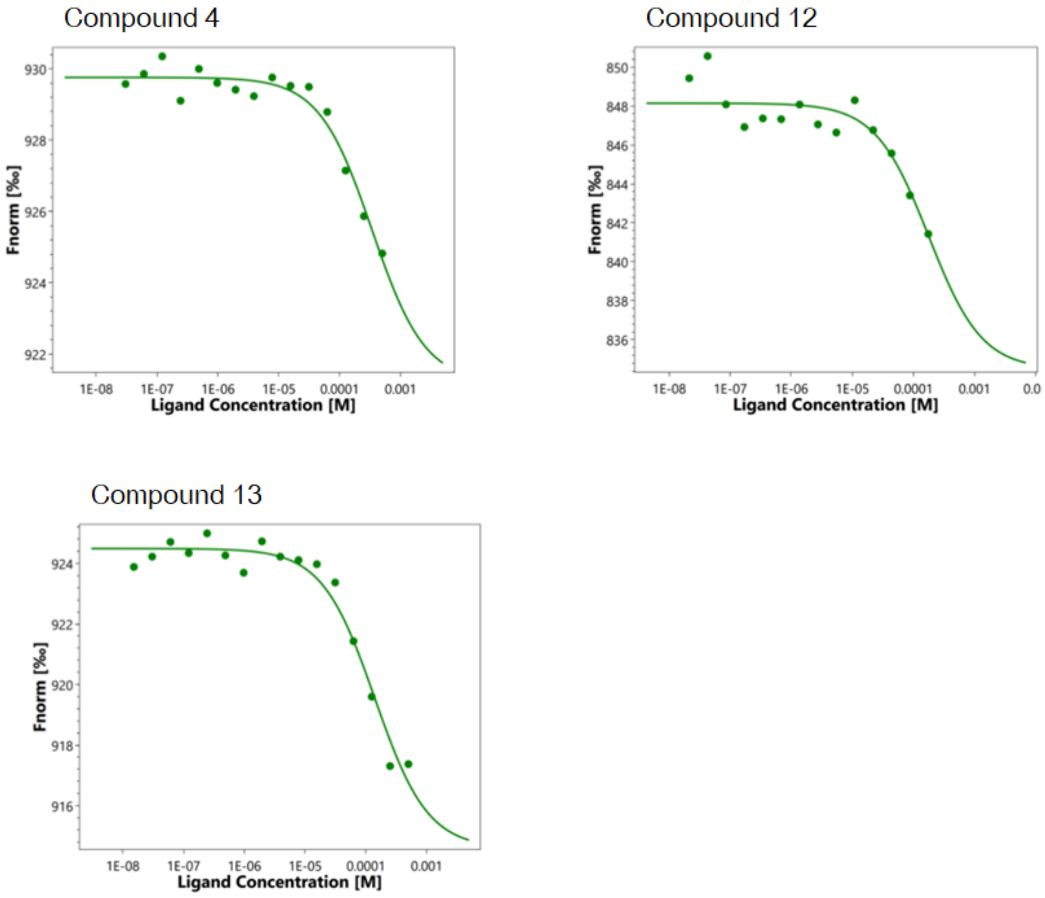

Figure 25. MST determination of compound binding to ArfGAP1.

To estimate K_d values of the binding event between ArfGAP1 and compounds 4, 12 and 13, sixteen MST capillaries containing a 1:2 serial dilution of each compound tested were assayed with 50 nM labelled 10xHis-ArfGAP1 added to each compound dilution. The capillaries were read in the Monolith NT.115 on the red channel at 20% excitation power of the detection laser and the medium setting of the infrared laser. After induction of the thermal gradient with the MST laser, MO.Control software plotted the fluorescence readings (F_{norm}, as a

(Figure 25 legend continues)

measure of protein movement) from each capillary as a function of compound concentration. This experiment was repeated three time for each compound and a representative graph of each is shown here.

Determining Human ArfGAP1 Enzyme Activity

The MST assay, while useful in assessing binding, does not answer the question of whether the compounds inhibit ArfGAP1 GAP activity. I sought to address this by performing an in vitro GTPase assay as a readout of enzymatic ArfGAP1 activity. An enzyme substrate for ArfGAP1 is required to determine its activating potential. Previous studies determined that yeast Arf1 (yArf1) is an excellent human ArfGAP1 substrate. In addition, yArf1 was chosen as LRRK2 is a very large 286 kDa protein that is very difficult to purify to homogeneity while maintaining activity.

Arf proteins require the addition of a 14 carbon myristoyl fatty acid on its second amino acid residue for activity. To achieve purification of an active form of a 6Hisx-tagged yArf1 a previously established *E. coli* expression system where there is co-expression of the His-tagged yArf1 along with a yeast myristoyltransferase (Nmt1) along with the addition of myristate to the culture medium. Several IPTG concentrations, time frames for gene expression, and growth temperatures were tested. The highest yield was obtained with induction of gene expression using 0.1mM IPTG for 14 hr at 22°C. The 6His-tagged Arf1 was purified using a Ni-NTA column and a stepwise imidazole gradient of 25 mM, 50 mM, 75 mM, and 150 mM. This produced a pure sample of yArf1 (**Figure 26**).

Figure 26. Yeast Arf1 was recombinantly expressed and purified from *E. coli.*

BL21(DE3) cells expressing polyhistidine-tagged yeast Arf1 were lysed by mechanical disruption and the resulting lysate purified with Ni-NTA beads. Yeast Arf1 was eluted with imidazole and fractions were concentrated and dialyzed with 20mM Tris pH 8/100 mM NaCl/1mM DTT/1mM $MgCl_2$. Final purity of the sample was assessed by SDS-PAGE and Coomassie staining. The 20 kDa band observed is at the expected MWt for yeast Arf1.

The sample was dialyzed versus 10 mM Tris-HCl buffer (pH 7.4) to remove imidazole prior to use in the GTPase assays.

The most common method to determine ArfGAP1 activity is measuring the free phosphate that is released upon the hydrolysis of GTP to GDP. This can be achieved by employing the dye malachite green which binds free phosphate and produces a colour change that can be measured spectrophotometrically. An alternative approach uses radioactive [^{32}P] γ-labelled GTP and determines the release of the radiolabeled phosphate that is then separated from its substrate, with radioactive phosphate release determined by scintillation counting as a readout of GTPase activity. Determining ArfGAP1 activity is complicated by the fact that the substrate yArf1 displays low intrinsic GTPase activity, hence adding more substrate results in higher background GTPase activity. In addition, ArfGAP1 contains an amphipathic lipid packing sensor motif that requires a curved membrane surface, preferably an in vitro ER/Golgi membrane mimetic for optimal activity. Also, Arf proteins are myristoylated and require embedding into a membrane for loading of GTP onto Arf1. Here, I tested several conditions using both the dye release and radiolabeled enzyme activity approaches to find optimal conditions for determining ArfGAP1 enzyme activity.

Using the colourimetric assay to assess the in vitro activity of ArfGAP1, yArf1 was first loaded with GTP in the presence of liposomes. Initially I used liposomes comprised solely of 1,2-dimyristoyl-sn-glycero-3-phosphocholine (DMPC) solubilized by the addition of cholate. ArfGAP1 was added to the Arf1-

liposome mixture to start the reaction. The samples were left to incubate for 30 minutes at room temperature prior to the reaction being stopped upon addition of a malachite-green dye solution and stabilizing buffer. The colour generated was read spectrophotometrically at Abs 595 nm. A GTP-only (no yArf1) sample was used to subtract background from the autohydrolysis of GTP during the reaction and for any free phosphate that may be present in the protein or GTP preparation. Various protein concentrations and ratios were tested and it was found that ArfGAP1 present in 10-fold excess over yArf1 was the optimal enzyme to substrate ratio for activity in this assay (**Figure 27**). Using this method, the increase in GAP-stimulated GTPase activity was found to not be statistically significant ($p = 0.2277$) and thus additional conditions were tested to optimize the assay.

Aside from DMPC liposomes, mixed-composition liposomes have also been used as a Golgi membrane mimetic to assay for in vitro ArfGAP1 activity. To that end, I repeated the assay using liposomes consisting of 5% phosphatidylserine, 50% phosphatidylcholine, 19% phosphatidylethanolamine, 10% phosphatidylinositol, and 16% cholesterol. Two concentrations of liposome were tested, 200 and 400 μM (**Figure 28**). A concentration of 200 μM resulted in increased Arf1-only hydrolysis and decreased ArfGAP1-stimulated hydrolysis. The increase in activity upon addition of ArfGAP1 was found to be non-significant ($p = 0.2329$). Using liposomes at a higher concentration (400 μM) yielded a 2-fold

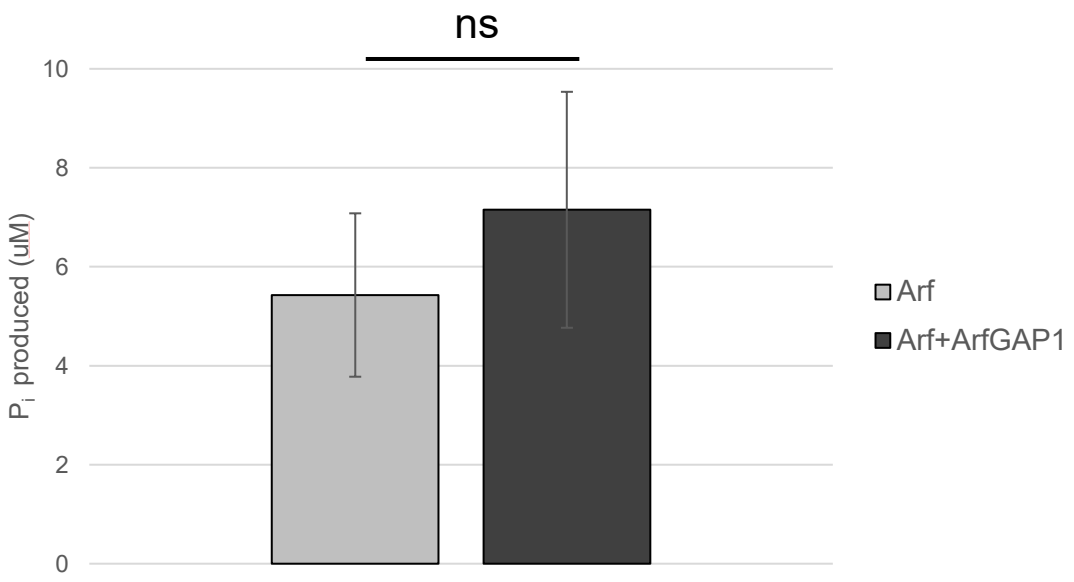

Figure 27. ArfGAP1 GTPase activation of Arf1 is not increased significantly in the presence of DMPC liposomes using the phosphate dye binding assay.

Purified Arf1 was loaded with GTP in the presence of DMPC liposomes and incubated alone or with ArfGAP1. Generation of free phosphate was detected by addition of a malachite green dye and spectrophotometric reading of absorbance at 595 nm. Mean values of triplicate reactions were plotted with error bars representing standard deviation. The data were analyzed with an unpaired two-tail t-test and a p value of less than 0.05 was deemed statistically significant.

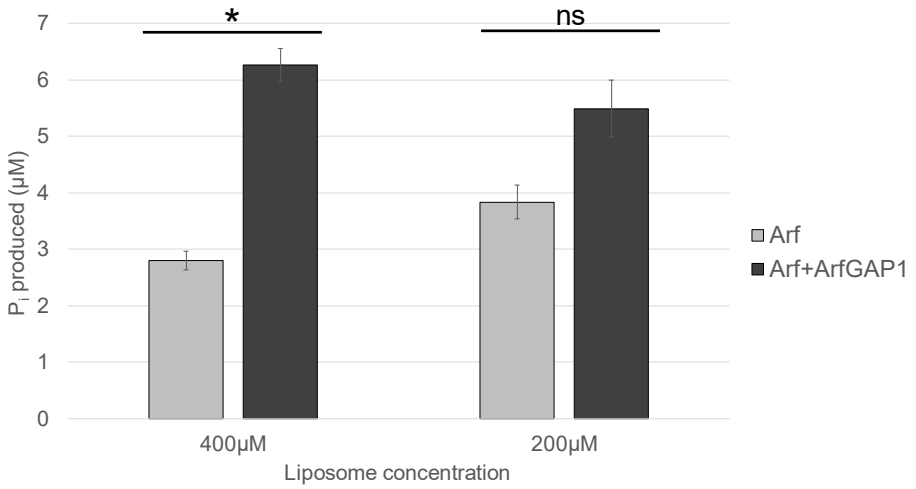

Figure 28. ArfGAP1 increases GTPase activity of Arf1 in the presence of mixed-composition liposomes.

Mixed-composition liposomes were prepared as an ER/Golgi membrane mimetic by combining 5% phosphatidylserine, 50% phosphatidylcholine, 19% egg phosphatidylethanolamine, 10% soy phosphatidylinositol, and 16% cholesterol, and extruding through a 50nm polycarbonate membrane. Purified Arf1 was loaded with GTP in the presence of the mixed-composition liposomes and incubated alone or with ArfGAP1. Generation of free phosphate was detected by addition of a malachite green dye and spectrophotometric reading of absorbance at 595 nm. Mean values of triplicate reactions were plotted with error bars representing standard deviation. The data were analyzed with an unpaired two-tail t-test and a p value of less than 0.05 was deemed statistically significant.

increase of hydrolysis due to GAP activity, a result that was found to be statistically significant ($p = 0.0016$), however, it was concluded that the malachite green assay for GTPase activity was not sensitive enough to test our putative GAP1 inhibitors, and a more sensitive approach was considered.

A radioactive ArfGAP1 assay was employed to determine if a larger signal to noise ratio could be attained. yArf1 is first loaded with GTP in the presence of the mixed-composition liposomes using a modified version of a previously published protocol (Singh et al. 2015). To do so, EDTA was added to chelate the Mg^{2+} that is integral for yArf1 GTP and GDP binding. Radiolabeled GTP was added in excess to enable substrate loading, and $MgCl_2$ was then added to stabilize the bound GTP. The goal of this step was to release yArf1-bound nucleotides and replace them with γ-[^{32}P]-GTP. The loaded yArf1 was then separated from free GTP, and the reaction was started upon the addition of 500 nM ArfGAP1. The reaction proceeded for 10 min at room temperature before being quenched with a charcoal solution that binds nucleotides but does not bind free phosphate. The charcoal solution was centrifuged and the supernatant containing released [^{32}P]-phosphate was assessed by scintillation counting.

The yArf1-only enzymatic activity was determined to be 2-fold increased above control (no yArf1) (**Figure 29**). When ArfGAP1 was incubated with yArf1 total activity was almost 7-fold over control. This level of measurable ArfGAP1 activity provided a more favourable assay to test inhibition of the small-molecule compounds 4, 12, and 13. Addition of compounds 4, 12, or 13 (each added at

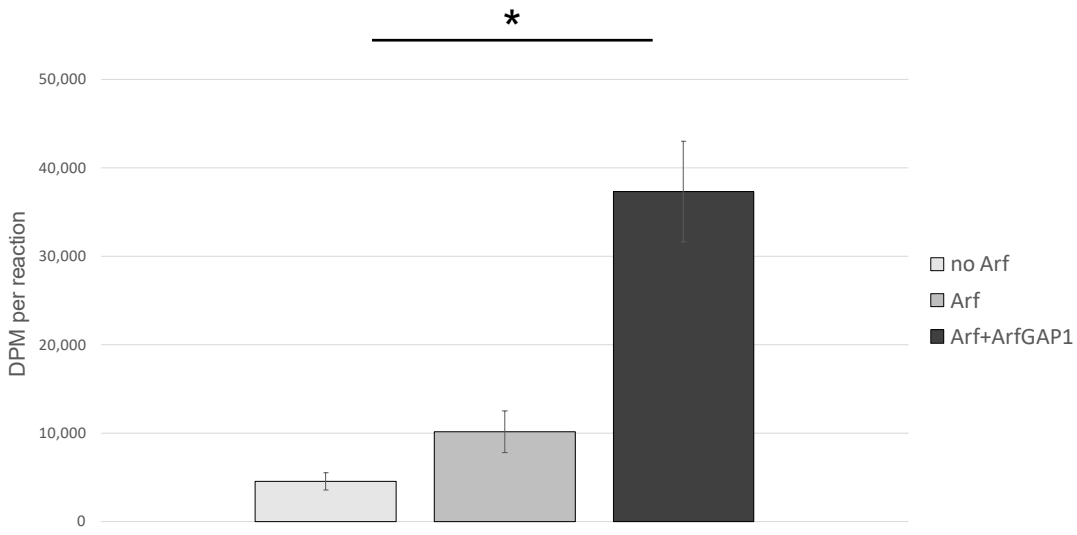

Figure 29. ArfGAP1 increases Arf1 GTPase activity in a radiolabelled in vitro assay.

Purified Arf1 was loaded with GTPγ^{32}P in the presence of the mixed-composition liposomes and incubated alone or with ArfGAP1. Samples were incubated at room temperature and the reaction was quenched upon the addition of a 5% charcoal solution. Free [^{32}P] phosphate was measured using a scintillation counter and disintegrations per minute (DPM) recorded. Mean values of triplicate reactions were plotted with error bars representing standard deviation. The data were analyzed with an unpaired two-tail t-test and a p value of less than 0.05 was deemed statistically significant.

different concentrations so as to test the upper limit of their solubility in the assay conditions) did not reveal inhibition of human ArfGAP1 GAP activity (**Figures 30-32**). The inability to observe inhibition of human ArfGAP1 enzymatic activity could be due to several factors. The compounds may affect ArfGAP1 function (i) through inhibition of a process that is not via direct inhibition of GAP function (point mutants have been made in mammalian ArfGAP1 that inhibit its role in Golgi-derived stability that do not affect its GAP activity), (ii) be weak inhibitors of GAP enzyme activity that require higher concentrations of compound than could be delivered in the enzyme assay, or (iii) be more specific to inhibition of GAP activity when using human LRRK2 as a substrate versus yArf1.

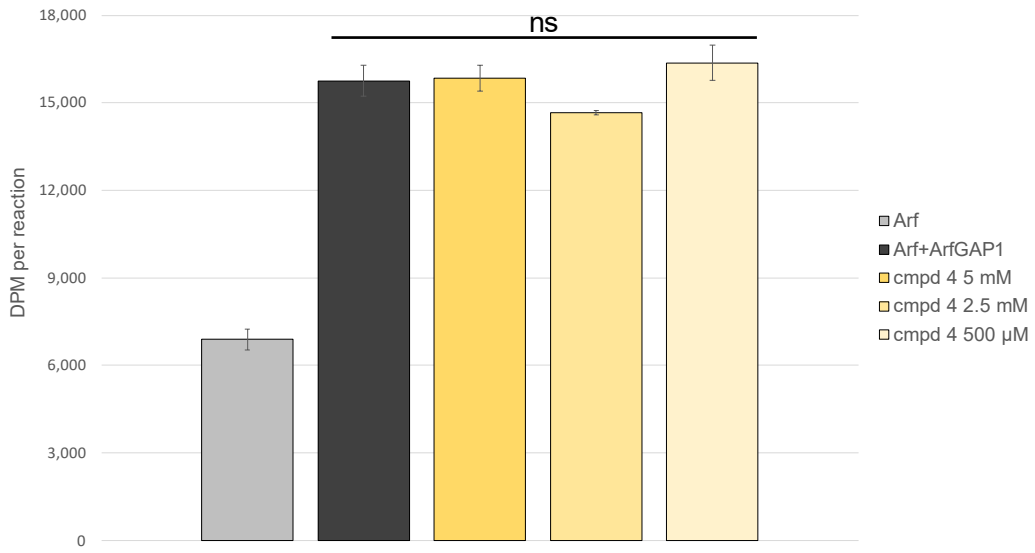

Figure 30. Compound 4 does not affect ArfGAP1 activity in a radiolabelled in vitro assay.

Purified Arf1 was loaded with GTPγ^{32}P in the presence of the mixed-composition liposomes and incubated alone or with ArfGAP1. Samples were incubated at room temperature with either DMSO or compound 4 (5 mM, 2.5 mM or 500 µM), and the reaction was quenched upon the addition of a 5% charcoal solution. Free [^{32}P] phosphate was measured using a scintillation counter and disintegrations per minute (DPM) recorded. Mean values of triplicate reactions were plotted with error bars representing standard deviation. The data were analyzed with a one-way ANOVA and a p value of less than 0.05 was deemed statistically significant.

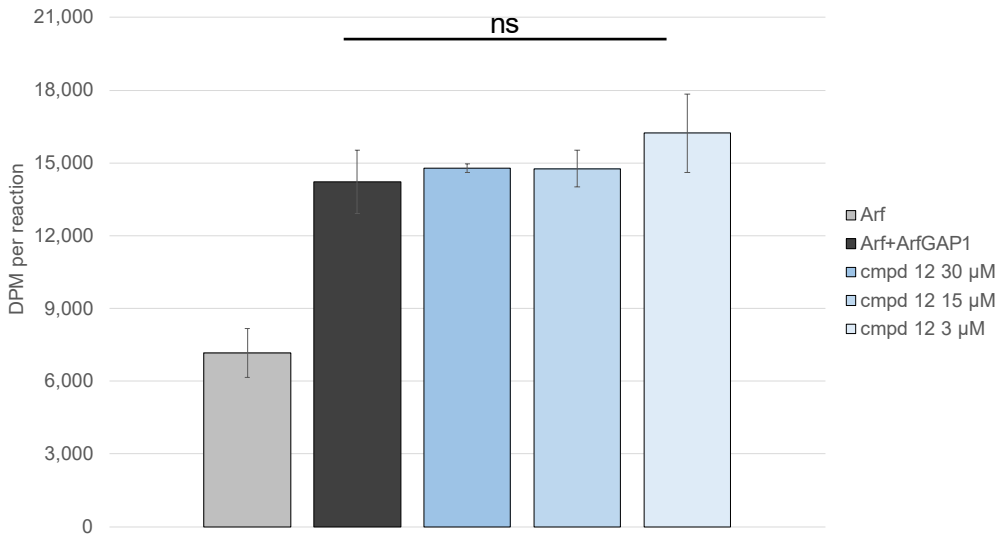

Figure 31. Compound 12 does not affect ArfGAP1 activity in a radiolabelled in vitro assay.

Purified Arf1 was loaded with GTPγ^{32}P in the presence of the mixed-composition liposomes and incubated alone or with ArfGAP1. Samples were incubated at room temperature with either DMSO or compound 12 (30, 15 or 3 µM), and the reaction was quenched upon the addition of a 5% charcoal solution. Free [^{32}P] phosphate was measured using a scintillation counter and disintegrations per minute (DPM) recorded. Mean values of triplicate reactions were plotted with error bars representing standard deviation. The data were analyzed with a one-way ANOVA and a p value of less than 0.05 was deemed statistically significant.

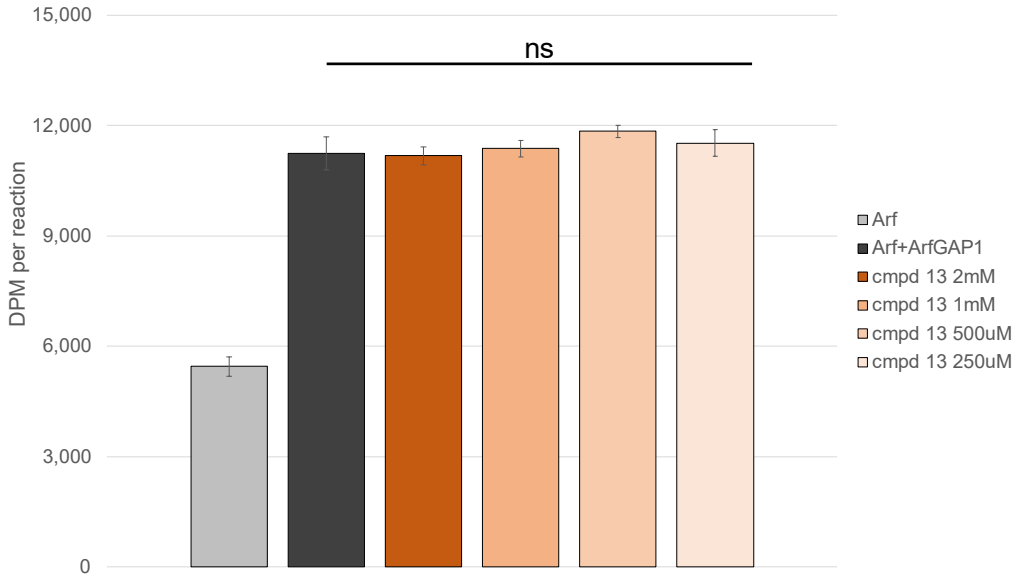

Figure 32. Compound 13 does not affect ArfGAP1 activity in a radiolabelled in vitro assay.

Purified Arf1 was loaded with GTPγ^{32}P in the presence of the mixed-composition liposomes and incubated alone or with ArfGAP1. Samples were incubated at room temperature with either DMSO or compound 13 (2mM, 1mM, 500 μM or 250 μM), and the reaction was quenched upon the addition of a 5% charcoal solution. Free [^{32}P] phosphate was measured using a scintillation counter and disintegrations per minute (DPM) recorded. Mean values of triplicate reactions were plotted with error bars representing standard deviation. The data were analyzed with a one-way ANOVA and a p value of less than 0.05 was deemed statistically significant.

Construction of Drosophila Strains to Determine the Effects of ArfGAP1 Interacting Compounds on LRRK2-mediated Parkinson's Disease

Typically defects in movement in human LRRK2 expressing *Drosophila* have been observed using the *ddc* driver, which drives expression in neurons that produce dopamine and serotonin. I sought to produce lines of flies that express human LRRK2 and human LRRK2 G2019S driven by the *ddc* promoter. All fly lines from outside sources were backcrossed to the lab reference line iso31 to isogenize the lines. This consisted of crossing red-eyed transgene-carrying virgin females to white-eyed iso31 males. Red-eyed progeny from the cross were isolated immediately after birth to prevent sibling mating, and virgin females were mated once again to white-eyed iso31 males. The red-eye phenotype was used as a visible marker and is genetically linked to the transgene. Females were used, as males do not undergo meiotic recombination. The process of backcrossing was repeated for a total of eight generations. Once fully isogenized, driver-*Gal4* lines and *UAS*-transgene lines were maintained separately as stocks and were only crossed immediately prior to characterization using the locomotion assay to produce a single generation of progeny carrying both genetic elements.

Previous work assessed the effect of expression of LRRK2 and LRRK2 G2019S on fly movement and observed differences in flies aged to 50-60 days and beyond. I determined movement at 50 days of age to determine if the

LRRK2 and LRRK2 G2019S strains generated decreased movement. Compared to control, LRRK2 fly movement during the evening peak was decreased by 60% and LRRK2 G2019S by 70% (**Figure 33**). The decrease in movement in flies expressing LRRK2 and LRRK2 G2019S at day 50 is similar to that observed in other studies (Liu et al., 2008; Ng et al., 2009).

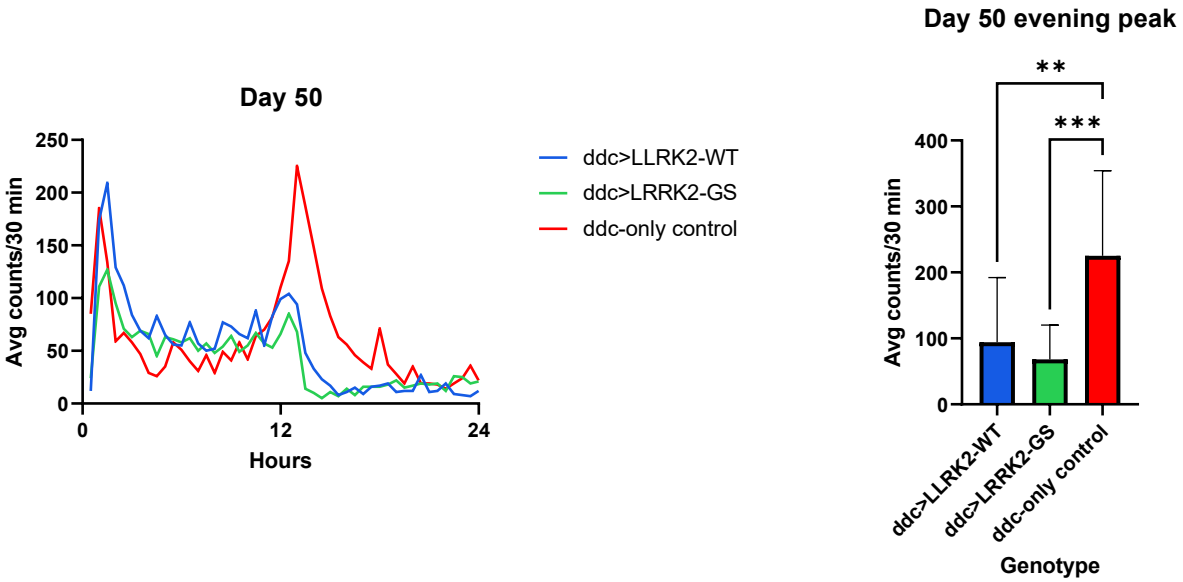

Figure 33. Expression of LRRK2 and LRRK2-G2019 decreases movement in flies.

Flies expressing either wild-type LRRK2 or mutant LRRK2-G2019S or control lines carrying only the *ddc* driver (and no LRRK2 variant) were aged for 50 days and then assayed for locomotion in activity monitors measuring the number of times a laser beam was broken by fly movement. Locomotion was monitored for a period of 24 hr on a 12 hr light/dark cycle and binned in 30 min increments. A line graph was plotted with average movement (measured as the number of laser beam breaks) of multiple flies (n = 8 to n = 16) as a function of time. Evening peaks (taken here at t = 13 h) of locomotor activity were plotted as a bar graph, with error bars representing standard deviation (*$p \leq 0.01$, **$p \leq 0.001$).

Maximum Tolerated Dose of the ArfGAP1 Binding Compounds to Drosophila

Three of the ArfGAP1 binding compounds, 4, 12, and 13 were chosen for in vivo studies in *Drosophila*. Compounds 4 and 12 were from the same structural class while compound 13 was from a different class. If a similar response is observed from compounds of differing structure that can both bind the same target, in this case human ArfGAP1, then the likelihood of the response observed being due to target inhibition is increased, versus that of an off-target effect. Prior to initiating the efficacy experiment a maximum tolerated dose experiment was performed to determine an appropriate concentration to deliver each compound. The compounds were dissolved into normal *Drosophila* food at final concentrations of 1-620 μM. The highest concentration used was the maximum solubility of each compound in the food.

Each compound was delivered in *Drosophila* food at various concentrations for one week and overt changes in behaviour and movement were monitored. No changes were observed including at the highest concentration of each compound (**Figure 34**). For the efficacity experiments a maximum concentration that could be dissolved in *Drosophila* food of 620 μM for compound 4, 123 μM for compound 12, and 366 μM for compound 13 was used. Flies supplied with DMSO-matched food or untreated fly food were included as controls.

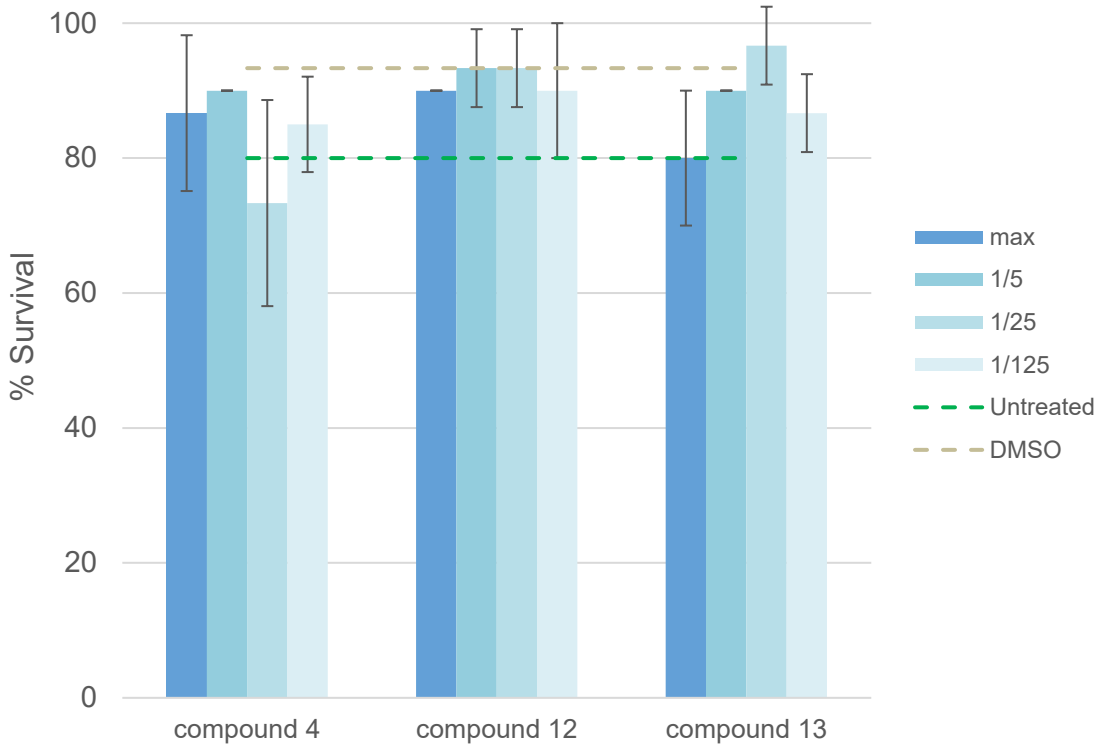

Figure 34. Compounds 4, 12 and 13 are not acutely toxic in Drosophila.

Iso31 flies were subjected to 7 days of treatment with either compound 4, compound 12, compound 13, DMSO, or untreated fly food. Maximum concentration of each compound in the food (compound 4 = 620 µM, compound 12 = 123 µM, compound 13 = 366 µM, DMSO = 0.5%) was compared to three dilutions (1/5, 1/25, 1/125). Flies were scored for survival post-treatment; error bars represent sample standard deviation of triplicate experiments.

Efficacy of ArfGAP1 Binding Compounds at Affecting Movement in Drosophila Models of LRRK2 Mediated Parkinson's Disease

ArfGAP1 binding compounds were presented to *Drosophila* expressing human LRRK2, or LRRK2-G2019S, under control of the *ddc* driver. Compounds were added to food at the maximum dissolvable dose from day 25 of life until endpoint experiments were conducted (day 55). Fresh food and drug were provided every 2-3 days. At day 55 movement was determined using the locomotion assay over 24 hours. Compounds 4 increased evening peak locomotion of the LRRK2-WT expressing strain, however, administration of compounds 12 or 13 resulted in a similar level of movement as controls (**Figure 35**). For the *Drosophila* expressing human LRRK2-G2019S, none of the compounds resulted in a significant change in peak locomotion compared to DMSO control (**Figure 36**).

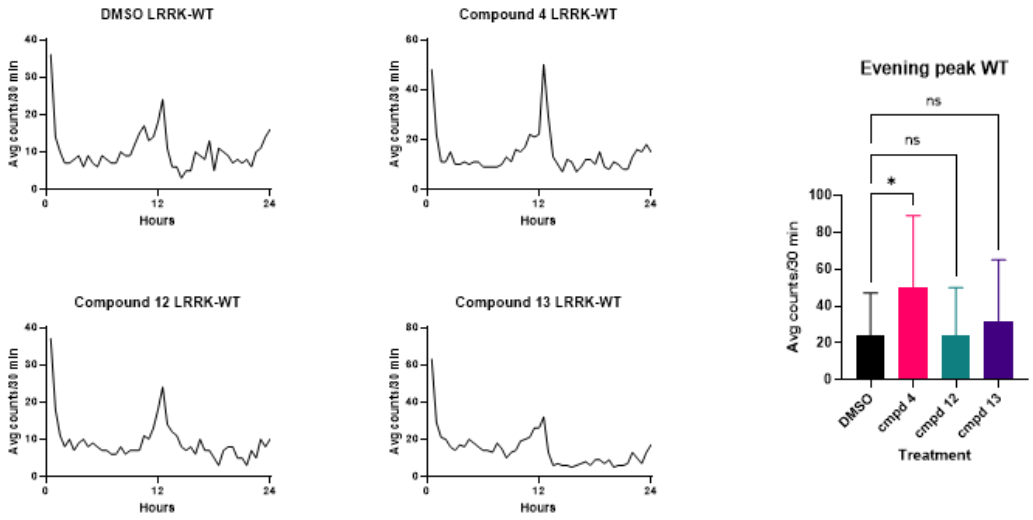

Figure 35. Effect of Potential ArfGAP1 Inhibitors on Drosophila Model of LRRK2 Mediated Parkinson's Disease.

Flies expressing wild-type LRRK2 from the *ddc* driver were aged for 25 days, then treated with a compound or DMSO for a further 30 days. At day 55, flies were analyzed for locomotor activity over a period of 96 hours, on a 12h L/D cycle in activity monitors measuring the number of times a laser beam was broken by fly movement. Locomotion was monitored for a period of 24 hr on a 12 hr light/dark cycle and binned in 30 min increments. A line graph was plotted with average movement (measured as the number of laser beam breaks) of multiple flies (n = 22 to n = 26) as a function of time. Evening peaks (taken here at t = 12.5 h) of locomotor activity were plotted as a bar graph, with error bars representing standard deviation (*$p \leq 0.05$, $^{ns}p \geq 0.05$).

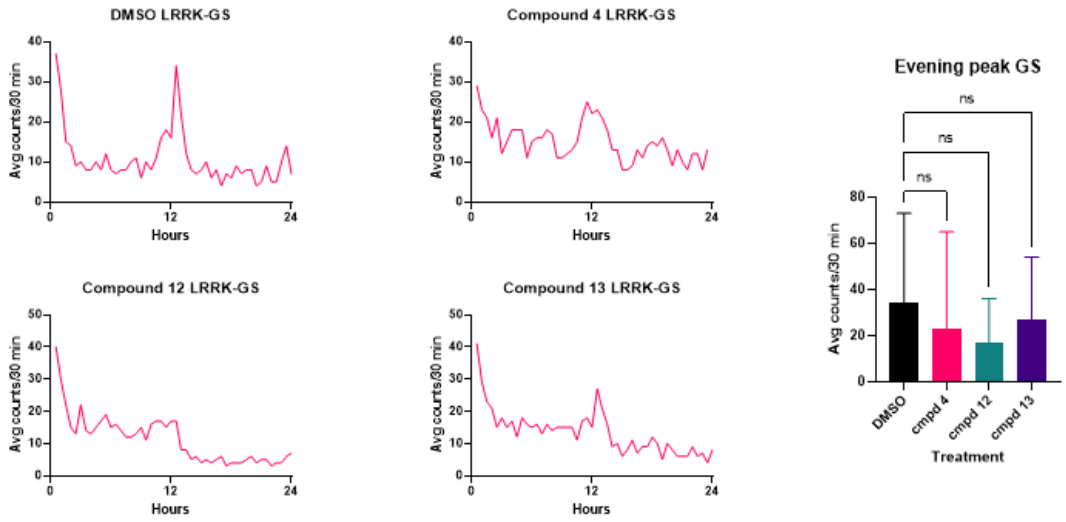

Figure 36. Effect of Potential ArfGAP1 Inhibitors on Drosophila Model of LRRK2-G2019S Mediated Parkinson's Disease.

Flies expressing mutant LRRK2-G2019S from the *ddc* driver were aged for 25 days, then treated with a compound or DMSO for a further 30 days. At day 55, flies were analyzed for locomotor activity over a period of 96 hours, on a 12h L/D cycle in activity monitors measuring the number of times a laser beam was broken by fly movement. Locomotion was monitored for a period of 24 hr on a 12 hr light/dark cycle and binned in 30 min increments. A line graph was plotted with average movement (measured as the number of laser beam breaks) of multiple flies (n = 14 to n = 26) as a function of time. Evening peaks (taken here at t = 12.5 h) of locomotor activity were plotted as a bar graph, with error bars representing standard deviation ($^{ns}p \geq 0.05$).

DISCUSSION

The major objectives of this work were to use a cell-based assay to screen for small molecule inhibitors of human ArfGAP1, assess if these inhibitors could directly bind to human ArfGAP1 to determine if they were direct inhibitors of ArfGAP1 function, and to test if they could be the basis of a potential new therapeutic approach for LRRK2-mediated PD based on their efficacy in an animal model. The cell-based small molecule screen of over 100,000 compounds led to the identification of four small molecules that prevented human ArfGAP1, and ArfGAP1-LRRK2, mediated toxicity based on their capacity to prevent the growth defect observed due to the over-expression of these proteins in yeast cells. The result from this initial screen suggested that I may have identified potential human ArfGAP1 inhibitors. I next used a biophysical method, MST, and determined that the small molecules could directly bind to human ArfGAP1 implying that their ability to inhibit ArfGAP1 function is direct. I then performed an in vitro ArfGAP1 assay to assess enzymatic activity in the presence of the ArfGAP1 substrate yArf1 and determined that none of the compounds inhibited enzymatic activity. This suggests that their capacity to prevent ArfGAP1 and ArfGAP1-LRRK2 mediated toxicity may not be due to direct inhibition of catalytic activity, but may be due to inhibition of some other function (*e.g.* inhibition of ArfGAP1 interaction with membranes or interaction with LRRK2). I went on to determine if the ability of a subset of these small molecule ArfGAP1 interacting compounds could decrease the movement disorder present in *Drosophila* models

of *LRRK2*-mediated PD. To do so, I produced two *Drosophila* models whereby wild type LRRK2, and the pathogenic LRRK2-G2019S variant, were expressed in dopaminergic neurons via inducible expression from the *ddc* promoter. Expression of LRRK2 or LRRK2-G2019S resulted in the expected decrease in movement as *Drosophila* aged. I went on to determine that compound 4 could reduce the movement defect in the *Drosophila* model of LRRK2-mediated PD.

Ameliorating Movement Defects in Drosophila Models of LRRK2 Mediated PD

Testing small molecules in human LRRK2 expressing *Drosophila* models has been previously conducted by several other groups. As movement is a primary defect in PD it is often measured in *Drosophila* to determine their potential capacity for amelioration of PD. There are two main assays used to monitor movement by *Drosophila*, the easiest and least expensive is the vertical climbing assay. In this assay, flies are tapped to the bottom of a pipette and their capacity to climb up the pipette a certain discrete distance over a predetermined time is measured. However, there is no standardization of this assay and protocols vary. For instance, the distance the fly must cover and the time allotted to do so in order to achieve a successful climb are arbitrarily set. Other factors that may influence fly climbing include the degree to which flies are tapped down to the bottom of the tube (in extreme cases too much force can concuss them)

and variations in light or time of day in which the assay is performed as flies display circadian-related patterns of movement. The climbing assay also presents results as binary data (successful or unsuccessful climb) and does not consider intermediate phenotypes (e.g. climbed 50% of the distance). A second method is the horizontal locomotion assay whereby flies are placed in a tube that enables crawling, and a computer automatically records locomotion continuously over time (normally 24-48 hrs) based on the number of times a fly breaks light beams placed at locations across the tube. Using this method there is no induction of the startle response and the flies are assayed over a longer period of time, versus one point in time, so as to analyze patterns over a typical day. This method also takes account the highly dependent circadian movement of flies but does require expensive equipment to perform. I used the horizontal locomotion assay and determined that compound 4 doubled movement of flies expressing human LRRK2 but did not ameliorate the movement defect of flies expressing the kinase gain of function variant LRRK2 G2019S.

Testing of inhibitors of LRRK2 kinase activity was an obvious approach to treat LRRK2 mediated PD. Testing of the direct LRRK2 kinase inhibitor GW5074 for protection versus movement defects in human LRRK2 G2019S expressing *Drosophila* has been previously assessed (Liu et al., 2011). GW5074 doubled the vertical climbing capacity for flies expressing human LRRK2 G2019S at 10 μM but was toxic at 100 μM. The *Drosophila* model of human LRRK2 expression was also used to investigate compounds identified in a high-throughput screen for in

vitro inhibitors of LRRK2 kinase activity which identified the anti-oxidants piceatannol, thymoquinone, and esculetin as LRRK2 kinase inhibitors. Treatment of human LRRK2 expressing flies with piceatannol, thymoquinone, or esculetin resulted in a 22% and 17% increase in vertical climbing ability for piceatannol and thymoquinone treated flies, with no increase observed for esculetin treated flies.

The vertical climbing assay was also used by Yang et al (2018) who subjected LRRK2-expressing flies with a chemical inhibitor of the hep pathway, a MAPK signalling cascade that includes ERK, JNK and p38. Chemical inhibition of hep kinase, or its genetic inhibition, partially ameliorated the LRRK-G2019S climbing phenotype. Prostaglandin PGA2 administration, which directly binds to the transcription factor Nurr1 and drives transcription of genes required for midbrain dopaminergic neuronal development and simultaneously reduces inflammation, also was found to improve the climbing defect due to expression of human LRRK2 and LRRK2 G2019S in *Drosophila* (Rajan et al., 2022). It is clear that inhibition of several processes have been determined to increase movement in *Drosophila* expressing human LRRK2 and LRRK2 G2019S in dopaminergic neurons. The best studied compounds in models beyond *Drosophila* are the direct inhibitors of the protein kinase activity of LRRK2.

The pathogenic G2019S variant of LRRK2 is known to result in gain-of-function (ie: hyperphosphorylating) protein kinase activity, therefore knockout models were first created to better understand the effects of inhibition of LRRK2

activity. The earliest mouse KO models found that 6 weeks into life, mice showed pathology in the proximal tubule cells of the cortex and outer medulla of the kidney and type II alveolar pneumocytes in the lung (Herzig et al., 2011). Specifically, kidneys of the animals appeared grossly darker and histological examination revealed increased vacuolization, which was also present in type II lung pneumocytes. A different *LRRK2* mouse knockout replicated the enlarged lamellar bodies in type II lung pneumocytes and also observed an increased number of lysosomes in proximal tubular epithelium of kidney. Kinase-dead LRRK2 knock-in mice had similar kidney pathology to the knockout mice, whereas knock-in of the G2019S variant of LRRK2 did not show any kidney/lung pathology. A subsequent study looked at *LRRK2* expression patterns across different types of cells (Fuji et al., 2015). In humans, the highest *LRRK2* mRNA level was detected in white blood cells (WBCs) and lung, followed by lymph, kidney, and bone marrow.

The most clinically advanced therapies for LRRK2 mediated PD are small molecule LRRK2 kinase activity inhibitors. Studies in non-human primates (NHPs) tested two structurally dissimilar compounds that could inhibit LRRK2 kinase activity: GNE-7915 and GNE-0877 (GNE-0877 was first identified as potential LRRK2 inhibitor from high-throughput biochemical screen) (Estrada et al., 2014). Cynomolgus macaques, sharing 97% identity to human LRRK2, were selected as the NHP model. Single administration of GNE-7915 was tested in macaques with dose ranging from 10-65 mg/kg. Upon completion of the study,

necropsy and subsequent immunohistology found increased number and size of lamellar bodies in lung pneumocytes, as well as an increase in median cell size as compared to controls. A follow-up study compared the effects of administration of GNE-7915 to GNE-0877 and observed that in the kidneys there was an increase in cellular lipid globules in both treatment groups, however no gross impairment of renal function was observed. Other side effects were also reported, such as dose-independent sedation, and dose-dependent transient tremors that resolved several hours after small-molecule administration. It is not known if the cause of these effects is directly attributable to inhibition of LRRK2 function or are a result of off-target toxicities. It was noted however, that the lung phenotype observed in monkeys treated with LRRK2 small molecule inhibitors was morphologically identical to that of *LRRK2* KO mice. Focusing on further characterization in the NHP lung, a recent study was conducted by Baptista et al, testing three structurally different LRRK kinase inhibitors (GNE-7915, Mli-2, PFE-360) in macaques to address several questions: i) whether lung toxicity is an on- or off-target effect; ii) to characterize the safety margin for lung toxicity (eg: is there a dose with no effect in the lung but still inhibits LRRK2 in the brain?); and iii) whether phenotypes are reversed upon discontinuation of drug (Baptista et al., 2020). In summary, this report published evidence of the same increase in vacuolation of pneumocytes corresponding to both enlarged size of, and increased number of, lamellar bodies as observed by various groups before. No deficits in pulmonary function tests were reported. In contrast to mice and rats, no unusual kidney phenotypes were seen. Ultimately, it remains unclear whether

it is possible to achieve a therapeutic level of LRRK inhibition in brain without stimulating toxic effects in lung.

A first-in-human clinical trial was recently concluded for lead compound DNL-201, previously investigated as GNE-0877, in healthy human volunteers in a clinical phase 1a trial, and in patients with PD in a phase 1b follow-up study (Jennings et al., 2022). Prior to administration to human subjects, lead compound DNL-201 was first tested for the ability to cross the blood-brain barrier (BBB) in NHPs; the compound was successfully detected in cerebrospinal fluid (CSF). A customary readout for LRRK2 activity in cell lines (LRRK autophosphorylation at site pS935 or pS1292, or phosphorylation of pT73 of downstream binding partner Rab10) was not easily achievable in primate subjects. Rather, this study on NHPs used an alternative biomarker of LRRK2 activity on lysosome function, measuring urinary levels of bis(monoacylglycero) phosphate (BMP), a phospholipid involved in lipid sorting in late endosomes and lysosomes. Administration of DNL-201 to NHPs achieved inhibition of LRRK2 activity, as measured by decreased BMP in urine. The authors also observed vacuolated type II pneumocytes in lungs of NHPs treated with DNL-201, consistent with previous reports. Increased pigment in renal tubular epithelial cells was also observed but had no effect on measured renal function; all phenotypes were reversed after treatment was discontinued. In humans, two additional studies (Phase1a and Phase1b trials) were performed to further probe for safety and tolerability of DNL-201: i) a double-blind placebo-controlled single-ascending and

multiple-ascending dose in healthy volunteers, and ii) a double-blind placebo-controlled trial in PD patients with and without *LRRK2* pathogenic variants. Readout for LRRK2 kinase activity was autophosphorylation at pS935 from whole blood or pT73 of Rab10 from peripheral blood mononuclear cells (PBMCs). In the Phase 1a study, 122 healthy volunteers were recruited. After 10 days of treatment (80-100 mg twice a day) a 75-82% decrease in LRRK2 kinase activity from baseline was observed, as measured by whole-blood pS935 LRRK2 and urinary BMP. Phase 1b evaluated 28 patients with mild to moderate PD after treatment with DNL-201 for 28 days (30-50 mg three times daily). A decrease in PBMC pT73 Rab10 was observed, ranging from 55-85% of baseline. The limited sample size prevented meaningful comparison between carriers and non-carriers of the G2019S variant in *LRRK2*. Safety and tolerability were assessed; only minor side effects such as headache, dizziness and nausea reported. Across both studies, no overt impairments in pulmonary or renal function were found. It is unclear at this stage if these compounds have the capacity to move to later stage clinical trials.

The findings of LRRK2 genetic loss-of-function in rodents (or chemical inhibition in NHPs) and the corresponding pathology in the kidney and lung pose potential concerns for the strategy of directly inhibiting LRRK2 kinase activity as a potential long-term therapy for PD. Our strategy, inhibition of the ArfGAP1 that drives LRRK2 GTPase activity that then enhances LRRK2 kinase activity was

proposed as an alternate strategy. To date, it is unclear if either strategy will be sufficient, or is one is superior to the other, to treat LRRK2 mediated PD.

Identification of ArfGAP Inhibitors

Beyond the identification of the ArfGAP1 binding compounds 4, 12, and 13 in my thesis research, there is currently one proposed ArfGAP1 inhibitor available, QS11 (Zhang et al., 2007). It is for research use only. QS11 was initially identified as a synergist of the Wnt signalling pathway using a cell-based screen whereby HEK293 cells were transfected with a reporter TopFlash assay (measuring dual luciferase activity as a readout for activated Wnt signalling in the presence of the ligand Wnt3a) and treated with a library of 100,000 compounds. Hits were identified as compounds that resulted in >3 SD from the mean increase in luciferase activity but did not have same effect in the absence of the ligand. QS11, a purine derivative, was identified as an activator of Wnt3a signalling. To identify the ligand for QS11, QS11 with a reactive linker was bound to Affi-gel resin and HEK293 protein extract was flowed over the column. Subsequent release of the QS11 bound protein and mass spectrometry identified ArfGAP1 as the ligand for QS11. The addition of QS11 to an ArfGAP1 assay with Arf1 as substrate decreased intrinsic Arf1 GTPase activity. QS11 was found to have an EC_{50} of 0.5 uM when delivered to HEK293 cells and ArfGAP1 activation was determined. QS11 showed little cytotoxicity in HEK293 cells and human primary

fibroblasts (Zhang et al., 2007). However, there are some limitations around the use of QS11 as a potential therapeutic agent or ArfGAP1 specific applications. First, it is considered a broad-spectrum ArfGAP inhibitor since it can inhibit other ArfGAPs. For example, QS11 has a higher affinity for the Arf6 effector AMAP1 with a K_d of 364 nM, versus 620 nM for ArfGAP1. Arf6/AMAP1 dysregulation by KRAS/TP53 mutation has been implicated in pancreatic cancer (Hashimoto et al., 2019). The consequence of inhibition of AMAP1 in the context of PD unknown, however the role of Arf6/AMAP1 in anterograde trafficking of mitochondria has been characterized (Onodera et al., 2018). Along these lines, I have not determined if compounds 4, 12, or 13 identified in my thesis work can bind to ArfGAPs beyond human ArfGAP1.

As far as we are aware, QS11 has not been tested in an animal model of PDs, including *Drosophila*. Indeed, certain aspects of QS11 pharmacokinetic properties may impede its potential as a therapeutic compound. Specifically, QS11 displays three violations of Lipinski's Rule of Five (RO5), a collection of parameters that estimate a compound's solubility and permeability (Lipinski et al., 2001). Lipinski's RO5 has a high predictive value of "drug-likeness"; approximately 77% of therapeutic drugs on the market have 2 or fewer violations (Ntie-Kang, 2013). Briefly, the RO5 state that an ideal drug has a molecular mass of less than 500 Daltons, no more than 5 hydrogen bond donors and 10 hydrogen bond acceptors, and an octanol-water partition coeeficient (logP) less than 5. Additional characteristics, proposed by Ghose and Veber, include ideal

total polar surface area (tPSA) of less than 140 $Å^2$ and molar refractivity from 40 to 130 (Bickerton et al., 2012). QS11 has a large molecular weight of 568, a logP of 6.8, and molar refractivity of 170 which all lie outside the optimal ranges defined in the RO5, making it an unlikely candidate to pursue as a lead compound. In this vein, I examined the fit of the RO5 for the small molecule compounds I tested in my in vitro assays, and on my LRRK2 fly model. Compounds 4 and 12, sharing a structural core, violated none of the RO5; however, the unrelated compound 13 violated one of the RO5 criteria, with a logP of 5.05, slightly above the desirable upper limit of 5 (**Table 7**). It may be worthwhile to note that 15% of FDA approved drugs have a logP greater than 5 (Ntie-Kang, 2013). As such, compounds 4, 12 and 13 may prove suitable candidates for further characterization and optimization as ArfGAP1 inhibitors and potential therapeutic agents. In addition to the RO5, a commonly used predictor of oral bioavailability is Jorgensen's RO3, which examine a molecule's aqueous solubility (logS > -5.7), apparent Caco2 (faster than 22nm/s), and number of primary metabolites (< 7); 90% of oral drugs have these properties (Lionta et al., 2014). Assessed in accordance with these criteria, compounds 4, 12 and 13 all include violations of the RO3, and may therefore require modification to the structure to improve oral bioavailability.

Cell-based Screens and Potential Human ArfGAP1 Inhibitors

Drilling down more specifically regarding the high throughput screen I used to identify potential human ArfGAP1 inhibitors via its inducible expression in

Table 7. Druglikeness properties for small molecules tested on *Drosophila* LRRK2 model.

Druglikeness property	Compound 4	Compound 12	Compound 13
Molecular weight (Da)	303	339	432
logP	3.5	4	5.05
H-bond acceptors + H-bond donors	4	3	1
Total polar surface area ($Å^2$)	80	24	21
Molar refractivity	94	111	100
Lipinski RO5 violations	0	0	1

yeast cells, I identified several compounds containing a piperazine core. Piperazine is found in the structures of therapeutic compounds across many different classes, including anthelmintic, antipsychotic, antihistamine, antidepressant and antineoplastic agents (Chaudhary et al., 2023). Piperazines have also been identified as chemical probes in vesicular trafficking. Interestingly, two separate studies investigating small molecules that affect Golgi mediated transport identified piperazine containing compounds similar to those that I identified in my screen for ArfGAP1 inhibitors. As ArfGAP1 functions at the Golgi, this links my screen with the results of these two screens. Specifically, a yeast high-throughput screen of 30,000 compounds was performed and 17 molecules were identified as modifiers of AP1-dependent Golgi to endosome transport; three of these compounds shared a piperazine-based structure observed in my set of human ArfGAP1 binding compounds (Duncan et al., 2007). Separately, Zouhar and colleagues performed a yeast screen of a library of 4,800 diverse compounds and identified 14 compounds that mislocalized a reporter protein trafficked in the Golgi-endosome-vacuole pathway; one of the three compounds selected for follow-up studies also shared the same piperazine structure present in my ArfGAP1 binding compounds (Zouhar et al., 2004). The discovery of piperazine-based compounds that share the same structure as those identified by me as ArfGAP1 binding compounds in two unbiased screens as modifiers of post-Golgi trafficking align with my findings that the piperazine-containing hits from my high-throughput screen may be ArfGAP1-targeting compounds. The cellular protein target for the piperazine-based compounds

identified in these yeast Golgi mediated trafficking screens has yet to be determined. Their binding to an inhibition of the activity of a Golgi acting yeast ArfGAP, such as Gcs1 (the yeast homologue of human ArfGAP1), merits further study. Conversely, I did not study the effect of expression of human ArfGAP1 and/or LRRK2 on yeast biology other than the observation that growth rate was decreased. Thus, how the compounds that ameliorate yeast growth due human ArfGAP1 or LRRK2 expression is not known other than they directly bind to human ArfGAP1.

The human ArfGAP1 binding compounds identified in this thesis were added to yeast cells in which the gene encoding the endogenous yeast ArfGAP1 (*GCS1*) was genetically inactivated. As human ArfGAP1 shares 64% homology and 43% identity to Gcs1 it is possible that over-expression of human ArfGAP1 in yeast may function in Gcs1 pathways (*e.g.* in post-Golgi transport) – with their increased expression compromising function of these pathways (Poon et al., 2001). The addition of compounds 4, 12, and 13 could be enabling an essential post-Golgi function being inhibited by expression of human ArfGAP1 in yeast. It would be interesting to monitor ArfGAP1 mediated Golgi egress pathways in the presence of over-expressed human ArfGAP1 and LRRK2 to assess if these were affected, and if the compounds that prevented ArfGAP1 mediated toxicity restored their function. This line of research could be interesting and may provide insight into some specifics of ArfGAP1 and LRRK2 mediated general cell biology.

Human ArfGAP1 Directly Interacts with the Compounds Discovered from the Cell-based Screen

One of the most ideal processes to determine if compounds isolated from a cell-based screen affect the activity of their target is to determine if they directly interact. In my case I sought to determine if compounds 4, 12, and 13 could directly interact with human ArfGAP1. To do so I used MST, a biophysical method that can both detect and provide a binding constant (K_d) for proteins with small molecules (Jerabek-Willemsen et al., 2011). For MST it is preferable if the target protein is purified to near homogeneity as this decreases signal to noise. Previous attempts to purify a full-length mammalian ArfGAP1 had not been successful. Purified mammalian ArfGAP1 had been purified as a GST-tagged version truncated at amino acid residue 257 (out of a total of 406) (Cukierman et al., 1995). This truncated form includes the functional GAP domain, Zn^{2+} finger, and only one of the two WxxF motifs. Importantly, the ALPS membrane binding motifs present in the C-terminus is missing from this truncated version, these are unstructured in solution but form amphipathic helices when interacting with lipid membranes where ArfGAP1 is in its most active state (Bigay et al., 2005). Finally, previous purifications had been from heterologous expression in *E. coli* from inclusion bodies requiring denaturing and subsequent and refolding of the protein (Huber et al., 2002). My purification of human ArfGAP1 was of the full-length protein with a 10x-His tag present at the C-terminus to enable purification over Ni^{2+} resin. To obtain full length protein expression, I explored numerous

expression conditions and was able to use a combination of reduced growth temperature, optimized expression time, and expression in the Rosetta strain of *E. coli* which is codon optimized from human proteins, to enable expression of and soluble full length human ArfGAP1 (Tegel et al., 2010) and its subsequent purification. To our knowledge, this is the first reported purification of full length human ArfGAP1.

Purified human ArfGAP1 was used for MST analysis by incubating human ArfGAP1 with varying concentrations of compounds 4, 12, or 13 in solution. The first MST attempt uses a version that monitors proteins by their intrinsic Trp fluorescence at 280 nm. ArfGAP1 has 11 Trp residues making it amenable to this type of MST. However, the compounds autofluoresced at 280 nm, with compound 13 having very high levels of autofluorescence, precluding the use of intrinsic fluorescence of ArfGAP1 in the MST assay. As human ArfGAP1 contained a 10xHis-tag to facilitate its rapid purification, dyes are available that bind to polyHis tracts that are fluorescent. I determined that the MST dye-label method was amenable for assessing if human ArfGAP1 could interact with the compounds 4, 12, and 13. Using MST, I determined that human ArfGAP1 (fluorescently labeled on its 10xHis tag) could directly bind to compounds 4, 12, and 13. Sigmoidal binding curves were obvious and evident as more compound was present, however, they were not complete as higher concentrations of each compound resulted in autofluorescence that overlapped with the emission spectrum of the fluorophore attached to the 10xHis-tag. This assay demonstrated

direct binding of each compound to human ArfGAP1, but precluded obtaining a K_d. To overcome this limitation in the future, fluorophores with different emission spectra could be tested for overlap with the autofluorescence of compounds 4, 12, and 13. These would require a version of human ArfGAP1 with built-in fluorophores such as mGFP, mCherry, or other endogenously fluorescent molecules to be subcloned in frame with the human ArfGAP1 open reading frame for expression and subsequent purification. However, these are large additions and may interfere with ArfGAP1 function which is a limitation of their use. A second issue is that the compounds were identified using a cell based screen, and active ArfGAP1 is thought to be membrane bound due to the presence of ALPS motifs in the protein. If the compounds preferentially bind active ArfGAP1 then the addition of liposomes that enable ArfGAP1 to the binding assay may result in higher affinity binding of the compounds to ArfGAP1 and allow for determination of an accurate K_d. Beyond MST, a different biophysical method such as surface plasmon resonance could be considered (Piliarik et al., 2009). Very generally, for surface plasmon resonance human 10xHis-ArfGAP1 would be immobilized and a solution containing a potential ArfGAP1 binding compound would be applied across the immobilized ArfGAP1. Next, a solution without the compound would be applied and over time the ArfGAP1-compound complex would dissociate. A decrease in binding signal would be observed and from this both association (K_a), and dissociation (K_d), rates could potentially be determined.

Human ArfGAP1-Binding Compounds and ArfGAP1 Activity

Preventing ArfGAP1 mediated toxicity in a cell-based assay, and direct binding of the compounds to ArfGAP1, are consistent with inhibition of ArfGAP1 biological activity. However, neither equates to inhibition of ArfGAP1 enzymatic activity. To assess if the compounds could inhibit ArfGAP1 enzymatic activity I required a substrate. A common substrate to assess human ArfGAP1 catalytic activity is yeast Arf1 (Huber et al., 2002). Yeast Arf1 with a polyHis tag was purified and two assay types (colourimetric versus radioactive) were tested. Although both assays resulted in measurable ArfGAP1 GTPase activation, the radiolabeled assay resulted in a higher signal to noise and was used for further assay optimization. ArfGAP1 possesses two tandem ALPS motifs which enable binding to highly curved membranes (Drin et al., 2009). Preferential binding to highly curved membranes is thought to enable ArfGAP1 to preferentially be most active at the Golgi endosome interface. To mimic highly curved membranes to optimize measurable ArfGAP1 activity (*i.e*. signal to noise as Arf1 itself has endogenous GTPase activity), ArfGAP1 activity in the presence of membrane of several compositions and concentrations was determined. Beyond membrane type, as Arf1 itself has endogenous GTPase activity the normal enzymatic assay process of saturating substrate was not viable, I also needed to determine the best substrate (yArf1) and enzyme (human ArfGAP1) ratio for optimal activity. To assess compounds 4, 12, or 13 for inhibition of ArfGAP1 I was limited by the fact

they that they were soluble in the assay buffer up only to 100 μM. None of the compounds inhibited human ArfGAP1 enzymatic activity at concentrations tested. There are several caveats to the interpretation of the inability of the compounds to inhibit ArfGAP1 activity. The substrate used was yArf1, whereas the GTPase activity most relevant to PD is that of human LRRK2. It is possible that the structure of compounds required to inhibit LRRK2 GTPase activity may be different than that for yArf1, for example differences at the substrate-enzyme interface. Second, the assay system for human ArfGAP1 requires the addition of lipid micelles and the compounds are somewhat hydrophobic, and a portion may partition into the lipids present in the assay lowering their effective concentration.

I screened over 100,000 compounds for those that prevent ArfGAP1 toxicity in a yeast cell-based assay, and subsequent counter screening including the ability of compounds to prevent the increased toxicity observed due to ArfGAP1 and LRRK2 mediated toxicity in yeast resulted in the identification of five compounds. Four were of a similar structural class and one was distinct. Further analysis of two of the compounds from the same class, compounds 4 and 12, and the single distinct compound, compound 13, determined that all three could directly bind to human ArfGAP1. However, we could not detect inhibition of human ArfGAP1 activity in vitro using yArf1 as substrate. This final result does not preclude usefulness of these compounds with respect to potentially inhibiting human ArfGAP1 in the context of LRRK2 mediated PD. Indeed, I did determine that compound 4 was able to partially ameliorate the

movement defect in *Drosophila* expressing human LRRK2 in dopaminergic neurons.

Implications of this research

The work described here represents a set of proof of concept experiments, from initial identification to validation and testing in an animal model. The yeast high-throughput screen that identified putative small molecule inhibitors is the first unbiased screen against human ArfGAP1. Given that all three compounds bind hArfGAP1 in vitro, and one compound has shown amelioration of a toxic phenotype in an animal model, lends credence to this pipeline as a viable approach for identifying future therapeutic compounds. Additionally, this work describes the first characterization of the piperazine-based compounds 4 and 12, and the structurally unrelated compound 13.

FUTURE DIRECTIONS

There are many avenues that offer up potential areas of future exploration. Using the yeast cell-based assay, it could be interesting to see if the compounds 4, 12, and 13 prevent both LRRK2 and LRRK2-G2019S toxicity, as only LRRK2 was tested. Indeed, this could provide and explanation for why each of these compounds ameliorated growth in *Drosophila* expressing human LRRK2, but not LRRK2 G2019S, in dopaminergic neurons. The mechanism by which expression of human ArfGAP1, LRRK2, and the additive capacity of both, to decrease yeast cell growth could be further explored. A logical starting point would be ArfGAP1 mediated vesicular trafficking pathways as compounds with the same structure of the compounds I identified as increasing growth in yeast cells were identified in chemical-genetic screens of small molecules that mediated Golgi mediated vesicular trafficking. Other vesicular trafficking pathways are also easily monitored in yeast including trafficking to the lysosome from various organelles.

The biochemical binding assay (MST) that determined compounds 4, 12, and 13 could directly bind to human ArfGAP1 could be optimized to determine a true K_d for each compound. Even without optimization, one could use the established MST protocol to determine the region of ArfGAP1 where the small molecules bind. This could be achieved by expressing and purifying truncations of ArfGAP1 and repeating the MST experiments. Identifying the binding motif may offer a glimpse into the potential mechanism of action. Once a region of

compound interaction with ArfGAP1 is known, one could test expected outcomes such as membrane interaction, or LRRK2 interaction, if the region is not in the catalytic domain. The specificity of compounds 4, 12, and 13 for binding to ArfGAP1 versus other human ArfGAP isoforms could also be determined. This information would be important if one decided to try to optimize one of the compounds to increase ArfGAP1 binding affinity and specificity.

In the enzymatic assay for ArfGAP1 activity, no decrease in activity was observed when ArfGAP1 was used to stimulate yArf1 GTP hydrolysis. This assay could be further optimized to increase the concentration of each compound in the assay buffer. The assay could also be repeated using LRRK2 as the ArfGAP1 substrate to see if the compounds are substrate specific as far as inhibition of GTPase activating activity.

Further in vivo experiments in the *Drosophila* model could be performed to determine if the movement increase by compound 4 in flies expressing human LRRK2 from the *ddc* promoter also increased dopaminergic neuron survival as well as dopamine level in fly brains. One could also assess pharmacokinetic and pharmacodynamic effects to determine if the compounds are able to reach the target in their active form. For example, HPLC-mass spectrometry could be performed on brain lysates from *Drosophila* to quantitate levels of compounds 4, 12, and 13 that were able to successfully penetrate the blood-brain barrier over time. Further refinement of these small molecules may involve modification of the structures and a quantitative structure-activity relationship analysis of the

compound 4 and 12 class, or compound 13, with the end goal being both increased binding to ArfGAP1 and increased penetrance into the brain.

REFERENCES

Abeliovich, A., & Gitler, A. D. (2016). Defects in trafficking bridge Parkinson's disease pathology and genetics. *Nature*, *539*(7628), 207–216.

Albrecht, D., Ceschin, J., Dompierre, J., Gueniot, F., Pinson, B., & Daignan-Fornier, B. (2016). Chemo-genetic interactions between histone modification and the antiproliferation drug AICAR are conserved in yeast and humans. *Genetics*, *204*(4), 1447–1460.

Alessi, D. R., & Sammler, E. (2018). LRRK2 kinase in Parkinson's disease. *Science*, *360*(6384), 36–37.

Andres-Mateos, E., Mejias, R., Sasaki, M., Li, X., Lin, B. M., Biskup, S., Zhang, L., Banerjee, R., Thomas, B., Yang, L., Liu, G., Beal, M. F., Huso, D. L., Dawson, T. M., & Dawson, V. L. (2009). Unexpected lack of hypersensitivity in LRRK2 knock-out mice to MPTP (1-methyl-4-phenyl-1,2,3,6-tetrahydropyridine). *The Journal of Neuroscience*, *29*(50), 15846–15850.

Aryal, B., & Lee, Y. (2019). Disease model organism for Parkinson disease: Drosophila melanogaster. *BMB Reports*, *52*(4), 250–258.

Bae, E.J., Kim, D.K., Kim, C., Mante, M., Adame, A., Rockenstein, E., Ulusoy, A., Klinkenberg, M., Jeong, G. R., Bae, J. R., Lee, C., Lee, H.J., Lee, B.D., Di Monte, D. A., Masliah, E., & Lee, S.J. (2018). LRRK2 kinase regulates α-synuclein propagation via RAB35 phosphorylation. *Nature Communications*, *9*(1), 3465.

Bae, E.J., Yang, N. Y., Lee, C., Lee, H.J., Kim, S., Sardi, S. P., & Lee, S.J. (2015). Loss of glucocerebrosidase 1 activity causes lysosomal dysfunction and α-synuclein aggregation. *Experimental & Molecular Medicine*, *47*, e153.

Bai, M., Gad, H., Turacchio, G., Cocucci, E., Yang, J.-S., Li, J., Beznoussenko, G. V., Nie, Z., Luo, R., Fu, L., Collawn, J. F., Kirchhausen, T., Luini, A., & Hsu, V. W. (2011). ARFGAP1 promotes AP-2-dependent endocytosis. *Nature Cell Biology*, *13*(5), 559–567.

Baptista, M. A. S., Merchant, K., Barrett, T., Bhargava, S., Bryce, D. K., Ellis, J. M., Estrada, A. A., Fell, M. J., Fiske, B. K., Fuji, R. N., Galatsis, P., Henry, A. G., Hill, S., Hirst, W., Houle, C., Kennedy, M. E., Liu, X., Maddess, M. L., Markgraf, C., Mei, H., … Sherer, T. B. (2020). LRRK2 inhibitors induce reversible changes in nonhuman primate lungs without measurable pulmonary deficits. *Science translational medicine*, *12*(540), eaav0820.

Behl, T., Kaur, G., Fratila, O., Buhas, C., Judea-Pusta, C. T., Negrut, N., Bustea, C., & Bungau, S. (2021). Cross-talks among GBA mutations, glucocerebrosidase, and α-synuclein in GBA-associated Parkinson's disease and their targeted therapeutic approaches: a comprehensive review. *Translational Neurodegeneration*, *10*(1), 4.

Benjamin, J. (2011). *Functions of the Yeast GTPase-Activating Proteins Age1 and Gcs1 for Post-Golgi Vesicular Transport* (G. Johnston (ed.)) [Doctor of Philosophy, Dalhousie University]. https://DalSpace.library.dal.ca//bitstream/10222/14218/1/Benjamin_Jeremy_PhD_MICI_August_2011.pdf

Benskey, M. J., Perez, R. G., & Manfredsson, F. P. (2016). The contribution of alpha synuclein to neuronal survival and function - Implications for Parkinson's disease. *Journal of Neurochemistry*, *137*(3), 331–359.

Berwick, D. C., Heaton, G. R., Azeggagh, S., & Harvey, K. (2019). LRRK2 Biology from structure to dysfunction: research progresses, but the themes remain the same. *Molecular Neurodegeneration*, *14*(1), 49.

Bezard, E., & Przedborski, S. (2011). A tale on animal models of Parkinson's disease. *Movement Disorders*, *26*(6), 993–1002.

Bickerton, G. R., Paolini, G. V., Besnard, J., Muresan, S., & Hopkins, A. L. (2012). Quantifying the chemical beauty of drugs. *Nature chemistry*, *4*(2), 90–98.

Bigay, J., Casella, J.-F., Drin, G., Mesmin, B., & Antonny, B. (2005). ArfGAP1 responds to membrane curvature through the folding of a lipid packing sensor motif. *The EMBO Journal*, *24*(13), 2244–2253.

Blumenreich, S., Barav, O. B., Jenkins, B. J., & Futerman, A. H. (2020). Lysosomal storage disorders shed light on lysosomal dysfunction in Parkinson's disease. *International Journal of Molecular Sciences*, *21*(14).

Boone, C., Bussey, H., & Andrews, B. J. (2007). Exploring genetic interactions and networks with yeast. *Nature Reviews. Genetics*, *8*(6), 437–449.

Bosgraaf, L., & Van Haastert, P. J. M. (2003). Roc, a Ras/GTPase domain in complex proteins. *Biochimica et Biophysica Acta*, *1643*(1-3), 5–10.

Boutros, M., Kiger, A. A., Armknecht, S., Kerr, K., Hild, M., Koch, B., Haas, S. A., Paro, R., Perrimon, N., & Heidelberg Fly Array Consortium. (2004). Genome-wide RNAi analysis of growth and viability in Drosophila cells. *Science*, *303*(5659), 832–835.

Boycott, K. M., Dyment, D. A., Sawyer, S. L., Vanstone, M. R., & Beaulieu, C. L. (2014). Identification of genes for childhood heritable diseases. *Annual Review of Medicine*, *65*, 19–31.

Bronstein, M. G., & Kakkis, E. D. (2016). Patients as key partners in rare disease drug development. *Nature Reviews. Drug Discovery*, *15*(11), 731–732.

Caldwell, K. A., Willicott, C. W., & Caldwell, G. A. (2020). Modeling neurodegeneration in Caenorhabditiselegans. *Disease Models & Mechanisms*, *13*(10).

Chartier-Harlin, M. C., Crawford, F., Houlden, H., Warren, A., Hughes, D., Fidani, L., Goate, A., Rossor, M., Roques, P., & Hardy, J. (1991). Early-onset Alzheimer's disease caused by mutations at codon 717 of the beta-amyloid precursor protein gene. *Nature*, *353*(6347), 844–846.

Chatr-Aryamontri, A., Oughtred, R., Boucher, L., Rust, J., Chang, C., Kolas, N. K., O'Donnell, L., Oster, S., Theesfeld, C., Sellam, A., Stark, C., Breitkreutz, B.J., Dolinski, K., & Tyers, M. (2017). The BioGRID interaction database: 2017 update. *Nucleic Acids Research*, *45*(D1), D369–D379.

Chaudhary, J., Sharma, V., Jain, A., Sharma, D., Chopra, B., & K Dhingra, A. (2023). A Profound Insight into the Structure-activity Relationship of Ubiquitous Scaffold Piperazine: An Explicative Review. *Medicinal chemistry (Shariqah (United Arab Emirates)*

Cha, Y., Erez, T., Reynolds, I. J., Kumar, D., Ross, J., Koytiger, G., Kusko, R., Zeskind, B., Risso, S., Kagan, E., Papapetropoulos, S., Grossman, I., & Laifenfeld, D. (2018). Drug repurposing from the perspective of pharmaceutical companies. *British Journal of Pharmacology*, *175*(2), 168–180.

Chen, C.Y., Weng, Y.H., Chien, K.Y., Lin, K.J., Yeh, T.H., Cheng, Y.P., Lu, C.S., & Wang, H.L. (2012). (G2019S) LRRK2 activates MKK4-JNK pathway and causes degeneration of SN dopaminergic neurons in a transgenic mouse model of PD. *Cell Death and Differentiation*, *19*(10), 1623–1633.

Chia, S. J., Tan, E.-K., & Chao, Y.-X. (2020). Historical Perspective: Models of Parkinson's Disease. *International Journal of Molecular Sciences*, *21*(7).

Chou, J.S., Chen, C.Y., Chen, Y.L., Weng, Y.H., Yeh, T.H., Lu, C.S., Chang, Y.M., & Wang, H.L. (2014). (G2019S) LRRK2 causes early-phase dysfunction of SNpc dopaminergic neurons and impairment of corticostriatal long-term depression in the PD transgenic mouse. *Neurobiology of Disease*, *68*, 190–199.

Chua, L. L., Ho, P., Toh, J., & Tan, E. K. (2020). Chetomin rescues pathogenic phenotype of LRRK2 mutation in drosophila. *Aging*, *12*(18), 18561–18570

Citron, M., Oltersdorf, T., Haass, C., McConlogue, L., Hung, A. Y., Seubert, P., Vigo-Pelfrey, C., Lieberburg, I., & Selkoe, D. J. (1992). Mutation of the beta-amyloid precursor protein in familial Alzheimer's disease increases beta-protein production. *Nature*, *360*(6405), 672–674.

Cooper, A. A., Gitler, A. D., Cashikar, A., Haynes, C. M., Hill, K. J., Bhullar, B., Liu, K., Xu, K., Strathearn, K. E., Liu, F., Cao, S., Caldwell, K. A., Caldwell, G. A., Marsischky, G., Kolodner, R. D., Labaer, J., Rochet, J.-C., Bonini, N. M., & Lindquist, S. (2006). Alpha-synuclein blocks ER-Golgi traffic and Rab1 rescues neuron loss in Parkinson's models. *Science*, *313*(5785), 324–328.

Cording, A. C., Shiaelis, N., Petridi, S., Middleton, C. A., Wilson, L. G., & Elliott, C. J. H. (2017). Targeted kinase inhibition relieves slowness and tremor in a Drosophila model of LRRK2 Parkinson's disease. *NPJ Parkinson's Disease*, *3*, 34.

Corsello, S. M., Bittker, J. A., Liu, Z., Gould, J., McCarren, P., Hirschman, J. E., Johnston, S. E., Vrcic, A., Wong, B., Khan, M., Asiedu, J., Narayan, R., Mader, C. C., Subramanian, A., & Golub, T. R. (2017). The drug repurposing hub: a next-generation drug library and information resource. *Nature Medicine*, *23*(4), 405–408.

Costanzo, M., Baryshnikova, A., Bellay, J., Kim, Y., Spear, E. D., Sevier, C. S., Ding, H., Koh, J. L. Y., Toufighi, K., Mostafavi, S., Prinz, J., St Onge, R. P., VanderSluis, B., Makhnevych, T., Vizeacoumar, F. J., Alizadeh, S., Bahr, S., Brost, R. L., Chen, Y., … Boone, C. (2010). The genetic landscape of a cell. *Science*, *327*(5964), 425–431.

Costanzo, M., VanderSluis, B., Koch, E. N., Baryshnikova, A., Pons, C., Tan, G., Wang, W., Usaj, M., Hanchard, J., Lee, S. D., Pelechano, V., Styles, E. B., Billmann, M., van Leeuwen, J., van Dyk, N., Lin, Z.-Y., Kuzmin, E., Nelson, J., Piotrowski, J. S., … Boone, C. (2016). A global genetic interaction network maps a wiring diagram of cellular function. *Science*, *353*(6306).

Cukierman, E., Huber, I., Rotman, M., & Cassel, D. (1995). The ARF1 GTPase-activating protein: zinc finger motif and Golgi complex localization. *Science*, *270*(5244).

Cunningham, L. A., & Moore, D. J. (2020). Endosomal sorting pathways in the pathogenesis of Parkinson's disease. *Progress in Brain Research*, *252*, 271–306.

Curwin, A. J., Fairn, G. D., & McMaster, C. R. (2009). Phospholipid transfer protein Sec14 is required for trafficking from endosomes and regulates distinct trans-Golgi export pathways. *The Journal of Biological Chemistry*, *284*(11), 7364–7375.

Deniston, C. K., Salogiannis, J., Mathea, S., Snead, D. M., Lahiri, I., Matyszewski, M., Donosa, O., Watanabe, R., Böhning, J., Shiau, A. K., Knapp, S., Villa, E., Reck-Peterson, S. L., & Leschziner, A. E. (2020). Structure of LRRK2 in Parkinson's disease and model for microtubule interaction. *Nature*, *588*, 344-349.

Dixon, S. J., Costanzo, M., Baryshnikova, A., Andrews, B., & Boone, C. (2009). Systematic mapping of genetic interaction networks. *Annual Review of Genetics*, *43*, 601–625.

Dodge, J. A., Chigladze, T., Donadieu, J., Grossman, Z., Ramos, F., Serlicorni, A., Siderius, L., Stefanidis, C. J., Tasic, V., Valiulis, A., & Wierzba, J. (2011). The importance of rare diseases: from the gene to society. *Archives of Disease in Childhood*, *96*(9), 791–792.

Dodson, M. W., Zhang, T., Jiang, C., Chen, S., & Guo, M. (2012). Roles of the Drosophila LRRK2 homolog in Rab7-dependent lysosomal positioning. *Human Molecular Genetics*, *21*(6), 1350–1363.

Do, J., McKinney, C., Sharma, P., & Sidransky, E. (2019). Glucocerebrosidase and its relevance to Parkinson disease. *Molecular Neurodegeneration*, *14*(1), 36.

Dowell, R. D., Ryan, O., Jansen, A., Cheung, D., Agarwala, S., Danford, T., Bernstein, D. A., Rolfe, P. A., Heisler, L. E., Chin, B., Nislow, C., Giaever, G., Phillips, P. C., Fink, G. R., Gifford, D. K., & Boone, C. (2010). Genotype to phenotype: a complex problem. *Science*, *328*(5977), 469.

Drin, G., Bigay, J., & Antonny, B. (2009). [Regulation of vesicular transport by membrane curvature]. *Medecine Sciences: M/S*, *25*(5), 483–488.

Dukes, A. A., Bai, Q., Van Laar, V. S., Zhou, Y., Ilin, V., David, C. N., Agim, Z. S., Bonkowsky, J. L., Cannon, J. R., Watkins, S. C., Croix, C. M. S., Burton, E. A., & Berman, S. B. (2016). Live imaging of mitochondrial dynamics in CNS dopaminergic neurons in vivo demonstrates early reversal of mitochondrial transport following MPP(+) exposure. *Neurobiology of Disease*, *95*, 238–249.

Duncan, M. C., Ho, D. G., Huang, J., Jung, M. E., & Payne, G. S. (2007). Composite synthetic lethal identification of membrane traffic inhibitors. *Proceedings of the National Academy of Sciences of the United States of America*, *104*(15), 6235–6240

Dung, V. M., & Thao, D. T. P. (2018). Parkinson's Disease Model. In M. Yamaguchi (Ed.), *Drosophila Models for Human Diseases* (pp. 41–61). Springer Singapore.

Dusonchet, J., Kochubey, O., Stafa, K., Young, S. M., Jr, Zufferey, R., Moore, D. J., Schneider, B. L., & Aebischer, P. (2011). A rat model of progressive nigral neurodegeneration induced by the Parkinson's disease-associated G2019S mutation in LRRK2. *The Journal of Neuroscience*, *31*(3), 907–912.

Eder, J., Sedrani, R., & Wiesmann, C. (2014). The discovery of first-in-class drugs: origins and evolution. *Nature Reviews. Drug Discovery*, *13*(8), 577–587.

Ekins, S. (2017). Industrializing rare disease therapy discovery and development. *Nature Biotechnology*, *35*(2), 117–118.

Enserink, J. M. (2012). Chemical genetics: budding yeast as a platform for drug discovery and mapping of genetic pathways. *Molecules*, *17*(8), 9258–9273.

Erb, M. L., & Moore, D. J. (2020). LRRK2 and the endolysosomal system in Parkinson's disease. *Journal of Parkinson's Disease*, *10*(4), 1271–1291.

Estrada, A. A., Chan, B. K., Baker-Glenn, C., Beresford, A., Burdick, D. J., Chambers, M., Chen, H., Dominguez, S. L., Dotson, J., Drummond, J., Flagella, M., Fuji, R., Gill, A., Halladay, J., Harris, S. F., Heffron, T. P., Kleinheinz, T., Lee, D. W., Le Pichon, C. E., Liu, X., … Sweeney, Z. K. (2014). Discovery of highly potent, selective, and brain-penetrant aminopyrazole leucine-rich repeat kinase 2 (LRRK2) small molecule inhibitors. *Journal of medicinal chemistry*, *57*(3), 921–936.

Fairn, G. D., MacDonald, K., & McMaster, C. R. (2007). A chemogenomic screen in Saccharomyces cerevisiae uncovers a primary role for the mitochondria in farnesol toxicity and its regulation by the Pkc1 pathway. *The Journal of Biological Chemistry*, *282*(7), 4868–4874.

Fairn, G. D., & McMaster, C. R. (2005). Studying phospholipid metabolism using yeast systematic and chemical genetics. *Methods*, *36*(2), 102–108.

Fletcher, E., Mercurio, K., Walden, E. A., & Baetz, K. (2021). A yeast chemogenomic screen identifies pathways that modulate adipic acid toxicity. *iScience*, *24*(4), 102327.

Foley, K. E. (2015). Model network: Canadian program aims to generate models for rare disease. *Nature Medicine*, *21*(11), 1242–1243.

Fox, S. H., & Brotchie, J. M. (2010). The MPTP-lesioned non-human primate models of Parkinson's disease. Past, present, and future. *Progress in Brain Research*, *184*, 133–157.

Fuji, R. N., Flagella, M., Baca, M., Baptista, M. A., Brodbeck, J., Chan, B. K., Fiske, B. K., Honigberg, L., Jubb, A. M., Katavolos, P., Lee, D. W., Lewin-Koh, S. C., Lin, T., Liu, X., Liu, S., Lyssikatos, J. P., O'Mahony, J., Reichelt, M., Roose-Girma, M., Sheng, Z., … Watts, R. J. (2015). Effect of selective LRRK2 kinase inhibition on nonhuman primate lung. *Science translational medicine*, *7*(273), 273ra15.

Gaspard, G. J., & McMaster, C. R. (2015). The mitochondrial quality control protein Yme1 is necessary to prevent defective mitophagy in a yeast model of Barth syndrome. *The Journal of Biological Chemistry*, *290*(14), 9284–9298.

Giaever, G., Flaherty, P., Kumm, J., Proctor, M., Nislow, C., Jaramillo, D. F., Chu, A. M., Jordan, M. I., Arkin, A. P., & Davis, R. W. (2004). Chemogenomic profiling: identifying the functional interactions of small molecules in yeast. *Proceedings of the National Academy of Sciences of the United States of America*, *101*(3), 793–798.

Giaever, G., Shoemaker, D. D., Jones, T. W., Liang, H., Winzeler, E. A., Astromoff, A., & Davis, R. W. (1999). Genomic profiling of drug sensitivities via induced haploinsufficiency. *Nature Genetics*, *21*(3), 278–283.

Gietz, R. D., & Schiestl, R. H. (2007). High-efficiency yeast transformation using the LiAc/SS carrier DNA/PEG method. *Nature Protocols*, *2*(1), 31–34.

Gitler, A. D., Bevis, B. J., Shorter, J., Strathearn, K. E., Hamamichi, S., Su, L. J., Caldwell, K. A., Caldwell, G. A., Rochet, J.-C., McCaffery, J. M., Barlowe, C., & Lindquist, S. (2008). The Parkinson's disease protein alpha-synuclein disrupts cellular Rab homeostasis. *Proceedings of the National Academy of Sciences of the United States of America*, *105*(1), 145–150.

Godena, V. K., Brookes-Hocking, N., Moller, A., Shaw, G., Oswald, M., Sancho, R. M., Miller, C. C. J., Whitworth, A. J., & De Vos, K. J. (2014). Increasing microtubule acetylation rescues axonal transport and locomotor deficits caused by LRRK2 Roc-COR domain mutations. *Nature Communications*, *5*, 5245.

Gómez-Benito, M., Granado, N., García-Sanz, P., Michel, A., Dumoulin, M., & Moratalla, R. (2020). Modeling Parkinson's disease with the alpha-synuclein protein. *Frontiers in Pharmacology*, *11*, 356.

Guernsey, D. L., Jiang, H., Campagna, D. R., Evans, S. C., Ferguson, M., Kellogg, M. D., Lachance, M., Matsuoka, M., Nightingale, M., Rideout, A., Saint-Amant, L., Schmidt, P. J., Orr, A., Bottomley, S. S., Fleming, M. D., Ludman, M., Dyack, S., Fernandez, C. V., & Samuels, M. E. (2009). Mutations in mitochondrial carrier family gene SLC25A38 cause nonsyndromic autosomal recessive congenital sideroblastic anemia. *Nature Genetics*, *41*(6), 651–653.

Guernsey, D. L., Matsuoka, M., Jiang, H., Evans, S., Macgillivray, C., Nightingale, M., Perry, S., Ferguson, M., LeBlanc, M., Paquette, J., Patry, L., Rideout, A. L., Thomas, A., Orr, A., McMaster, C. R., Michaud, J. L., Deal, C., Langlois, S., Superneau, D. W., … Samuels, M. E. (2011). Mutations in origin recognition complex gene ORC4 cause Meier-Gorlin syndrome. *Nature Genetics*, *43*(4), 360–364.

Gündner, A. L., Duran-Pacheco, G., Zimmermann, S., Ruf, I., Moors, T., Baumann, K., Jagasia, R., van de Berg, W. D. J., & Kremer, T. (2019). Path mediation analysis reveals GBA impacts Lewy body disease status by increasing α-synuclein levels. *Neurobiology of Disease*, *121*, 205–213.

Hang, L., Thundyil, J., & Lim, K.-L. (2015). Mitochondrial dysfunction and Parkinson disease: a Parkin-AMPK alliance in neuroprotection. *Annals of the New York Academy of Sciences*, *1350*(1), 37–47.

Hashimoto, S., Furukawa, S., Hashimoto, A., Tsutaho, A., Fukao, A., Sakamura, Y., Parajuli, G., Onodera, Y., Otsuka, Y., Handa, H., Oikawa, T., Hata, S., Nishikawa, Y., Mizukami, Y., Kodama, Y., Murakami, M., Fujiwara, T., Hirano, S., & Sabe, H. (2019). ARF6 and AMAP1 are major targets of *KRAS* and *TP53* mutations to promote invasion, PD-L1 dynamics, and immune evasion of pancreatic cancer. *Proceedings of the National Academy of Sciences of the United States of America*, *116*(35), 17450–17459.

Haun, R. S., Tsai, S. C., Adamik, R., Moss, J., & Vaughan, M. (1993). Effect of myristoylation on GTP-dependent binding of ADP-ribosylation factor to Golgi. *The Journal of Biological Chemistry*, *268*(10), 7064–7068.

Herzig, M. C., Kolly, C., Persohn, E., Theil, D., Schweizer, T., Hafner, T., Stemmelen, C., Troxler, T. J., Schmid, P., Danner, S., Schnell, C. R., Mueller, M., Kinzel, B., Grevot, A., Bolognani, F., Stirn, M., Kuhn, R. R., Kaupmann, K., van der Putten, P. H., Rovelli, G., … Shimshek, D. R. (2011). LRRK2 protein levels are determined by kinase function and are crucial for kidney and lung homeostasis in mice. *Human molecular genetics*, *20*(21), 4209–4223.

Hillenmeyer, M. E., Fung, E., Wildenhain, J., Pierce, S. E., Hoon, S., Lee, W., Proctor, M., St Onge, R. P., Tyers, M., Koller, D., Altman, R. B., Davis, R. W., Nislow, C., & Giaever, G. (2008). The chemical genomic portrait of yeast: uncovering a phenotype for all genes. *Science*, *320*(5874), 362–365.

Hindle, S., Afsari, F., Stark, M., Middleton, C. A., Evans, G. J. O., Sweeney, S. T., & Elliott, C. J. H. (2013). Dopaminergic expression of the Parkinsonian gene LRRK2-G2019S leads to non-autonomous visual neurodegeneration, accelerated by increased neural demands for energy. *Human Molecular Genetics*, *22*(11), 2129–2140.

Hobert, O. (2016). A map of terminal regulators of neuronal identity in Caenorhabditis elegans. *Wiley Interdisciplinary Reviews. Developmental Biology*, *5*(4), 474–498.

Ho, C. H., Piotrowski, J., Dixon, S. J., Baryshnikova, A., Costanzo, M., & Boone, C. (2011). Combining functional genomics and chemical biology to identify targets of bioactive compounds. *Current Opinion in Chemical Biology*, *15*(1), 66–78.

Howe, D. G., Bradford, Y. M., Eagle, A., Fashena, D., Frazer, K., Kalita, P., Mani, P., Martin, R., Moxon, S. T., Paddock, H., Pich, C., Ramachandran, S., Ruzicka, L., Schaper, K., Shao, X., Singer, A., Toro, S., Van Slyke, C., & Westerfield, M. (2017). The zebrafish model organism database: new support for human disease models, mutation details, gene expression phenotypes and searching. *Nucleic Acids Research*, *45*(D1), D758–D768.

Hsieh, C.-H., Shaltouki, A., Gonzalez, A. E., Bettencourt da Cruz, A., Burbulla, L. F., St Lawrence, E., Schüle, B., Krainc, D., Palmer, T. D., & Wang, X. (2016). Functional impairment in Miro degradation and mitophagy is a shared feature in familial andsSporadic Parkinson's disease. *Cell Stem Cell*, *19*(6), 709–724.

Huang, M., Wang, B., Li, X., Fu, C., Wang, C., & Kang, X. (2019). α-Synuclein: A multifunctional player in exocytosis, endocytosis, and vesicle recycling. *Frontiers in Neuroscience*, *13*, 28.

Huang, X., Wu, C., Park, Y., Long, X., Hoang, Q. Q., & Liao, J. (2019). The Parkinson's disease-associated mutation N1437H impairs conformational dynamics in the G domain of LRRK2. *FASEB Journal*, *33*(4), 4814–4823.

Huang, Y., Shenoy, S., Lu, B., Liu, W., & Li, C. (2012). Kinase signaling dysfunction in Parkinson's disease: a reverse genetic approach in Drosophila. *Journal of Neurogenetics*, *26*(2), 158–167.

Huber, I., Cukierman, E., Rotman, M., & Cassel, D. (2002). ARF GTPase-activating protein 1. *Methods in Molecular Biology, 189*, 199–206.

Imai, Y., Gehrke, S., Wang, H.-Q., Takahashi, R., Hasegawa, K., Oota, E., & Lu, B. (2008). Phosphorylation of 4E-BP by LRRK2 affects the maintenance of dopaminergic neurons in Drosophila. *The EMBO Journal*, *27*(18), 2432–2443.

Inoshita, T., Arano, T., Hosaka, Y., Meng, H., Umezaki, Y., Kosugi, S., Morimoto, T., Koike, M., Chang, H.-Y., Imai, Y., & Hattori, N. (2017). Vps35 in cooperation with LRRK2 regulates synaptic vesicle endocytosis through the endosomal pathway in Drosophila. *Human Molecular Genetics*, *26*(15), 2933–2948.

Islam, M. S., & Moore, D. J. (2017). Mechanisms of LRRK2-dependent neurodegeneration: role of enzymatic activity and protein aggregation. *Biochemical Society Transactions*, *45*(1), 163–172.

Ito, G., Katsemonova, K., Tonelli, F., Lis, P., Baptista, M. A. S., Shpiro, N., Duddy, G., Wilson, S., Ho, P. W.-L., Ho, S.-L., Reith, A. D., & Alessi, D. R. (2016). Phos-tag analysis of Rab10 phosphorylation by LRRK2: a powerful assay for assessing kinase function and inhibitors. *Biochemical Journal*, *473*(17), 2671–2685.

Jaiswal, M., Sandoval, H., Zhang, K., Bayat, V., & Bellen, H. J. (2012). Probing mechanisms that underlie human neurodegenerative diseases in Drosophila. *Annual Review of Genetics*, *46*, 371–396.

Jennings, D., Huntwork-Rodriguez, S., Henry, A. G., Sasaki, J. C., Meisner, R., Diaz, D., Solanoy, H., Wang, X., Negrou, E., Bondar, V. V., Ghosh, R., Maloney, M. T., Propson, N. E., Zhu, Y., Maciuca, R. D., Harris, L., Kay, A., LeWitt, P., King, T. A., Kern, D., … Troyer, M. D. (2022). Preclinical and clinical evaluation of the LRRK2 inhibitor DNL201 for Parkinson's disease. *Science translational medicine*, *14*(648), eabj2658.

Jerabek-Willemsen, M., Wienken, C. J., Braun, D., Baaske, P., & Duhr, S. (2011). Molecular interaction studies using microscale thermophoresis. *Assay and Drug Development Technologies*, *9*(4), 342–353.

Joppi, R., Gerardi, C., Bertele', V., & Garattini, S. (2016). Letting post-marketing bridge the evidence gap: the case of orphan drugs. *BMJ*, *353*, i2978.

Kachroo, A. H., Laurent, J. M., Yellman, C. M., Meyer, A. G., Wilke, C. O., & Marcotte, E. M. (2015). Evolution. Systematic humanization of yeast genes reveals conserved functions and genetic modularity. *Science*, *348*(6237), 921–925.

Kahn, R. A., Bruford, E., Inoue, H., Logsdon, J. M., Jr, Nie, Z., Premont, R. T., Randazzo, P. A., Satake, M., Theibert, A. B., Zapp, M. L., & Cassel, D. (2008). Consensus nomenclature for the human ArfGAP domain-containing proteins. *The Journal of Cell Biology*, *182*(6), 1039–1044.

Langston, J. W. (2017). The MPTP Story. *Journal of Parkinson's Disease*, *7*(s1), S11–S19.

Langston, J. W., Ballard, P., Tetrud, J. W., & Irwin, I. (1983). Chronic parkinsonism in humans due to a product of meperidine-analog synthesis. *Science*, *219*(4587), 979–980.

Lee, A. Y., St Onge, R. P., Proctor, M. J., Wallace, I. M., Nile, A. H., Spagnuolo, P. A., Jitkova, Y., Gronda, M., Wu, Y., Kim, M. K., Cheung-Ong, K., Torres, N. P., Spear, E. D., Han, M. K. L., Schlecht, U., Suresh, S., Duby, G., Heisler, L. E., Surendra, A., … Giaever, G. (2014). Mapping the cellular response to small molecules using chemogenomic fitness signatures. *Science*, *344*(6180), 208–211.

Lee, S. B., Kim, W., Lee, S., & Chung, J. (2007). Loss of LRRK2/PARK8 induces degeneration of dopaminergic neurons in Drosophila. *Biochemical and Biophysical Research Communications*, *358*(2), 534–539.

Lehner, B. (2013). Genotype to phenotype: lessons from model organisms for human genetics. *Nature Reviews. Genetics*, *14*(3), 168–178.

Lemieux, G. A., & Ashrafi, K. (2015). Neural regulatory pathways of feeding and fat in Caenorhabditis elegans. *Annual Review of Genetics*, *49*, 413–438.

Leschziner, A. E., & Reck-Peterson, S. L. (2021). Scientific perspectives: Structural biology of LRRK2 and its interaction with microtubules. *Movement Disorders*.

Li, H., Jiang, H., Zhang, B., & Feng, J. (2018). Modeling Parkinson's disease using patient-specific induced pluripotent stem cells. *Journal of Parkinson's Disease*, *8*(4), 479–493.

Lin, C.H., Tsai, P.I., Wu, R.M., & Chien, C.T. (2010). LRRK2 G2019S mutation induces dendrite degeneration through mislocalization and phosphorylation of tau by recruiting autoactivated GSK3ß. *The Journal of Neuroscience*, *30*(39), 13138–13149.

Lin, K.J., Lin, K.L., Chen, S.D., Liou, C.W., Chuang, Y.C., Lin, H.Y., & Lin, T.K. (2019). The overcrowded crossroads: Mitochondria, alpha-synuclein, and the endo-lysosomal system interaction in Parkinson's disease. *International Journal of Molecular Sciences*, *20*(21).

Lionta, E., Spyrou, G., Vassilatis, D. K., & Cournia, Z. (2014). Structure-based virtual screening for drug discovery: principles, applications and recent advances. *Current topics in medicinal chemistry*, *14*(16), 1923–1938.

Lipinski, C. A., Lombardo, F., Dominy, B. W., & Feeney, P. J. (2001). Experimental and computational approaches to estimate solubility and permeability in drug discovery and development settings. *Advanced drug delivery reviews*, *46*(1-3), 3–26.

Liu, Z., Hamamichi, S., Lee, B. D., Yang, D., Ray, A., Caldwell, G. A., Caldwell, K. A., Dawson, T. M., Smith, W. W., & Dawson, V. L. (2011). Inhibitors of LRRK2 kinase attenuate neurodegeneration and Parkinson-like phenotypes in Caenorhabditis elegans and Drosophila Parkinson's disease models. *Human Molecular Genetics*, *20*(20), 3933–3942.

Liu, Z., Wang, X., Yu, Y., Li, X., Wang, T., Jiang, H., Ren, Q., Jiao, Y., Sawa, A., Moran, T., Ross, C. A., Montell, C., & Smith, W. W. (2008). A Drosophila model for LRRK2-linked parkinsonism. *Proceedings of the National Academy of Sciences of the United States of America*, *105*(7), 2693–2698.

MacLeod, D. A., Rhinn, H., Kuwahara, T., Zolin, A., Di Paolo, G., McCabe, B. D., Marder, K. S., Honig, L. S., Clark, L. N., Small, S. A., & Abeliovich, A. (2013). RAB7L1 interacts with LRRK2 to modify intraneuronal protein sorting and Parkinson's disease risk. *Neuron*, *77*(3), 425–439.

Malpartida, A. B., Williamson, M., Narendra, D. P., Wade-Martins, R., & Ryan, B. J. (2020). Mitochondrial dysfunction and mitophagy in Parkinson's disease: From mechanism to therapy. *Trends in Biochemical Sciences*.

Manning-Bog, A. B., & Langston, J. W. (2007). Model fusion, the next phase in developing animal models for Parkinson's disease. *Neurotoxicity Research*, *11*(3-4), 219–240.

Matlack, K. E. S., Tardiff, D. F., Narayan, P., Hamamichi, S., Caldwell, K. A., Caldwell, G. A., & Lindquist, S. (2014). Clioquinol promotes the degradation of metal-dependent amyloid-β (Aβ) oligomers to restore endocytosis and ameliorate Aβ toxicity. *Proceedings of the National Academy of Sciences of the United States of America*, *111*(11), 4013–4018.

Matta, S., Van Kolen, K., da Cunha, R., van den Bogaart, G., Mandemakers, W., Miskiewicz, K., De Bock, P.-J., Morais, V. A., Vilain, S., Haddad, D., Delbroek, L., Swerts, J., Chávez-Gutiérrez, L., Esposito, G., Daneels, G., Karran, E., Holt, M., Gevaert, K., Moechars, D. W., … Verstreken, P. (2012). LRRK2 controls an EndoA phosphorylation cycle in synaptic endocytosis. *Neuron*, *75*(6), 1008–1021.

Mattiazzi Usaj, M., Styles, E. B., Verster, A. J., Friesen, H., Boone, C., & Andrews, B. J. (2016). High-content screening for quantitative cell biology. *Trends in Cell Biology*, *26*(8), 598–611.

Mawuenyega, K. G., Sigurdson, W., Ovod, V., Munsell, L., Kasten, T., Morris, J. C., Yarasheski, K. E., & Bateman, R. J. (2010). Decreased clearance of CNS beta-amyloid in Alzheimer's disease. *Science*, *330*(6012), 1774.

Mazzulli, J. R., Xu, Y.H., Sun, Y., Knight, A. L., McLean, P. J., Caldwell, G. A., Sidransky, E., Grabowski, G. A., & Krainc, D. (2011). Gaucher disease glucocerebrosidase and α-synuclein form a bidirectional pathogenic loop in synucleinopathies. *Cell*, *146*(1), 37–52.

McLornan, D. P., List, A., & Mufti, G. J. (2014). Applying synthetic lethality for the selective targeting of cancer. *The New England Journal of Medicine*, *371*(18), 1725–1735.

Mehra, S., Sahay, S., & Maji, S. K. (2019). α-Synuclein misfolding and aggregation: Implications in Parkinson's disease pathogenesis. *Biochimica et Biophysica Acta - Proteins and Proteomics*, *1867*(10), 890–908.

Meng, D., Yang, Q., Melick, C. H., Park, B. C., Hsieh, T.-S., Curukovic, A., Jeong, M.-H., Zhang, J., James, N. G., & Jewell, J. L. (2021). ArfGAP1 inhibits mTORC1 lysosomal localization and activation. *The EMBO Journal*, *40*(12), e106412.

Millburn, G. H., Crosby, M. A., Gramates, L. S., Tweedie, S., & FlyBase Consortium. (2016). FlyBase portals to human disease research using Drosophila models. *Disease Models & Mechanisms*, *9*(3), 245–252.

Moffat, J. G., Vincent, F., Lee, J. A., Eder, J., & Prunotto, M. (2017). Opportunities and challenges in phenotypic drug discovery: an industry perspective. *Nature Reviews. Drug Discovery*, *16*(8), 531–543.

Mor, D. E., Tsika, E., Mazzulli, J. R., Gould, N. S., Kim, H., Daniels, M. J., Doshi, S., Gupta, P., Grossman, J. L., Tan, V. X., Kalb, R. G., Caldwell, K. A., Caldwell, G. A., Wolfe, J. H., & Ischiropoulos, H. (2017). Dopamine induces soluble α-synuclein oligomers and nigrostriatal degeneration. *Nature Neuroscience*, *20*(11), 1560–1568.

Mullan, M., Crawford, F., Axelman, K., Houlden, H., Lilius, L., Winblad, B., & Lannfelt, L. (1992). A pathogenic mutation for probable Alzheimer's disease in the APP gene at the N-terminus of beta-amyloid. *Nature Genetics*, *1*(5), 345–347.

Myasnikov, A., Zhu, H., Hixson, P., Xie, B., Yu, K., Pitre, A., Peng, J., & Sun, J. (2021). Structural analysis of the full-length human LRRK2. *Cell*, *184*(13), 3519–3527.e10.

Nalls, M. A., Pankratz, N., Lill, C. M., Do, C. B., Hernandez, D. G., Saad, M., DeStefano, A. L., Kara, E., Bras, J., Sharma, M., Schulte, C., Keller, M. F., Arepalli, S., Letson, C., Edsall, C., Stefansson, H., Liu, X., Pliner, H., Lee, J. H., … Singleton, A. B. (2014). Large-scale meta-analysis of genome-wide association data identifies six new risk loci for Parkinson's disease. *Nature Genetics*, *46*(9), 989–993.

Ng, C.-H., Mok, S. Z. S., Koh, C., Ouyang, X., Fivaz, M. L., Tan, E.-K., Dawson, V. L., Dawson, T. M., Yu, F., & Lim, K.-L. (2009). Parkin protects against LRRK2 G2019S mutant-induced dopaminergic neurodegeneration in Drosophila. *The Journal of Neuroscience*, *29*(36), 11257–11262.

Nguyen, A. P. T., Daniel, G., Valdés, P., Islam, M. S., Schneider, B. L., & Moore, D. J. (2018). G2019S LRRK2 enhances the neuronal transmission of tau in the mouse brain. *Human Molecular Genetics*, *27*(1), 120–134.

Nguyen, A. P. T., & Moore, D. J. (2017). Understanding the GTPase Activity of LRRK2: Regulation, Function, and Neurotoxicity. *Advances in Neurobiology*, *14*, 71–88.

Ntie-Kang F. (2013). An in silico evaluation of the ADMET profile of the StreptomeDB database. *SpringerPlus*, *2*, 353.

Nuber, S., Rajsombath, M., Minakaki, G., Winkler, J., Müller, C. P., Ericsson, M., Caldarone, B., Dettmer, U., & Selkoe, D. J. (2018). Abrogating native α-Synuclein tetramers in mice causes a L-DOPA-responsive motor syndrome closely resembling Parkinson's disease. *Neuron*, *100*(1), 75–90.e5.

Onodera, Y., Nam, J. M., Horikawa, M., Shirato, H., & Sabe, H. (2018). Arf6-driven cell invasion is intrinsically linked to TRAK1-mediated mitochondrial anterograde trafficking to avoid oxidative catastrophe. *Nature communications*, *9*(1), 2682.

Outeiro, T. F., & Lindquist, S. (2003). Yeast cells provide insight into alpha-synuclein biology and pathobiology. *Science*, *302*(5651), 1772–1775.

Paisán-Ruíz, C., Jain, S., Evans, E. W., Gilks, W. P., Simón, J., van der Brug, M., López de Munain, A., Aparicio, S., Gil, A. M., Khan, N., Johnson, J., Martinez, J. R., Nicholl, D., Martí Carrera, I., Pena, A. S., de Silva, R., Lees, A., Martí-Massó, J. F., Pérez-Tur, J., … Singleton, A. B. (2004). Cloning of the gene containing mutations that cause PARK8-linked Parkinson's disease. *Neuron*, *44*(4), 595–600.

Piliarik, M., Vaisocherová, H., & Homola, J. (2009). Surface plasmon resonance biosensing. *Methods in Molecular Biology, 503*, 65–88.

Polymeropoulos, M. H., Lavedan, C., Leroy, E., Ide, S. E., Dehejia, A., Dutra, A., Pike, B., Root, H., Rubenstein, J., Boyer, R., Stenroos, E. S., Chandrasekharappa, S., Athanassiadou, A., Papapetropoulos, T., Johnson, W. G., Lazzarini, A. M., Duvoisin, R. C., Di Iorio, G., Golbe, L. I., & Nussbaum, R. L. (1997). Mutation in the alpha-synuclein gene identified in families with Parkinson's disease. *Science*, *276*(5321), 2045–2047.

Poon, P. P., Nothwehr, S. F., Singer, R. A., & Johnston, G. C. (2001). The Gcs1 and Age2 ArfGAP proteins provide overlapping essential function for transport from the yeast trans-Golgi network. *The Journal of Cell Biology*, *155*(7), 1239–1250.

Poon, P. P., Wang, X., Rotman, M., Huber, I., Cukierman, E., Cassel, D., Singer, R. A., & Johnston, G. C. (1996). Saccharomyces cerevisiae Gcs1 is an ADP-ribosylation factor GTPase-activating protein. *Proceedings of the National Academy of Sciences of the United States of America*, *93*(19), 10074–10077.

Prabhudesai, S., Bensabeur, F. Z., Abdullah, R., Basak, I., Baez, S., Alves, G., Holtzman, N. G., Larsen, J. P., & Møller, S. G. (2016). LRRK2 knockdown in zebrafish causes developmental defects, neuronal loss, and synuclein aggregation. *Journal of Neuroscience Research*, *94*(8), 717–735.

Qiang, W., Yau, W.M., Lu, J.X., Collinge, J., & Tycko, R. (2017). Structural variation in amyloid-β fibrils from Alzheimer's disease clinical subtypes. *Nature*, *541*(7636), 217–221.

Rajan, S., Toh, H.T., Ye, H., et al. Prostaglandin A2 Interacts with Nurr1 and Ameliorates Behavioral Deficits in Parkinson's Disease Fly Model. *Neuromolecular Med*. 2022;24(4):469-478.

Ramonet, D., Daher, J. P. L., Lin, B. M., Stafa, K., Kim, J., Banerjee, R., Westerlund, M., Pletnikova, O., Glauser, L., Yang, L., Liu, Y., Swing, D. A., Beal, M. F., Troncoso, J. C., McCaffery, J. M., Jenkins, N. A., Copeland, N. G., Galter, D., Thomas, B., … Moore, D. J. (2011). Dopaminergic neuronal loss, reduced neurite complexity and autophagic abnormalities in transgenic mice expressing G2019S mutant LRRK2. *PloS One*, *6*(4), e18568.

Ren, G., Xin, S., Li, S., Zhong, H., & Lin, S. (2011). Disruption of LRRK2 does not cause specific loss of dopaminergic neurons in zebrafish. *PloS One*, *6*(6), e20630.

Reynolds, A., Doggett, E. A., Riddle, S. M., Lebakken, C. S., & Nichols, R. J. (2014). LRRK2 kinase activity and biology are not uniformly predicted by its autophosphorylation and cellular phosphorylation site status. *Frontiers in Molecular Neuroscience*, *7*, 54.

Saha, S., Guillily, M. D., Ferree, A., Lanceta, J., Chan, D., Ghosh, J., Hsu, C. H., Segal, L., Raghavan, K., Matsumoto, K., Hisamoto, N., Kuwahara, T., Iwatsubo, T., Moore, L., Goldstein, L., Cookson, M., & Wolozin, B. (2009). LRRK2 modulates vulnerability to mitochondrial dysfunction in Caenorhabditis elegans. *The Journal of Neuroscience*, *29*(29), 9210–9218.

Sämann, J., Hegermann, J., von Gromoff, E., Eimer, S., Baumeister, R., & Schmidt, E. (2009). Caenorhabditits elegans LRK-1 and PINK-1 act antagonistically in stress response and neurite outgrowth. *The Journal of Biological Chemistry*, *284*(24), 16482–16491.

Schirle, M., & Jenkins, J. L. (2016). Identifying compound efficacy targets in phenotypic drug discovery. *Drug Discovery Today*, *21*(1), 82–89.

Schmidt, S. H., Knape, M. J., Boassa, D., Mumdey, N., Kornev, A. P., Ellisman, M. H., Taylor, S. S., & Herberg, F. W. (2019). The dynamic switch mechanism that leads to activation of LRRK2 Is embedded in the DFGψ motif in the kinase domain. *Proceedings of the National Academy of Sciences of the United States of America,* 116(30): 14979–88.

Seegobin, S. P., Heaton, G. R., Liang, D., Choi, I., Blanca Ramirez, M., Tang, B., & Yue, Z. (2020). Progress in LRRK2-associated Parkinson’s disease animal models. *Frontiers in Neuroscience*, *14*, 674.

Sejwal, K., Chami, M., Rémigy, H., Vancraenenbroeck, R., Sibran, W., Sütterlin, R., Baumgartner, P., McLeod, R., Chartier-Harlin, M.C., Baekelandt, V., Stahlberg, H., & Taymans, J.M. (2017). Cryo-EM analysis of homodimeric full-length LRRK2 and LRRK1 protein complexes. *Scientific Reports*, *7*(1), 8667.

Sekigawa, M., Kunoh, T., Wada, S.I., Mukai, Y., Ohshima, K., Ohta, S., Goshima, N., Sasaki, R., & Mizukami, T. (2010). Comprehensive screening of human genes with inhibitory effects on yeast growth and validation of a yeast cell-based system for screening chemicals. *Journal of Biomolecular Screening*, *15*(4), 368–378.

Sekine, S. (2020). PINK1 import regulation at a crossroad of mitochondrial fate: the molecular mechanisms of PINK1 import. *Journal of Biochemistry*, *167*(3), 217–224.

Senchuk, M. M., Van Raamsdonk, J. M., & Moore, D. J. (2021). Multiple genetic pathways regulating lifespan extension are neuroprotective in a G2019S LRRK2 nematode model of Parkinson's disease. *Neurobiology of Disease*, *151*, 105267.

Shadrina, M., & Slominsky, P. (2021). Modeling Parkinson's disease: Not only rodents? *Frontiers in Aging Neuroscience*, *13*, 695718.

Sheng, D., Qu, D., Kwok, K. H. H., Ng, S. S., Lim, A. Y. M., Aw, S. S., Lee, C. W. H., Sung, W. K., Tan, E. K., Lufkin, T., Jesuthasan, S., Sinnakaruppan, M., & Liu, J. (2010). Deletion of the WD40 domain of LRRK2 in Zebrafish causes Parkinsonism-like loss of neurons and locomotive defect. *PLoS Genetics*, *6*(4), e1000914.

Sheng, Z., Zhang, S., Bustos, D., Kleinheinz, T., Le Pichon, C. E., Dominguez, S. L., Solanoy, H. O., Drummond, J., Zhang, X., Ding, X., Cai, F., Song, Q., Li, X., Yue, Z., van der Brug, M. P., Burdick, D. J., Gunzner-Toste, J., Chen, H., Liu, X., … Zhu, H. (2012). Ser1292 autophosphorylation is an indicator of LRRK2 kinase activity and contributes to the cellular effects of PD mutations. *Science Translational Medicine*, *4*(164), 164ra161.

Singh, M. K., Gao, H., Sun, W., Song, Z., Schmalzigaug, R., Premont, R. T., & Zhang, Q. (2015). Structure-activity relationship studies of QS11, a small molecule Wnt synergistic agonist. *Bioorganic & Medicinal Chemistry Letters*.

Singleton, A. B., Farrer, M., Johnson, J., Singleton, A., Hague, S., Kachergus, J., Hulihan, M., Peuralinna, T., Dutra, A., Nussbaum, R., Lincoln, S., Crawley, A., Hanson, M., Maraganore, D., Adler, C., Cookson, M. R., Muenter, M., Baptista, M., Miller, D., … Gwinn-Hardy, K. (2003). alpha-Synuclein locus triplication causes Parkinson's disease. *Science*, *302*(5646), 841.

Sitaraman, D., Zars, M., Laferriere, H., Chen, Y.-C., Sable-Smith, A., Kitamoto, T., Rottinghaus, G. E., & Zars, T. (2008). Serotonin is necessary for place memory in Drosophila. *Proceedings of the National Academy of Sciences of the United States of America*, *105*(14), 5579–5584.

Smith, A. M., Ammar, R., Nislow, C., & Giaever, G. (2010). A survey of yeast genomic assays for drug and target discovery. *Pharmacology & Therapeutics*, *127*(2), 156–164.

Smith, W. W., Pei, Z., Jiang, H., Dawson, V. L., Dawson, T. M., & Ross, C. A. (2006). Kinase activity of mutant LRRK2 mediates neuronal toxicity. *Nature Neuroscience*, *9*(10), 1231–1233.

Spang, A., Shiba, Y., & Randazzo, P. A. (2010). Arf GAPs: Gatekeepers of vesicle generation. *FEBS Letters*, 584(12), 2646–51.

Stafa, K., Trancikova, A., Webber, P. J., Glauser, L., West, A. B., & Moore, D. J. (2012). GTPase activity and neuronal toxicity of Parkinson's disease-associated LRRK2 is regulated by ArfGAP1. *PLoS Genetics*, *8*(2), e1002526.

Stayte, S., & Vissel, B. (2014). Advances in non-dopaminergic treatments for Parkinson's disease. *Frontiers in Neuroscience*, *8*, 113.

Steger, M., Tonelli, F., Ito, G., Davies, P., Trost, M., Vetter, M., Wachter, S., Lorentzen, E., Duddy, G., Wilson, S., Baptista, M. A., Fiske, B. K., Fell, M. J., Morrow, J. A., Reith, A. D., Alessi, D. R., & Mann, M. (2016). Phosphoproteomics reveals that Parkinson's disease kinase LRRK2 regulates a subset of Rab GTPases. *eLife*, *5*.

Steinberg, T. H. (1994). Cellular transport of drugs. *Clinical Infectious Diseases*, *19*(5), 916–921.

Steinmetz, L. M., Scharfe, C., Deutschbauer, A. M., Mokranjac, D., Herman, Z. S., Jones, T., Chu, A. M., Giaever, G., Prokisch, H., Oefner, P. J., & Davis, R. W. (2002). Systematic screen for human disease genes in yeast. *Nature Genetics*, *31*(4), 400–404.

Stormo, A. E. D., FitzGibbon, M., Shavarebi, F., Earley, E. M., Lum, L. S., Verschueren, E., Swaney, D. L., Skibinski, G., Ravisankar, A., van Haren, J., Davis, E. J., Johnson, J. R., Von Dollen, J., Mirescu, C., Iaccarino, C., Dauer, W. T., Nichols, R. J., Wittmann, T., Cox, T. C., … Hiniker, A. (2020). The E3 ligase TRIM1 ubiquitinates LRRK2 and controls its localization, degradation, and toxicity. In *bioRxiv* (p. 2020.10.21.336578).

Sun, S., Yang, F., Tan, G., Costanzo, M., Oughtred, R., Hirschman, J., Theesfeld, C. L., Bansal, P., Sahni, N., Yi, S., Yu, A., Tyagi, T., Tie, C., Hill, D. E., Vidal, M., Andrews, B. J., Boone, C., Dolinski, K., & Roth, F. P. (2016). An extended set of yeast-based functional assays accurately identifies human disease mutations. *Genome Research*, *26*(5), 670–680.

Szabo, M., Svensson Akusjärvi, S., Saxena, A., Liu, J., Chandrasekar, G., & Kitambi, S. S. (2017). Cell and small animal models for phenotypic drug discovery. *Drug Design, Development and Therapy*, *11*, 1957–1967.

Tang, B. L. (2017). Rabs, membrane dynamics, and Parkinson's disease. *Journal of Cellular Physiology*, *232*(7), 1626–1633.

Tang, F.L., Liu, W., Hu, J.X., Erion, J. R., Ye, J., Mei, L., & Xiong, W.C. (2015). VPS35 deficiency or mutation causes dopaminergic neuronal loss by impairing mitochondrial fusion and function. *Cell Reports*, *12*(10), 1631–1643.

Tardiff, D. F., Khurana, V., Chung, C. Y., & Lindquist, S. (2014). From yeast to patient neurons and back again: powerful new discovery platform. *Movement Disorders*, *29*(10), 1231–1240.

Tcw, J., & Goate, A. M. (2017). Genetics of β-amyloid precursor protein in Alzheimer's disease. *Cold Spring Harbor Perspectives in Medicine*, *7*(6).

Tegel, H., Tourle, S., Ottosson, J., & Persson, A. (2010). Increased levels of recombinant human proteins with the Escherichia coli strain Rosetta(DE3). *Protein Expression and Purification*, *69*(2), 159–167.

Tolosa, E., Vila, M., Klein, C., & Rascol, O. (2020). LRRK2 in Parkinson disease: challenges of clinical trials. *Nature Reviews. Neurology*, *16*(2), 97–107.

Tong, A. H., Evangelista, M., Parsons, A. B., Xu, H., Bader, G. D., Pagé, N., Robinson, M., Raghibizadeh, S., Hogue, C. W., Bussey, H., Andrews, B., Tyers, M., & Boone, C. (2001). Systematic genetic analysis with ordered arrays of yeast deletion mutants. *Science*, *294*(5550), 2364–2368.

Tong, A. H. Y., Lesage, G., Bader, G. D., Ding, H., Xu, H., Xin, X., Young, J., Berriz, G. F., Brost, R. L., Chang, M., Chen, Y., Cheng, X., Chua, G., Friesen, H., Goldberg, D. S., Haynes, J., Humphries, C., He, G., Hussein, S., … Boone, C. (2004). Global mapping of the yeast genetic interaction network. *Science*, *303*(5659), 808–813.

Tong, Y., Yamaguchi, H., Giaime, E., Boyle, S., Kopan, R., Kelleher, R. J., & Shen, J. (2010). Loss of leucine-rich repeat kinase 2 causes impairment of protein degradation pathways, accumulation of alpha-synuclein, and apoptotic cell death in aged mice. *Proceedings of the National Academy of Sciences of the United States of America*, *107*(21), 9879–9884.

Treusch, S., Hamamichi, S., Goodman, J. L., Matlack, K. E. S., Chung, C. Y., Baru, V., Shulman, J. M., Parrado, A., Bevis, B. J., Valastyan, J. S., Han, H., Lindhagen-Persson, M., Reiman, E. M., Evans, D. A., Bennett, D. A., Olofsson, A., DeJager, P. L., Tanzi, R. E., Caldwell, K. A., … Lindquist, S. (2011). Functional links between Aβ toxicity, endocytic trafficking, and Alzheimer's disease risk factors in yeast. *Science*, *334*(6060), 1241–1245.

Ugur, B., Chen, K., & Bellen, H. J. (2016). Drosophila tools and assays for the study of human diseases. *Disease Models & Mechanisms*, *9*(3), 235–244.

Usmani, A., Shavarebi, F., & Hiniker, A. (2021). The Cell Biology of LRRK2 in Parkinson's Disease. *Molecular and Cellular Biology*. https://doi.org/10.1128/MCB.00660-20

van Leeuwen, J., Pons, C., Mellor, J. C., Yamaguchi, T. N., Friesen, H., Koschwanez, J., Ušaj, M. M., Pechlaner, M., Takar, M., Ušaj, M., VanderSluis, B., Andrusiak, K., Bansal, P., Baryshnikova, A., Boone, C. E., Cao, J., Cote, A., Gebbia, M., Horecka, G., … Boone, C. (2016). Exploring genetic suppression interactions on a global scale. *Science*, *354*(6312).

Vaz, R. L., Outeiro, T. F., & Ferreira, J. J. (2018). Zebrafish as an animal model for drug discovery in Parkinson's disease and other movement disorders: A systematic review. *Frontiers in Neurology*, *9*, 347.

Venderova, K., Kabbach, G., Abdel-Messih, E., Zhang, Y., Parks, R. J., Imai, Y., Gehrke, S., Ngsee, J., Lavoie, M. J., Slack, R. S., Rao, Y., Zhang, Z., Lu, B., Haque, M. E., & Park, D. S. (2009). Leucine-rich repeat kinase 2 interacts with Parkin, DJ-1 and PINK-1 in a Drosophila melanogaster model of Parkinson's disease. *Human Molecular Genetics*, *18*(22), 4390–4404.

Vidyadhara, D. J., Lee, J. E., & Chandra, S. S. (2019). Role of the endolysosomal system in Parkinson's disease. *Journal of Neurochemistry*, *150*(5), 487–506.

Vilariño-Güell, C., Wider, C., Ross, O. A., Dachsel, J. C., Kachergus, J. M., Lincoln, S. J., Soto-Ortolaza, A. I., Cobb, S. A., Wilhoite, G. J., Bacon, J. A., Behrouz, B., Melrose, H. L., Hentati, E., Puschmann, A., Evans, D. M., Conibear, E., Wasserman, W. W., Aasly, J. O., Burkhard, P. R., … Farrer, M. J. (2011). VPS35 mutations in Parkinson disease. *American Journal of Human Genetics*, *89*(1), 162–167.

Volta, M., & Melrose, H. (2017). LRRK2 mouse models: dissecting the behavior, striatal neurochemistry and neurophysiology of PD pathogenesis. *Biochemical Society Transactions*, *45*(1), 113–122.

Wagner, B. K. (2016). The resurgence of phenotypic screening in drug discovery and development. *Expert Opinion on Drug Discovery*, *11*(2), 121–125.

Watanabe, R., Buschauer, R., Böhning, J., Audagnotto, M., Lasker, K., Lu, T.-W., Boassa, D., Taylor, S., & Villa, E. (2020). The in situ structure of Parkinson's disease-linked LRRK2. *Cell*, *182*(6), 1508–1518.e16.

Wauters, F., Cornelissen, T., Imberechts, D., Martin, S., Koentjoro, B., Sue, C., Vangheluwe, P., & Vandenberghe. W. (2020). LRRK2 mutations impair depolarization-induced mitophagy through inhibition of mitochondrial accumulation of RAB10. *Autophagy,*16(2), 203–22.

Williams, E. T., Chen, X., & Moore, D. J. (2017). VPS35, the retromer complex and Parkinson's disease. *Journal of Parkinson's Disease*, *7*(2), 219–233.

Winslow, A. R., Chen, C.W., Corrochano, S., Acevedo-Arozena, A., Gordon, D. E., Peden, A. A., Lichtenberg, M., Menzies, F. M., Ravikumar, B., Imarisio, S., Brown, S., O'Kane, C. J., & Rubinsztein, D. C. (2010). α-Synuclein impairs macroautophagy: implications for Parkinson's disease. *The Journal of Cell Biology*, *190*(6), 1023–1037.

Wint, J. M., & Sirotkin, H. I. (2020). Lrrk2 modulation of Wnt signaling during zebrafish development. *Journal of Neuroscience Research*, *98*(10), 1831–1842.

Wong, L. H., Sinha, S., Bergeron, J. R., Mellor, J. C., Giaever, G., Flaherty, P., & Nislow, C. (2016). Reverse chemical genetics: Comprehensive fitness profiling reveals the spectrum of drug target interactions. *PLoS Genetics*, *12*(9), e1006275.

Woods, I. G., Kelly, P. D., Chu, F., Ngo-Hazelett, P., Yan, Y. L., Huang, H., Postlethwait, J. H., & Talbot, W. S. (2000). A comparative map of the zebrafish genome. *Genome Research*, *10*(12), 1903–1914.

Xiong, Y., Coombes, C. E., Kilaru, A., Li, X., Gitler, A. D., Bowers, W. J., Dawson, V. L., Dawson, T. M., & Moore, D. J. (2010). GTPase activity plays a key role in the pathobiology of LRRK2. *PLoS Genetics*, *6*(4), e1000902.

Xiong, Y., Yuan, C., Chen, R., Dawson, T. M., & Dawson, V. L. (2012). ArfGAP1 is a GTPase activating protein for LRRK2: reciprocal regulation of ArfGAP1 by LRRK2. *The Journal of Neuroscience*, *32*(11), 3877–3886.

Xiong, Y., & Yu, J. (2018). Modeling Parkinson's Disease in Drosophila: What Have We Learned for Dominant Traits? *Frontiers in Neurology*, *9*, 228

Xu, Q., Shenoy, S., & Li, C. (2012). Mouse models for LRRK2 Parkinson's disease. *Parkinsonism & Related Disorders*, *18 Suppl 1*, S186–S189.

Yao, C., Johnson, W. M., Gao, Y., Wang, W., Zhang, J., Deak, M., Alessi, D. R., Zhu, X., Mieyal, J. J., Roder, H., Wilson-Delfosse, A. L., & Chen, S. G. (2013). Kinase inhibitors arrest neurodegeneration in cell and C. elegans models of LRRK2 toxicity. *Human Molecular Genetics*, *22*(2), 328–344.

Yang, D., Thomas, J. M., Li, T., Lee, Y., Liu, Z., & Smith, W. W. (2018). The Drosophila hep pathway mediates Lrrk2-induced neurodegeneration. *Biochemistry and cell biology*, *96*(4), 441–449.

Yap, T. L., Gruschus, J. M., Velayati, A., Westbroek, W., Goldin, E., Moaven, N., Sidransky, E., & Lee, J. C. (2011). Alpha-synuclein interacts with Glucocerebrosidase providing a molecular link between Parkinson and Gaucher diseases. *The Journal of Biological Chemistry*, *286*(32), 28080–28088.

Yoboue, E. D., & Valente, E. M. (2020). PINK1 and Parkin: The odd couple. *Neuroscience Research*, *159*, 25–33.

Zhang, Q., Major, M. B., Takanashi, S., Camp, N. D., Nishiya, N., Peters, E. C., Ginsberg, M. H., Jian, X., Randazzo, P. A., Schultz, P. G., Moon, R. T., & Ding, S. (2007). Small-molecule synergist of the Wnt/beta-catenin signaling pathway. *Proceedings of the National Academy of Sciences of the United States of America*, *104*(18), 7444–7448.

Zhang, S. L., Yue, Z., Arnold, D. M., Artiushin, G., & Sehgal, A. (2018). A circadian clock in the blood-brain barrier regulates xenobiotic efflux. *Cell*, *173*(1), 130–139.e10.

Zhao, Y., & Dzamko, N. (2019). Recent developments in LRRK2-targeted therapy for Parkinson's disease. *Drugs*, *79*(10), 1037–1051.

Zimprich, A., Biskup, S., Leitner, P., Lichtner, P., Farrer, M., Lincoln, S., Kachergus, J., Hulihan, M., Uitti, R. J., Calne, D. B., Stoessl, A. J., Pfeiffer, R. F., Patenge, N., Carbajal, I. C., Vieregge, P., Asmus, F., Müller-Myhsok, B., Dickson, D. W., Meitinger, T., … Gasser, T. (2004). Mutations in LRRK2 cause autosomal-dominant parkinsonism with pleomorphic pathology. *Neuron*, *44*(4), 601–607.

Zon, L. (2016). Modeling human diseases: an education in interactions and interdisciplinary approaches. *Disease Models & Mechanisms*, *9*(6), 597–600.

Zouhar, J., Hicks, G. R., & Raikhel, N. V. (2004). Sorting inhibitors (Sortins): Chemical compounds to study vacuolar sorting in Arabidopsis. *Proceedings of the National Academy of Sciences of the United States of America*, *101*(25), 9497–9501.